Towards a parameter-free theory for electrochemical process at the nano-scale

Ashwinee Kumar

Supervisor:
Prof. S. Sanvito

Co-Supervisor:
Dr. C. Cucinotta

Department of Physics
Trinity College Dublin
Ireland
2019

Declaration

I Ashwinee Kumar, hereby declare that this thesis has not been submitted as an exercise for a degree at this or any other university. It comprises work performed entirely by myself during the course of my PhD studies at Trinity College Dublin. I was involved in a number of collaborations, and where it is appropriate my collaborators are acknowledged for their contributions.

I agree that Library may lend or copy this thesis upon request.

_____

Abstract

The mass and charge distribution at electrochemical interfaces plays a key role in driving electrochemical phenomena. However, in spite of its importance, even the structure of the Pt/water interface under bias, the most basic electrochemical interface, is still almost entirely unknown. Here we present the first *ab initio* simulation of the double layer structure at the Pt/water interface in realistic solution conditions and its dependence on an applied potential. Our results are enabled by a newly developed *ab initio* charging approach, which is here briefly described. We reveal that the double layer structure, number density and charge distribution, strongly depends on the applied potential. Furthermore, we show that the metal/surface charging state cannot be described using a traditional simple capacitor model. In fact, the interfacial dipole is not merely determined by the reorientation of the first water layer in contact with the metal surface, but also by its charging state in combination with its number density. Water reorientation becomes relevant only in the second water layer. The dependence of the structure of the Pt/water double layer on the applied potential will likely affect the catalytic processes therein.

Acknowledgements

I am indebted to many people for their help and guidance in the last 4 years.

First of all, I would like to thank my supervisor Prof. Stefano Sanvito for his continuous help, guidance and support during my PhD. His enthusiasm, insight into science and dedication to research have been an inspiration for me. Working under his supervision has been an incredible privilege. I would like to express my gratitude to Dr. Clotilde Cucinotta, from her I learned about the *ab initio* simulation of metal/water interfaces. Her input to this work through her ideas, insights and expertise is very much appreciated.

Next, I would like to thank my lab mates - Maria, Mario, Yanhui, Emanuele, Urvesh, Rajarshi, Anais, Sabin for their constant help and support. I would especially like to thank Tom for the technical support and advice. I would also like to thank Stefania Negro, she was of great help in the starting of my PhD. I would also like to thank many friends from different societies especially DUHAC, they have been a great support from me in college.

I would also like to thank TCHPC for providing me the computational power, and their staff members who all have been very helpful. I would also like to thank the Irish Research Council for providing the fund to carry out the research work.

Finally, I would like to thank my family members, they have been a great support throughout my life.

Contents

1 Introduction **1**

1.1 My PhD work 5

1.2 Choice of time scale 7

1.3 Literature Review 8

2 Theoretical tools and approximations **13**

2.1 Methodological Approach 13

2.1.1 The Many-Body Problem 13

2.1.2 Hartree-Fock Approximation 15

2.1.3 Density Functional Theory (DFT) 16

2.1.4 Exchange-Correlation Functionals 18

2.1.5 The Bloch Theorem 20

2.2 Computational Approach 20

2.2.1 Basis Sets Expansion 20

2.2.2 Supercells 21

2.2.3 Pseudopotentials 22

2.2.4 Periodic Boundary Conditions (PBC) 22

2.2.5 Density of States (DOS) 23

2.2.6 *ab initio* Molecular Dynamics (AIMD) 25

2.2.7 Radial Distribution Function 28

2.2.8 Work Function 28

2.2.9 Band Alignment 29

2.2.10 The *ion unbalance* model 31

3 Models and Convergency Tests **33**

3.1 Bulk Platinum and Surface 34

3.1.1 Platinum Bulk 34

3.1.2 Platinum Surface 35

3.2 Starting Pt-Water Simulation 48

4 Platinum/water interface under bias **51**

4.1 The model system 53

4.2 Methodology Used 54

4.3 Electronic analysis 55

4.3.1 Bader charges 55

4.3.2 The charge at the electrode-electrolyte interface 64

4.3.3 Evaluation of the electrode/electrolyte potential drop 67

4.3.4 The Interface Capacitance 69

4.4 Structural analysis 73

4.4.1 Water structure and orientation 73

4.4.2 Computational SFG spectra 78

4.5 Methodology assessment 79

5 A Comparative Study of Pt/Water And The Ag/Water Interfaces **83**

6 Smaller Simulation Cell **93**

6.1 Platinum/Water interface 94

6.2 *ab initio* MD of smaller Pt/water system 102

7 Conclusion and Future work **107**

7.1 Conclusion 107

7.2 Future work 110

A Water Molecule **113**

B Sum-Frequency-Generation Spectroscopy (SFG) **119**

C Solvation shell **121**

D Timestep and K points **125**

E Publications **127**

List of Figures

1-1 A hydrogen fuel cell vehicle, which uses hydrogen as fuel and converts it into electricity. This in turn is used to drive the car, while leaving water as the combustion product [1]. 1

1-2 The working principles of different electrolytic devices. Panel (a) shows the working principle of a solid oxide fuel cell. Oxygen molecules turn into oxygen ions on coming in contact with the cathode. O ions travel to the anode through the electrolyte where they combine with hydrogen producing water. Panel (b) shows the working principle of a simple electrolytic cell. As soon as the electrodes are immersed in the electrolyte, the flow of anions to the anode and cations to the cathode begins, starting reduction and oxidation reactions at the respective electrodes and producing electricity in return. Panel (c) shows the working principle of superacapacitor (an irregular electrode can be seen over here, this is to increase the surface area of electrodes). The application of potential across the electrodes leads to anode and cathode covered with oppositely charged ions [2]. 2

1-3 A simplified illustration of the Helmholtz double layer near the electrode-electrolyte interface. The electrode is positively charge, the electrolyte oriented with negative dipole towards it and solvated ions distributed inside the electrolyte. A steep decrease in the potential profile can also be observed within the double layer. 'd2' marks the boundary of the DL (also known as outer Helmholtz plane), after that there is diffuse layer where diffusion of ions take place and further away to the right the seperator separates this layer from the bulk electrolyte [3]. 4

1-4 The STM image of D_2O clusters on Pd(111) surface at 100 Kelvin. The formation of hexagonal honeycomb clusters can easily be seen in this figure [4]. 5

1-5 Various materials modelling methods along with their associated time and length scales. 7

1-6 Filhol and Neurock model showing the polarization of a bare Cu(111) slab by either a sodium ion pseudopotential at the outer Helmholtz plane (Na) or the use of a continuum countercharge (1e), is illustrated by comparing plots of the electrostatic potential (top), electric field (center), and the change in electron density (bottom). Gradual decrease of electrostatic potential can be seen in top [5]. 10

1-7 Rossmeisl model showing a charged Pt(111) slab with 3 water layers outside and one solvated hydronium ion (yellow) per unit cell. The electrode potential, due to the charged interface and averaged parallel to the surface is shown for systems with 1, 2 and 3 relaxed water layers along with results [6]. 11

2-1 Figure showing a unit cell and different types of supercells in a 2D cubic crystal [7]. 21

2-2 Replication of the all atoms of white box throughout the space to form an infinite lattice. 22

2-3 DOS of Pt(111) surface,the DOS does not have a HOMO-LUMO as it is a metal. Fermi level aligned with 0 eV. 24

2-4 PDOS of O and H of liquid water, shows separately the contribution of electron density of O and H. Fermi level aligned with 0 eV. 24

2-5 Figure shows the number of particles within a distance of r and $r+dr$ (shown in green colour) away from the reference point (shown in blue colour) [8]. . 28

2-6 Figure shows the schematic energy level diagram for the calculation of work function in a metal. It is defined as the energy difference between the electrostatic potential in the vacuum and the Fermi level of the material (E_F) [9]. 29

2-7 Figure shows different scenarios for substrate-molecule energy alignment. The solid substrate is depicted by red and blue colour for low and high work function respectively. The molecule is depicted by green colour and molecular levels are depicted by horizontal lines (two for HOMO and two for LUMO). Gray line at the intrerface represents lack of interface states, Δ and E_T are interface potential step and the tunneling barrier (defined as the distance between the metal Fermi level and the molecular HOMO level) respectively. (A) Vacuum level alignment in the state of non electrical equilibrium. (B) Hybrid states (bonding groups) localised at the substrate-molecule interface, the interface can be polarised in order to maintain a net equilibrium between the electron chemical potential of the molecule (μ) and the fermi level of the solid (E_F), this results in an extremely sharp induced potential energy step (Δ). (C) In cases where the substrate's Fermi level is outside the molecular gap, (In this example IP$<$WF) the charging of the moleule takes place. However, the low interface permittivity enforces a nonzero E_T [10]. 30

2-8 Single electron energy levels alignment and schematic picture of a Pt/electrolyte half-cell. E_F(Pt) separates filled and empty electronic states. Filled and empty water molecular states lay well below and above E_F, respectively. The highest occupied state for Na (here HOMO(Na), by analogy with the nomenclature for highest occupied molecular orbitals) is above E_F, and thus this species is expected to be fully ionised in solution. Correspondingly, the lowest unoccupied state for Cl, (namely, the degenerate Semi Occupied Molecular Orbital, SOMO(Cl)), is below E_F, therefore it becomes filled in the system under consideration. Notably, a frozen picture of the single electron energy levels in our system is adopted here. 32

3-1 Figure showing energy vs K points grid for bulk platinum showing the variation of total energy with variation in K points. 35

3-2 Figure showing energy vs lattice parameter at different K points grid for bulk platinum, used for optimizing the lattice parameter using the equation of states. 35

3-3 Figure shows the supercell of platinum used for modelling the 7 layers slab (a) (001) surface and (b) (111) surface. 37

3-4 The numbering of different layers of platinum with respect to vacuum, starting with layer 1 from top to 7 at the bottom. 38

3-5 Figure shows the interlayer distance as a function of the K-points grid (XxXx1) in Pt (001), it can be seen that as one moves from surface to centre the interlayer spacing comes closer to that of bulk. The convergence of the curves with increase in K points can also be seen. 39

3-6 Interlayer distance as a function of K-points grid in Pt (111), it can be seen that as one moves from surface to centre the interlayer spacing comes closer to that of bulk. The convergence of the curves with increase in K points can also be seen. 40

3-7 PDOS of middle layer of 7 layers platinum surfaces (001) and (111) compared with bulk (surfaces calculated using 8X8X1 K points while bulk using 8X8X8 K points). It can be seen that the PDOS of (001) and (111) are all very similar to the bulk, so we conclude that they are able to mimic the property of the bulk to a large extent. 40

3-8 PDOS of symmetric layers(e.g 1 and 7, 2 and 6, 3 and 5 shown in figure (a), (b) and (c)) of the 7 layers Pt (001) slab compared with each other, the symmetric layers superimpose each other, confirming the same density of states (calculated with 8X8X1 K points grid). 41

3-9 PDOS of symmetric layer(e.g 1 and 7, 2 and 6, 3 and 5 shown in figure (a), (b) and (c)) of the 7 layers Pt (111) slab compared with each other, the symmetric layers superimpose each other, confirming the same density of states (calculated with 8X8X1 K points grid). 42

3-10 Work function vs K-points density Figure shows the work function as a function of the K-points grid (XxXx1) in 7 layers Pt (a) (111) slab and (b) (001) slab. The convergence of the curves with increase in K points grid can be observed. 43

3-11 PDOS of middle layer of 4 layers platinum surfaces (001) and (111) compared with bulk Pt (surfaces calculated using 8X8X1 K points while bulk using 8X8X8 K points grid). 45

3-12 Interlayer distance as a function of K-points grid in Pt(001) 4 layers slab (calculated using 8X8X1 K points grid). Both the curves are showing a convergence behaviour with increasing K points grid. 45

3-13 Interlayer distance as a function of K-points grid in Pt(111) 4 layers slab (calculated using 8X8X1 K points grid). layer 1-2 is showing a consistent convergence behavior while layer 2-3 has yet not converged. 46

3-14 PDOS of symmetric layers(e.g 1 and 4, 2 and 3) of Pt(001) 4 layers slab compared with each other (a) PDOS of top and bottom layer (b) PDOS of both middle layer (both calculated using 8X8X1 K points grid). All the symmetric layers are superimposing on each other, confirming the symmetry. 46

3-15 PDOS of symmetric layer(e.g 1 and 4, 2 and 3) of 4 layers Pt(111) compared with each other (a) PDOS of top and bottom layer (b) PDOS of both middle layer (both calculated using 8X8X1 K points grid). All the symmetric layers are superimposing on each other, confirming the symmetry. 47

3-16 Work function vs K-points density of a 4 layers Pt slab (a) for 4 layers Pt(111) slab (b) for 4 layers Pt(001) slab (both calculated using 8X8X1 K points grid). Both the curves are showing a convergence behaviour with increasing K points grid. 47

3-17 Figure shows Pt/water solution model system. Here we present a snapshot of the trajectory of the 0Na:0Cl system. Red, white and olive-green colour represent oxygen, hydrogen and platinum respectively. 48

3-18 0Na:0Cl system: graph of water density variation throughout the electrolyte, it shows different region of water layers near the electrode i.g. first (min1) and second (min2) minimum of the water density profile. The subscript 'l' and 'r' represent the left and right position of the respective minima. 49

3-19 Figure shows average atomic density profiles for the O and H atoms belonging to the aqueous electrolyte in contact with the electrode (in units of atoms per Å) for 0Na:0Cl system. Here (a) represents the water molecules belonging to the first water layer, in contact with the electrode. In (b) the water molecules of the second water layer. The plain and dashed lines stand for the O and H atoms' contributions, respectively. Z1 and Z2 mark the end of the first and second layer. 50

4-1 Our Pt/water solution model system. Here we present a snapshot of the trajectory of the 10Na:12Cl system (with 10 Na and 12 Cl ions in solution). The horizontal bar on top of the snapshot marks the external boundary of the first and second water layer (Z_1 and Z_2, respectively). $Z = 0$ labels the average position of the surface Pt layers in contact with the aqueous electrolyte. Red, white, olive green, cyan and blue spheres represent O, H, Pt, Cl and Na atoms, respectively. 53

4-2 Average density profile of the O atom in the aqueous solution. To facilitate the reading, the results are vertically shifted. The separation between first and second water layer is identified by Z_1, while the separation between the second region and the rest (bulk) of the solution is marked by the Z_2 interval, as the coordinate is not the same for the three interfaces. The zero of the Z scale is aligned to the position of the centre of the metal slab. . . . 58

4-3 10Na:12Cl system: graph of water density variation throughout the electrolyte, it shows different region of water layers near the electrode i.g. first minimum (min1), second minimum (min2) and shoulder of the water density profile. The subscript 'l' and 'r' represent the left and right position of the respective label. It has the highest density of water in first layer compared to other two systems. 61

4-4 10Na:10Cl system: graph of water density variation throughout the electrolyte, it shows different region of water layers near the electrode i.g. first minimum (min1), second minimum (min2) and shoulder of the water density profile. The subscript 'l' and 'r' represent the left and right position of the respective label. 62

4-5 12Na:10Cl system: graph of water density variation throughout the electrolyte, it shows different region of water layers near the electrode i.g. first minimum (min1), second minimum (min2) and shoulder of the water density profile. The subscript 'l' and 'r' represent the left and right position of the respective label. It has the least density of water in first layer clearly showing density dependense of water near the electrodes on the concentration of ions in solution. 63

4-6 Graphical representation of the overall excess (nominal-calculated) Bader valence charge distribution along the double layer. The charge is averaged along the trajectory and between the two surfaces present in our cell. The black dashed line (joining the Pt subsurface layers and the region in their middle) signals that in the middle of the metal slab the actual charge is 0 (see Fig. 4-10). 66

4-7 *Effective* potential drop, ΔV, versus time for the three interfaces studied. The *effective* ΔV is obtained by subtracting from the electrostatic potential of the total system (with charged electrode and electrolyte) that of its neutral separate components (i.e. the neutral electrode and the electrolyte, both surrounded by vacuum) in the same atomic configuration assumed in the charged system. 67

4-8 *Absolute* potential drop, ΔV, versus time, for the three interfaces studied. The *absolute* ΔV is obtained as the difference between vacuum potential energy and the Fermi level. 68

4-9 Standard potential drop for the three interfaces studied, calculated as the difference between the potential energy in the bulk electrolyte and the potential energy in the bulk electrode. 69

4-10 Macroscopic total (ionic cores + valence electrons) charge (inset at the bottom, representation not to the scale) and electrostatic potential energy (top inset) profiles along z (perpendicularly to the electrode surface), for the representative 10Na:10Cl system (represented in the central inset). These profiles are calculated along the trajectory every 1 ps (black lines). The average of these profiles is represented with a red line. Similar charge and potential drop trends are observed for all the systems. 70

4-11 Double layer charge versus potential drop ΔV , as averaged along the trajectory for 12Na:10Cl (electrode charge -1.1 $|e|$), 10Na:10Cl (electrode charge -0.6 $|e|$) and 10Na:12Cl (electrode charge -0.03 $|e|$) systems. Charge and potential drop are provided in units of $|e|$ and Volts, respectively. Also reported, the system's capacitance ($C = 8.29\ \mu\mathrm{F{\cdot}cm^{-2}}$), evaluated from the slope of the charge/potential linear fit (dashed black line). The continuous vertical red line represents the experimental PZC. Aligning this potential to the point where the linear fit crosses zero charge, allowed to define ad absolute potential scale for our electrodes, referred to the standard hydrogen electrode potential. The dashed vertical red line represents our evaluation of the PZC, where ΔV is evaluated relating the interfacial Fermi energy in every system to the vacuum level, and this latter to the SHE. 71

4-12 Average atomic density profiles for the O and H atoms belonging to the aqueous electrolyte in contact with the electrode (in units of atoms per Å). 12Na:10Cl, 10Na:10Cl, and 10Na:12Cl systems are represented in black, red and blue, respectively. Differently unbalanced ion populations in solution lead to differently charged electrodes. The charge on the metal moiety of the interface is reported in the brackets next to each label (in units of $|e|$). For each system, the atomic density profiles are averaged over 50 ps long trajectories obtained performing DFT based Born Oppenheimer molecular dynamics. First and second water layers are defined as described in Tab. 4.3. Here (a) represents the water molecules belonging to the first water layer, in contact with the electrode. In (b) the water molecules of the second water layer. The plain and dashed lines stand for the O and H atoms' contributions, respectively. The separation between first and second water layer is identified by Z_1, while the separation between the second region and the rest (bulk) of the solution is marked by the Z_2 interval. 74

4-13 Integrated O-H radial distribution profile ("Running" Coordination number), where O belongs to the molecules of the first water layer in contact with the electrode. Black, red and blue lines represent the profiles relative to 12Na:10Cl, 10Na:10Cl and 10Na:12Cl systems, respectively. 75

4-14 (a) Prototypical configuration of first and second water layer for 10Na:12Cl, 10Na:10Cl and 12Na:10Cl systems, respectively. Red lines highlight hexagonal and pentagonal motives. (b) Trajectories of O atoms belonging to first and second water layer in contact with the electrode, marked with blue and red lines, respectively. The charge on the metal electrode is also reported (units of $|e|$). Wat. nb. indicates the average number of molecules in the first water layer. 76

4-15 Schematic view of the water bilayer at the Pt/H_2O interface for different state of charges (this is a cartoon showing the trend in the result, it's not to the scale.). (a) Poorly charged Pt, typically with 10 Na and 12 Cl in solution, (b) negatively charge Pt, typically with 10 Na and 10 Cl in solution, (c) highly negatively charged Pt, typically with 12 Na and 10 Cl in solution. 77

4-16 Layer resolved surface sensitive vibrational density of states (VDOS), for 12Na:10Cl, 10Na:10Cl and 10Na:12Cl systems, represented with black, red and blue lines, respectively. The charge on the metal moiety of each DL is also reported in brackets, in units of $|e|$. In (a) the VDOS obtained from the water molecules of layer 1, an increasing number of which points towards the bulk of the electrolyte, as the electrode becomes more positive. In (b) the VDOS obtained taking into account only water molecules of the second layer, where the number of water molecules reorienting their dipole towards the electrode becomes increasingly larger, as the electrode becomes more negative. 79

4-17 PDOS. Average projected density of states on Pt, Na and Cl species along the trajectory. The zero of the energy scale is aligned to the Fermi level. The PDOS on Pt atoms is represented in green. The PDOS on ions in 12Na:10Cl, 10Na:10Cl and 10Na:12Cl systems are magnified ($\times$ 3) and represented by a red, blue and black line, respectively. In every system, the same colour code is used to represent both PDOS on Na and Cl, however there is no ambiguity, as they do not overlap. 80

5-1 Comparison of the projected density of states (PDOS) on O, Cl and Na atomic species, for the 10Na:12Cl-Ag (blue) and 10Na:12Cl-Pt (green) systems. The zero of the energy scale in these graphs is aligned to the Fermi level of the interface under consideration, so Cl and O PDOSes in Ag/water interface (upper inset) are lower in energy with respect to the Fermi level than those in Pt/water interface. This marks the lower value of Pt Fermi level with respect to vacuum. In the lower inset, the PDOS on Pt and the ions. A larger gap between Cl LUMO and Na HOMO is observed in the Ag/water interface. 84

5-2 Average density profile of the water in the electrolytic solution. The separation between first and second water layer is identified by Z1, while the separation between the second region and the rest (bulk) of the solution is marked by the Z2 interval. The shoulder is also clearly visible here similar to that of platinum electrode systems. The zero of the Z scale is aligned to the position of the centre of the metal slab. 87

5-3 Figure shows average atomic density profiles for the O and H atoms belonging to the aqueous electrolyte in contact with the electrode (in units of atoms per Å) for 10Na:12Cl-Ag system. Here (a) represents the water molecules belonging to the first water layer, in contact with the electrode. In (b) the water molecules of the second water layer. The plain and dashed lines stand for the O and H atoms' contributions, respectively. Z1 and Z2 mark the end of the first and second layer. 88

6-1 Figure shows both the symmetric layer of the smaller system have symmetric PDOS. In (a) PDOS of 1st and 4th layer of the smaller system is comapred and in (b) PDOS of 2nd and 3rd layer of the smaller system is compared. 94

6-2 Comparison of 2nd layer DOS of the smaller system, with that of the bulk platinum. 95

6-3 Figure shows the relaxation process of a 4 layer platinum (111) slab with 1 water molecule. It shows the orientation of the molecule at the beginning and end of the simulation (after relaxation), (a) shows top view of initial configuration, (b) shows top view of final configuration, (c) shows sideview of initial configuration and (d) shows sideview of final configuration. The red sphere represent the 'Oxygen', white 'Hydrogen' and olive green 'Platinum'. 96

6-4 Figure shows the relaxation process of 4 layer platinum (111) slab with 2 water molecule, it shows the orientation of the molecule at the beginning and end of the simulation (after relaxation), (a) shows top view of initial configuration, (b) shows top view of final configuration, (c) shows sideview of initial configuration and (d) shows sideview of final configuration. The red sphere represent the 'Oxygen', white 'Hydrogen' and olive green 'Platinum'. 97

6-5 Figure shows the relaxation process of 4 layer platinum (111) slab with 13 water molecule, it shows the orientation of the molecule at the beginning and end of the simulation (after relaxation), (a) shows top view of initial configuration, (b) shows top view of final configuration, (c) shows sideview of initial configuration and (d) shows sideview of final configuration. The red sphere represent the 'Oxygen', white 'Hydrogen' and olive green 'Platinum'. 98

6-6 Figure shows the relaxation process of 4 layer platinum (111) slab with 26 water molecule, it shows the orientation of the molecule at the beginning and end of the simulation (after relaxation), (a) shows top view of initial configuration, (b) shows top view of final configuration, (c) shows sideview of initial configuration and (d) shows sideview of final configuration. The red sphere represent the 'Oxygen', white 'Hydrogen' and olive green 'Platinum'. 99

6-7 Figure shows the average potential profile of 4 layers platinum (111) surface on interaction with different number of water molecules- (a) potential profile of platinum with 1 water molecule on its surface, (b) potential profile of platinum with 2 water molecule on its surface, (c) potential profile of platinum with 13 water molecule on its surface and (d) Potential profile of platinum with 26 water molecule on its surface. 100

6-8 Variation of work function of Pt(111) with increasing number of water molecule on its surface. 101

6-9 Distribution of water molecules on both side of Pt(111) surface, in new smaller system. The middle layers of the slab are fixed. The red sphere represent the 'Oxygen', white 'Hydrogen' and olive green 'Platinum' 103

6-10 Distribution of water density in smaller system, measured as distance from the surface (surface=0Å) 104

6-11 Average potential profile of Pt(111)-water (small system). The potential shows uniformity on both side of platinum surface. 104

6-12 Charge variation in the small system, starting from the subsurface platinum layer (SS), surface platinum (S), first layer of water (L1), second layer of water (L2), rest of water (RW). 105

7-1 Electrolytic cell in working condition [11, 12] 112

A-1 Shown is the convergence of total energy as a function of force cutoff of a water molecule at a fixed box size. 114

A-2 Shown is the plot of variation of total energy of a water molecule as a function of box size. 115

A-3 Shown is the graph of ΔE as a function of box size for the water molecule, it can be seen that the ΔE fluctuates around 0 116

A-4 Shown are the charge density isosurface of the occupied molecular orbitals of water, starting from lowest energy (a) to highest (d). 117

A-5 Shown are the charge density isosurface of the unoccupied molecular orbitals of water starting from lowest energy (a) to highest (d). 118

C-1 The figure shows the solvations of anion (Cl) and cation (Na). It can be easily seen that in the anion solvation shell '(a)' hydrogen of water molecules are pointing towards Cl, while in the cation solvation shell '(b)' hydrogen of water molecules are pointing away from Na. Due to the polar nature of water molecule it is behaving in such a way. 122

C-2 The figure shows the radial distribution function of different systems for Cl-H. The first minima of G(r) curve is taken as cut off distance, defining the solvation shell. 122

C-3 The figure shows the radial distribution function of different systems for Na-O. The first minima of G(r) curve is taken as cut off distance, defining the solvation shell. 123

List of Tables

3.1 Table showing the platinum lattice parameter and bulk modulus obtained by varying the K points grid. 36

3.2 Total energy E and ΔE with variation in vacuum gap in 7 layers Pt(001). The '$*$' marks the vacuum gap sufficient for modelling the surface. 37

3.3 Total energy E and ΔE with variation in vacuum gap in 7 layers Pt(111). The '$*$' marks the vacuum gap sufficient for modelling the surface. 38

3.4 Interlayer distance in Platinum(001) using a 8x8x1 k point grid [(bulk =1.995 Å)], it can be seen that symmetric layers have same interlayer distance. 43

3.5 Interlayer distance in Platinum(111) using a 8x8x1 k point grid [(bulk =2.304 Å)], it can be seen that symmetric layers have same interlayer distance. 43

3.6 Total energy E and Δ E as a function of the vacuum gap in a 4 layers Pt(111) slab. 44

3.7 Total energy E and Δ E as a function of the vacuum gap in a 4 layers Pt(001) slab. 44

4.1 Excess Bader charges within the first solvation shell of Cl ion. Water No., O, H-away and H-towards and Water average represent the average number of water molecules, the average charge on O and H atoms - pointing away or towards the ion - and on each water molecule in the first solvation shell around Cl atom, respectively. Cl+Water and Cl represent the total average charge in each solvation shell and on Cl ion, respectively 56

4.2 Excess Bader charges within the first solvation shell of Na ion. Water No., O, H and Water average represent the average number of water molecules, the average charge on O and H atoms, and on each water molecule in the first solvation shell around Na atom, respectively. Na+Water and Na represent the total average charge in each solvation shell and on Na ion, respectively. 56

4.3 Cartesian coordinates in Å used to define position and boundaries of first and second water layer. Z_i mark the external boundary of layer i and correspond to the density minima of the O mass density profile. z_{Mi} mark the position of the i^{th} peak in the O mass density profile. All distances are measured from the Pt external surface layer 57

4.4 Excess Bader charges in the first layer of water near the electrode. Water No., Total-Water, Avg.-Water, O and H represent the average number of water molecules, the total charge on the water layer, the average charge per water molecule, average charge per O and H atoms, respectively. 58

4.5 Excess Bader charges in the second layer of water near the electrode. Water No., Total-Water, Avg.-Water, O and H represent the average number of water molecules, the total charge on the water layer, the average charge per water molecule, average charge per O and H atoms, respectively. 58

4.6 Excess Bader charges in free water. Free water is the water which is neither part of solvation shells nor of first or second water layers. Water No., Total-Water, Avg.-Water, O and H represent the average number of water molecules, the total charge on free water, the average charge per water molecule and average charge per O and H atoms, respectively. 59

4.7 10Na:12Cl system: comparison of water number density (per unit of cell surface) and excess Bader charges in the water layers near the electrode as calculated using either the minimum or the shoulder of the O density profile. Water No., Total-Water, Avg.-Water, O, H represent the average number of water in the first layer, total excess charge in the layer, average charge per water molecule, per oxygen and hydrogen atoms, respectively. . 60

4.8 10Na:10Cl system: comparison of water density and excess Bader charges in the water layers near the electrode as calculated using either the minimum or the shoulder of the O density profile. Water No., Total-Water, Avg.-Water, O, H represent the average number of water in the first layer, total excess charge in the layer, average charge per water molecule, per oxygen and hydrogen atoms, respectively. 60

4.9 12Na:10Cl system: comparison of water density and excess Bader charges in the water layers near the electrode as calculated using either the minimum or the shoulder of the O density profile. Water No., Total-Water, Avg.-Water, O, H represent the average number of water in the first layer, total excess charge in the layer, average charge per water molecule, per oxygen and hydrogen atoms, respectively. 60

4.10 Bader excess (nominal-calculated) valence charges in units of $|e|$. In column 'system', the name of the system under consideration, defined by the number of Na^+ and Cl^- ions in solution and the type of metal electrode. In columns 2-6 the total, subsurface and external surface charge and the charge on first and second layer of water in contact with the electrode, respectively. These values are averaged along the trajectory and between the two interfaces present in our cell. Columns "Cl + H" and "Na" report the charge localised around Cl and Na ions. Due to the crude definition of the boundary of the volume defining the Bader charge around each atom, part of the charge actually localised on Cl was accounted by the Bader scheme to the charge of the H atoms pointing towards it. In this table the sum of Cl and this *artificial* H charges are reported. In the last two columns, "Solvation Shells" and "DL", we report the total charge in the first solvation shells of Na and Cl ions and the total charge on the double layer, DL, including electrode, first and second water layer. 64

4.11 Average number density of water molecules per surface in the cell and per system, in the first and second layer in contact with the electrode. The cross section of our cell is (A=286 $Å^2$), corresponding to 42 surface Pt atoms. 75

5.1 Excess Bader charges within the first solvation shell of Cl ion. Water No., O, H-away and H-towards and Water average represent the average number of water molecules, the average charge on O and H atoms - pointing away or towards the ion - and on each water molecule in the first solvation shell around Cl atom, respectively. Cl+Water and Cl represent the total average charge in each solvation shell and on Cl ion, respectively 86

5.2 Excess Bader charges within the first solvation shell of Na ion. Water No., O, H and Water average represent the average number of water molecules, the average charge on O and H atoms, and on each water molecule in the first solvation shell around Na atom, respectively. Na+Water and Na represent the total average charge in each solvation shell and on Na ion, respectively. 89

5.3 Excess Bader charges in the first layer of water near the electrode. Water No., Total-Water, Avg.-Water, O and H represent the average number of water molecules, the total charge on the water layer, the average charge per water molecule, average charge per O and H atoms, respectively. 89

5.4 Excess Bader charges in the second layer of water near the electrode. Water No., Total-Water, Avg.-Water, O and H represent the average number of water molecules, the total charge on the water layer, the average charge per water molecule, average charge per O and H atoms, respectively. 90

5.5 Excess Bader charges in free water. Free water is the water which is neither part of solvation shells nor of first or second water layers. Water No., Total-Water, Avg.-Water, O and H represent the average number of water molecules, the total charge on free water, the average charge per water molecule and average charge per O and H atoms, respectively. 90

5.6 Bader excess (nominal-calculated) valence charges in units of $|e|$. In column 'system', the name of the system under consideration, defined by the number of Na^+ and Cl^- ions in solution and the type of metal electrode. In columns 2-6 the total, subsurface and external surface charge and the charge on first and second layer of water in contact with the electrode, respectively. These values are averaged along the trajectory and between the two interfaces present in our cell. Columns "Cl + H" and "Na" report the charge localised around Cl and Na ions. Due to the crude definition of the boundary of the volume defining the Bader charge around each atom, part of the charge actually localised on Cl was accounted by the Bader scheme to the charge of the H atoms pointing towards it. In this table the sum of Cl and this *artificial* H charges are reported. In the last two columns, "Solvation Shells" and "DL", we report the total charge in the first solvation shells of Na and Cl ions and the total charge on the double layer, DL, including electrode, first and second water layer. 91

6.1 Average distance of water molecules from Pt(111) surface in various sytem before and after relaxation 100

6.2 Excess of Bader charges in the first layer of the water near the electrode. Water No., Total-Water, Avg.-Water, O and H represent the average number of water molecules, the total charge on the water layer, the average charge per water molecule, the average charge per O and H atoms, respectively (for the small system). 102

6.3 Bader excess (nominal-calculated) valence charges in units of $|e|$ per unit area of electrode in units of $Å^2$, for electrode is compared under the section of Metallic electrode, then Interfacial water. Finally the number of interfacial water molecules per unit area in units of $Å^2$, under the Water No. (see figure 6-12 for more detail). 102

Chapter 1

Introduction

The study of the interface between water and other substrates is very important for understanding the various processes taking place in biology, electrochemistry, fuel cell, battery, supercapacitor and more generally in science. There is a never-ending list of examples for the interaction of water with other substrates where surface interaction plays a crucial role.

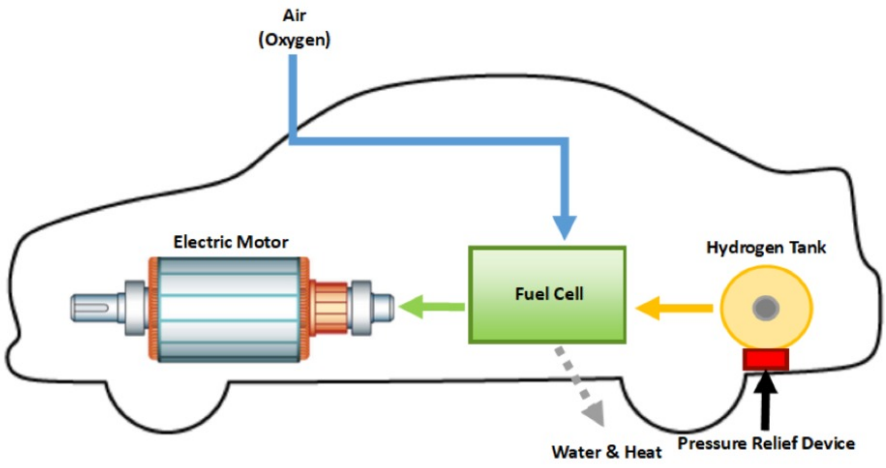

Figure 1-1: A hydrogen fuel cell vehicle, which uses hydrogen as fuel and converts it into electricity. This in turn is used to drive the car, while leaving water as the combustion product [1].

Figure 1-1 shows the working principle of a fuel cell inside a car. It uses hydrogen as

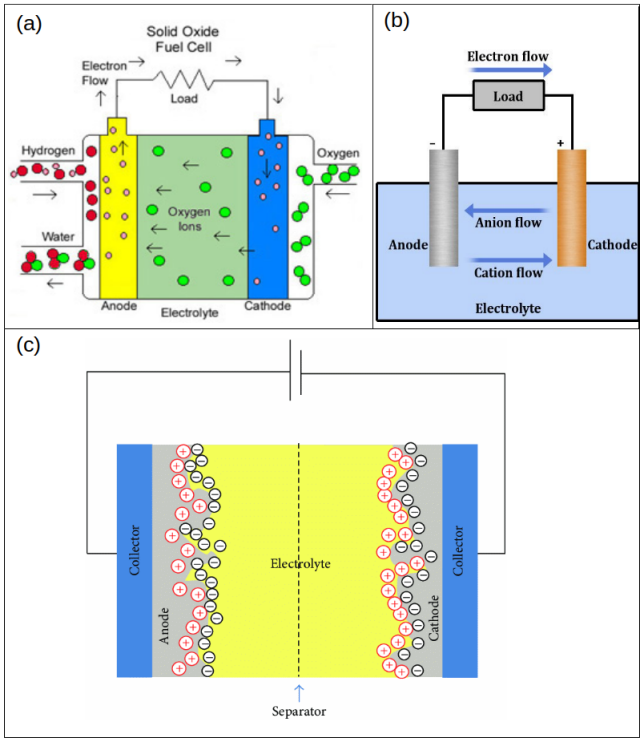

Figure 1-2: The working principles of different electrolytic devices. Panel (a) shows the working principle of a solid oxide fuel cell. Oxygen molecules turn into oxygen ions on coming in contact with the cathode. O ions travel to the anode through the electrolyte where they combine with hydrogen producing water. Panel (b) shows the working principle of a simple electrolytic cell. As soon as the electrodes are immersed in the electrolyte, the flow of anions to the anode and cations to the cathode begins, starting reduction and oxidation reactions at the respective electrodes and producing electricity in return. Panel (c) shows the working principle of superacapacitor (an irregular electrode can be seen over here, this is to increase the surface area of electrodes). The application of potential across the electrodes leads to anode and cathode covered with oppositely charged ions [2].

a fuel and it converts it into electrical energy, which is used to drive the electric motor. The product of the combustion is water. Electricity being a very efficient form of energy, will help solving the energy problem of the world. Figure 1-2 shows the working principle of a solid oxide fuel cell, battery and supercapacitor. It can be seen in the figure 1-2 that all these systems involve electrode-electrolyte interfaces and application of a potential across the electrodes. The application of a potential leads to the formation of a double layer (DL) at the electrode-electrolyte interface, and the migration of charge and mass inside the electrolyte. The double layer involves a complex interface with charge and mass

transfer, bond formation and bond breakage. It is described by the presence of long-range and short-range orders, hydrogen bonding and Van-der walls interaction. This system is very complex and difficult to study.

A successful model for the DL was first proposed by Helmholtz in 1853 [3]. He described the DL as a molecular dielectric which stores charge electrostatically (like a capacitor) independent of electrode charge density and dependent on dielectric constant of electrolyte. A simplified illustration of the Helmholtz double layer is shown in the Fig. 1-3. It clearly shows a steep potentail drop in the DL, a positively charged electrode and polarized electrolyte next to it. This model provides a good description of the interface but it did not consider the adsorption of ions on the surface of the electrode, the diffusion of ions in solution and the interaction between the solvent dipole moment and the electrodes.

Gouy-Chapman-Stern [13, 14] further modified Helmholtz model. They found out that the capacitance of the DL is not constant but vary with the application of the potential to the electrode as well as the ionic concentration. They also considered diffusion of the ions in the DL as well as adsorption on the electrodes. This model is the base of the study untill present day.

For decades these systems have been the subject of theoretical and experimental investigations. Even with the rapid technological growth witnessed in the last few years the study of such interfaces has continued to interest the experimental and theoretical communities. There are many experimental techniques developed to study liquid-metal interfaces: low-energy electron diffraction (LEED), surface vibrational spectroscopies, such as surface enhanced Raman spectroscopy (SERS) and sum-frequency generation (SFG), high-resolution microscopy, like atomic force microscopy (AFM) and scanning tunneling microscope (STM), to name a few.

STM is a great tool for the study of surfaces, but it is not useful in ambient conditions since cryogenic temperatures and ultra-high vacuum are usually required to perform the experiments. Figure 1-4 shows a STM image of D_2O clusters on Pd(111) at 100 Kelvin. Clusters of D_2O limited to few unit cell can be easily seen. Although this experiment reveals the structure of D_2O on the Pd(111) surface, it lacks continuity due to formation

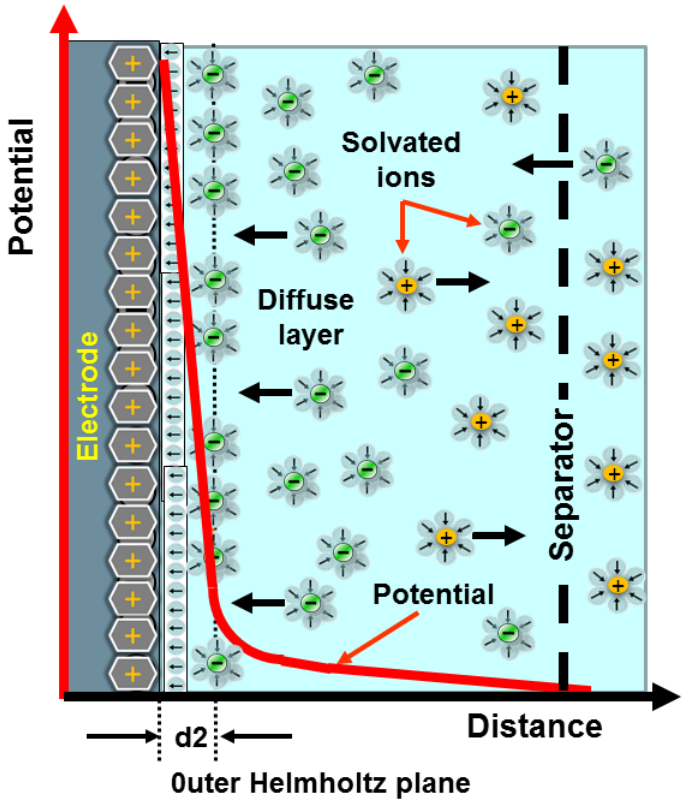

Figure 1-3: A simplified illustration of the Helmholtz double layer near the electrode-electrolyte interface. The electrode is positively charge, the electrolyte oriented with negative dipole towards it and solvated ions distributed inside the electrolyte. A steep decrease in the potential profile can also be observed within the double layer. 'd2' marks the boundary of the DL (also known as outer Helmholtz plane), after that there is diffuse layer where diffusion of ions take place and further away to the right the seperator separates this layer from the bulk electrolyte [3].

of segregated clusters as well as it is far away from the experimental set up. AFM serves as a great tool to study the interfaces in ambient conditions, but it fails to achieve an atomic resolution of complex interfaces as well as in describing the dynamics. Spectroscopic techiniques are not suitable either for atomic scale manipulation nor real-space imaging. In ambient conditions processes like bond formation, bond breaking, charge transfer between the liquid electrolyte and the solid interface are very difficult to investigate using experimental techniques. Some of these, for example charge transfer, may occur on a timescale of femtoseconds [15, 16].

From this short review we can appreciate the level of difficulty related to the understanding of the double layer. A full understanding will help us to take a step towards solving the energy and pollution problem of the world, by providing a clean and green source of energy, which is possible with the commercialization of fuel cells.

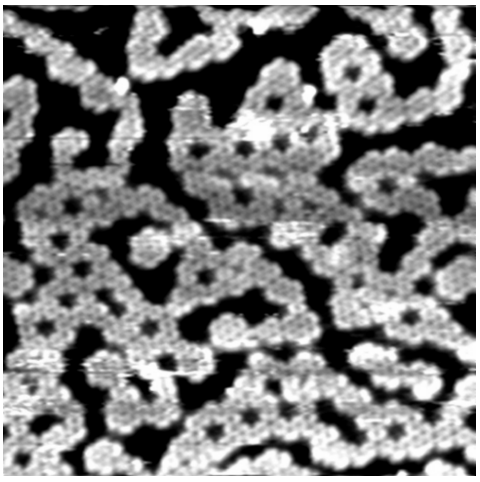

Figure 1-4: The STM image of D_2O clusters on Pd(111) surface at 100 Kelvin. The formation of hexagonal honeycomb clusters can easily be seen in this figure [4].

With the recent advances in computational techniques, the modelling of the interfaces is moving closer to realistic "liquid-water" interfaces. The best-suited theoretical tools to simulate these systems atomistic models, as they have turned out to be better for predicting experimental results [17]. They are even more useful for describing the processes occurring in extreme conditions of temperature and pressure [18]. Nowaday atomistic simulation are considered to be the best tool for the prediction of material properties, and for finding new materials for suitable processes. A large group of scientists is working to find new materials for aerospace, magnetism, elctrochemical applications using atomistic simulations [19].

1.1 My PhD work

My PhD work involves contributions towards the understanding of the DL. Although a lot of work has been carried out in the area of fuel cells and supercapacitors, their efficiency and power output remains very low. As such, much research is carried out

in order to increase the energy output to fulfill the world energy demands. My study will mostly focus on the structure and properties of the double layer. Since, as already discussed, the formation of the double layer is the fundamental phenomenon occuring in an electrochemical environment. In particular we will look at the modeling of the electrostatic potential applied to the electrochemical cell at the molecular level. This can be used to monitor the reactions as well as developing better materials for water splitting [20]. Since there are different theoretical methods to model the double layer, it is very important to choose the appropriate one, which can predict the experimental phenomenon accurately. Many different types of modelling methods are available depending on the process to study. Each one of them has limitations and advantages, so the selection should be made carefully. Major issues in modelling the application of a potential to an interface are:

- The size of the system (In atomistic simulations, depending on the type of system to equalize, it varies from thousands to tens of thousands of atoms. This is very far away from any practical system, a problem that is solved by using periodic boundary conditions (PBC) and supercells approach. These are disscussed in detail in chapter 2.)

- Application of potential (Due to the implementation of PBC, to avoid the finite size effect, it is not possible to apply the potential directly to the electrode. In our model we will be using an imbalance population of ions in the electrolyte to charge the electrode, in turn applying the potential. This aspect will be discussed in detail in chapter 2.)

- Simulation time (The time of a simulation depends upon the kind of simulation going to be performed. Atomistic simulation can be performed upto picosecond time scale due to the large amount of intricate interactions to be taken into account. In contrast large-scale molecular dyanmics calculations can calculate properties changes in time interval upto a second [in this case the intricate interaction can be replaced by a suitable potential profile]. This aspect will be discussed in more detail in the next section.)

1.2 Choice of time scale

Figure 1-5 shows the various time and length scales addressed by the available theoretical tools. Accuracy is inversely proportional to the computational cost, so depending on the observable quantity a balance between accuracy and throughput should be reached before starting calculation of the selected system [21].

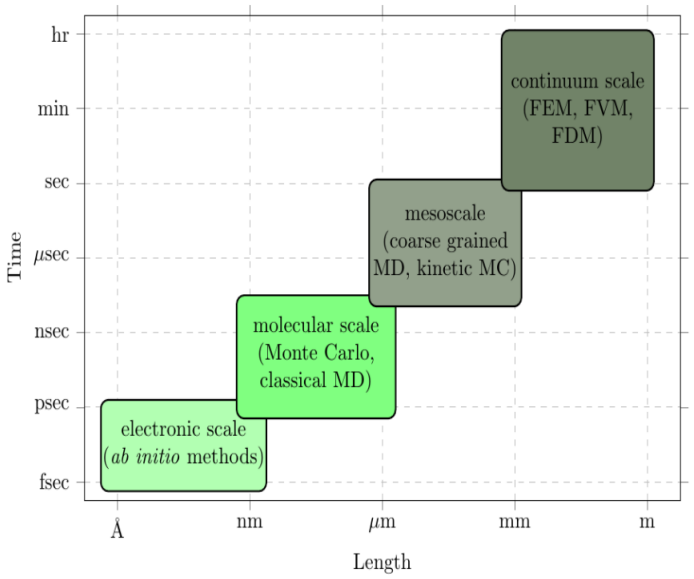

Figure 1-5: Various materials modelling methods along with their associated time and length scales.

In the bottom left corner there are *ab initio* or first principle methods, which include a description of the electronic interaction of the system. Their main limitation is that they can compute a maximum of few thousands atoms. The second approach after the *ab initio* one is, classical molecular dynamics(MD) [22, 23]. This method does not precisely take into account the electronic interactions, but instead replaces them with an atomic potential energy surface, thus reducing the computational cost significantly. The parameters for calculations can be assigned empirically in the form of interaction potentials. They can also be derived from *ab initio* computational results or experiments. Moving further to the right on the length scale we find kinetic Monte Carlo approaches [24], which deal with much larger systems and for longer times. As the computation time decreases due

to grouping of atoms, they also require some knowledge of the behaviour of the system in question prior to running the simulation. The required knowledge of the system can conveniently be extracted from *ab initio* or classical molecular dynamics results.

In the right corner there are the continuum-scale methods (e.g. finite-elements modelling (FEM), finite-volume method (FVM), finite-difference method (FDM)) [25]. At this scale the interactions between the electrons are incorporated indirectly using partial differential equations. The resulting equations are coupled energy-balance equations, mass-balance equations and momentum-balance equations. These equations can be used to describe the transport of the constituting species by the means of conduction, convection and diffusion. These approaches are widely used in mechanical and civil engineering.

1.3 Literature Review

My work involves the study of the double layer equilibrium structure and the effects of an applied electrode potential. This will give me a deep insight into the structure and the reactivity of the interfaces and a comprehensive mechanistic description of the atomic and electronic scale processes at the electrode surfaces under an applied potential. Such understanding is still missing in the science community. Therefore, an *ab initio* approach is the best modelling method, which can be used. It has been already used for a long time [26, 27, 28] in modeling surfaces [29, 30, 31], but mostly focusing on reactivity of interfaces [32, 33, 34, 35, 36]. A comprehensive mechanistic description of atomic and electronic scale processes at the electrode surfaces under an applied potential is still missing. In particular, it is remarkable how limited our microscopic knowledge is of the double layer's equilibrium structure and the effect of an applied electrode potential on it. This is true even for the most fundamental interfaces, such as Pt/water. Modelling the application of an external potential is a key challenge in the field of theoretical electrochemistry.

One successfull model was developed by Filhol and Neurock [5] for tuning the electrochemical potential of half of an electrochemical cell. In this method two reference potentials are established, one describing the potential of H_2O far away from the elec-

trode and the other associated to the free electron. Excess/deficiency of charge can be introduced in the system by adjusting the surface potential and the method was used to analyse the case of Cu(111). Fig. 1-6 shows the variation of the charge and potential at the Cu(111) surface [5]. The problem of this method is that the potential drop is too gradual. This is not the case with the real electrolytic interfaces, where the potential drop is very sharp. However the method was successful in controlling the potential of the coupled interface system and in the introduction of fraction charge. Otani and Sugino [37, 38] tried to improve the model by introducing counter charges $15 - 20$Å in front of the electrode surface, since most of the potential drop takes place outside the surface. Also this model was unable to correctly show the polarization of water at the interface. Rossmeisl [6] used a better approach by introducing a hydronium ion in the water layer outside the charged interface. In this way, the electrified interface is explicitly modelled. However, the ion is at a fixed distance from the electrode and no dynamical simulation of the double layer was performed. The Rossmeisl model is shown in the Fig. 1-7. This model was successful in constructing the energy diagram for the hydrogen evolution reaction at different potentials and it established the potential dependent nature of the reaction.

The potential drop at the interface is determined by several factors, such as the type of ions in solution and their dynamics, the work function of the metal, the surface charge density, the electric field at the interface and the polarizability. Most of the standard approaches achieve cell neutrality and the description of the potential drop at the interface. However, a reliable description of an electrified interface has yet to be obtained.

An alternative computational standard hydrogen electrode method, devised to investigate coupled proton-electron transfer reactions, was developed by Sprik and co-workers [39, 40, 41]. This approach allows one to refer the computed potential to the standard hydrogen electrode (SHE) using the solvation free energy of the proton, calculated by measuring free energies from a common reference point, corresponding to the free energy of an aqueous hydronium ion H_3O^+. The method is sophisticated and powerful, but its obvious downside is the high computational cost, which has limited its application to realistic metal/electrolyte interfaces. More recently an extension of the standard hydrogen

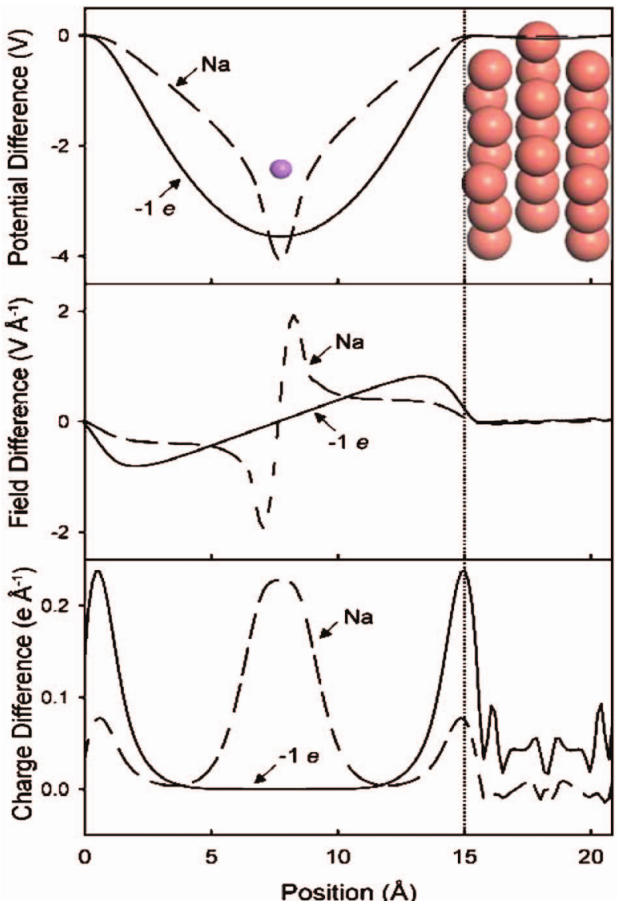

Figure 1-6: Filhol and Neurock model showing the polarization of a bare Cu(111) slab by either a sodium ion pseudopotential at the outer Helmholtz plane (Na) or the use of a continuum countercharge (1e), is illustrated by comparing plots of the electrostatic potential (top), electric field (center), and the change in electron density (bottom). Gradual decrease of electrostatic potential can be seen in top [5].

electrode method that avoids the expensive calculation of the solvation free energy of the proton has been introduced and applied to a few metal/water interfaces [35]. However, this does not include ions and does not address the problem of charging. Perhaps more importantly, it does not provide a description of the over-potential related to the transfer of species to, from or across the interface.

For these reasons, we propose here a realistic description of the interface, which uses MD simulations of the inhomogeneous metal/electrolyte system. In many respects, part of the theoretical sophistications of the previous methods is lacking in our approach, which however follows the trend towards a simpler and intuitive description of the system,

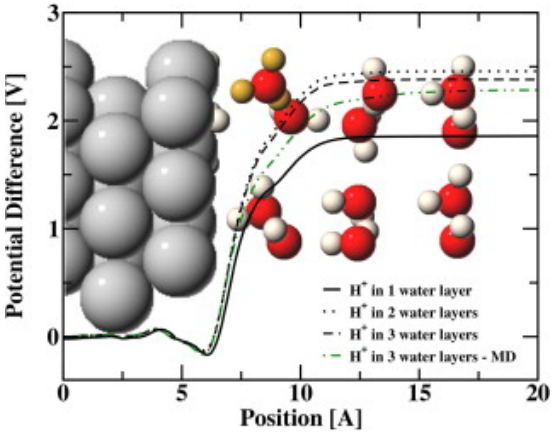

Figure 1-7: Rossmeisl model showing a charged Pt(111) slab with 3 water layers outside and one solvated hydronium ion (yellow) per unit cell. The electrode potential, due to the charged interface and averaged parallel to the surface is shown for systems with 1, 2 and 3 relaxed water layers along with results [6].

using simulations to reproduce reality and to carry out virtual experiments. In order to understand the electrolytic system thoroughly there is the need to address the problem by using a more comprehensive approach. In this approach we introduce imbalanced population of ions (e.g. 12Na:10Cl, 10Na:10Cl and 10Na:12Cl) in Pt-water system. They are expected to generate a charge of -1, 0 and +1 |e| on each electrode surface, respectively. This different status of charge will lead to the application of different potentials across the electrode, which will facilitate the study of the application of potential under PBC.

Due to the limited availability of computational power one can only model a system with a few hundreds or maybe thousand of atoms, which is very far away from the real system size. In order to avoid these finite-size effects most of the standard methods use periodic boundary conditions, which in turn make it difficult to apply a bias across the electrodes. One central open issue in electrochemistry is to model the effect of an applied potential to an electrochemical cell. Since the potential must be periodic, in order to simulate this effect standard simulation methods resort to a trick, which involves changing the charge on the electrode. The use of periodic boundary conditions also implies cell neutrality, which is enforced by adding counter charges to the system. Most of these methods reproduce a localised electric field and a potential energy drop within a micro-

scopic distance from the metal surface. However, none of them provides a realistic and self-consistent view of the structure and charge polarization within DL, able to capture the subtle interplay of electronic, ionic and thermal effects. This is due to the small size of the samples used and the lack of an extended dynamic description of its formation based on first principles. It has been experimentally proven [42] that the nature, structure and composition of the solvent at the interface with the electrode plays an essential role in determining its activity. Therefore a comprehensive modelling of the electro chemical (EC) environment overcoming traditional simplified models for the double layer, in combination with well-controlled experiment, is urgent and crucial to progress in the field. Here we present a realistic description from first principles of the Pt-water and Ag-water double layer structure and the charge distribution under an applied potential. In order to achieve this we have developed a general approach, which evolves previous methods towards a more comprehensive description of the metal/electrolyte interface. This is made possible as our model is extremely realistic and accounts explicitly and fully from first principles for charge polarization effects at both sides of the interface, the full dynamics of solvent rearrangment and electronic structures details. Besides unravelling for the first time the structure of the DL under an applied potential, our scheme also allowed us to directly evaluate the capacitance, the point of zero charge and the absolute electrode potential - by connecting the electrode Fermi level to the vacuum level and the standard hydrogen electrode. More in general, our approach also enables the estimation from first principles, the internal energy, the entropy and the free energies in a realistic environment. This information is also needed to develop and tune semi-empirical models able to simulate the steady state of large systems over time scales longer than those currently achievable with fully ab initio simulations.

Since the study of the above system is computationally intensive we have developed a smaller system, which can imitate the properties of the larger one. We will be discussing these systems in great details in chapters 4, 5 and 6.

Chapter 2

Theoretical tools and approximations

2.1 Methodological Approach

2.1.1 The Many-Body Problem

All the quantum mechanical properties of a system of N nuclei and n electrons can be, in principle, obtained by solving the many-body Schrödinger equations. The time independent non-relativistic Schrödinger equation is

$$\hat{H}\psi(\boldsymbol{r}, \boldsymbol{R}) = E\psi(\boldsymbol{r}, \boldsymbol{R}), \tag{2.1}$$

where $\hat{H}$ is the Hamiltonian operator and $\psi(\boldsymbol{r}, \boldsymbol{R})$ is the many-body wave function. The solution of this equation depends on $3(n + N)$ interacting degrees of freedom (excluding spin). More explicitly the Hamiltonian takes the form

$$\hat{H} = \hat{T}_e + \hat{V}_{ion-el} + \hat{V}_{el-el} + \hat{T}_{ion} + \hat{V}_{ion-ion}, \tag{2.2}$$

where,

$\hat{T}_e = -\frac{\hbar^2}{2m_e}\sum_i \nabla_i^2$ is the kinetic energy operator for the electrons,
$\hat{V}_{ion-el} = \sum_{i,I} \frac{Z_I e^2}{|\boldsymbol{r}_i - \boldsymbol{R}_I|}$ is the operator for the electron-nuclei interaction,
$\hat{V}_{el-el} = \frac{1}{2}\sum_{i \neq j} \frac{e^2}{|\boldsymbol{r}_i - \boldsymbol{r}_j|}$ is the operator for the electron-electron interaction,

$\hat{T}_{ion} = -\sum_I \frac{\hbar^2}{2M_I}\nabla_I^2$ is the operator for kinetic the energy of nuclei,

$\hat{V}_{ion-ion} = \frac{1}{2}\sum_{I\neq J} \frac{Z_I Z_J e^2}{|\boldsymbol{R}_I - \boldsymbol{R}_J|}$ is the operator for nucleus-nucleus interaction.

Here $\hbar$ is the reduced Planck's constant, m_e, e, $\boldsymbol{r}$ are the mass, charge and position of the electrons, while M, Z, $\boldsymbol{R}$ are the mass, charge and position of the nuclei.

Solving the Schrödinger equation for $3(n+N)$ interacting degrees of freedom is possible only for the simplest model systems (e.g. where $(n+N)$ is very small). However several approximations have been developed to address the many-body problem.

The first simplification consists in the Born-Oppenheimer (BO) approximation, which allows one to separate off the nuclear degrees of freedom from the electronic ones. The BO approximation is based on the consideration that the mass of the nuclei is typically three to five orders of magnitude larger than that of the electrons, thus they move much slower. As a consequence their dynamics can be separated from that of the electrons [43].

The wavefunction of a system described by two independent variables can be written as the general solution of the Schrödinger equation $\psi(\boldsymbol{r}, \boldsymbol{R}) = \psi(\boldsymbol{r})\chi(\boldsymbol{R})$. Due to the presence of the $\hat{V}_{ion-el}$ term it is not possible to express the wave function in this way. However, it can be written in a general way $\psi(\boldsymbol{r}, \boldsymbol{R}) = \psi(\boldsymbol{r}; \boldsymbol{R})\chi(\boldsymbol{R})$, meaning that the electronic component of the wave function, $\psi(\boldsymbol{r})$ depends on the nuclear coordinates.

Substituting $\psi(\boldsymbol{r}, \boldsymbol{R}) = \psi(\boldsymbol{r}; \boldsymbol{R})\chi(\boldsymbol{R})$ in equation (2.1) allows us to separate the electronic equation from that of the nuclei. The electronic wavefunction can be solved at a fixed positions $\boldsymbol{R}$ for $\boldsymbol{r}$. Solving for a range of $\boldsymbol{R}$ gives the potential energy surface on which the nuclei move. The equation for the electronic part can then be written as

$$\hat{H}_e \psi(\boldsymbol{r}, \boldsymbol{R}) = E_{ee}(\boldsymbol{R}), \tag{2.3}$$

where,

$$\hat{H}_e = \hat{T}_e + \hat{V}_{ion-el} + \hat{V}_{el-el}. \tag{2.4}$$

Solving this equation is still enormously complicated because it depends on $3n$ interacting degrees of freedom. However the problem can be further simplified by taking the Hartree-Fock approximation.

2.1.2 Hartree-Fock Approximation

Hartree proposed an approximation in 1927 in which he replaced the n electron wavefunction $\boldsymbol{\psi}(\boldsymbol{r}_i)$ by a product of single-electron wavefunctions $\psi_i(\boldsymbol{r}_i)$

$$\boldsymbol{\psi}(\boldsymbol{r}_1, \boldsymbol{r}_2, \boldsymbol{r}_3, \ldots, \boldsymbol{r}_n) = \psi_1(\boldsymbol{r}_1)\psi_2(\boldsymbol{r}_2)\psi_3(\boldsymbol{r}_3)\ldots\psi_n(\boldsymbol{r}_n). \tag{2.5}$$

The expression (2.5) is known as the Hartree product. In this the many electron problem is reduced to solving a one electron problem in the effective field generated by the other electrons. The Hartree product, however, fails to satisfy the antisymmetry principle, which states that a wavefunction describing fermions should be antisymmetric with respect to the interchange of any set of space-spin coordinates ($\boldsymbol{x}$). In order to take into account the spin, a new orbital is defined $\chi(\boldsymbol{x} = (\boldsymbol{r}, \alpha))$, related to $\psi(\boldsymbol{r})$ in the following way

$$\chi(\boldsymbol{x}) = \psi(\boldsymbol{r})\alpha, \tag{2.6}$$

where α is a spin function. Using $\chi(\boldsymbol{r})$, the Hartree product can be written as:

$$\boldsymbol{\psi}(\boldsymbol{x}_1, \boldsymbol{x}_2, \boldsymbol{x}_3, \ldots, \boldsymbol{x}_n) = \chi_1(\boldsymbol{x}_1)\chi_2(\boldsymbol{x}_2)\chi_3(\boldsymbol{x}_3)\ldots\chi_n(\boldsymbol{x}_n). \tag{2.7}$$

Considering the two electron problem, the wavefunction which satisfy the antisymmetry principle can be written as

$$\boldsymbol{\psi}_s = \frac{1}{\sqrt{2}}[\chi_1(\boldsymbol{x}_1)\chi_2(\boldsymbol{x}_2) - \chi_1(\boldsymbol{x}_2)\chi_2(\boldsymbol{x}_1)]. \tag{2.8}$$

Generalizing for n electrons gives the Slater determinant:

$$\boldsymbol{\psi}_s = \frac{1}{(n!)^{1/2}} \begin{vmatrix} \chi_1(\boldsymbol{x}_1) & \chi_2(\boldsymbol{x}_1) & \chi_3(\boldsymbol{x}_1) & \dots & \chi_n(\boldsymbol{x}_1) \\ \chi_1(\boldsymbol{x}_2) & \chi_2(\boldsymbol{x}_2) & \chi_3(\boldsymbol{x}_2) & \dots & \chi_n(\boldsymbol{x}_2) \\ \chi_1(\boldsymbol{x}_3) & \chi_2(\boldsymbol{x}_3) & \chi_3(\boldsymbol{x}_3) & \dots & \chi_n(\boldsymbol{x}_3) \\ \vdots & \vdots & \vdots & \ddots & \vdots \\ \chi_1(\boldsymbol{x}_n) & \chi_2(\boldsymbol{x}_n) & \chi_3(\boldsymbol{x}_n) & \dots & \chi_n(\boldsymbol{x}_n) \end{vmatrix}$$

Expressing the wave function as a Slater determinant is equivalent to the assumption that each electron moves independently of all the others except that it feels the Coulomb repulsion due to the average positions of all electrons and it also experiences the exchange interaction due to antisymmetrization of the wavefunction. Some concepts of this description also apply to Kohn-Sham density functional theory, which bears resemblance to Hartree-Fock theory.

2.1.3 Density Functional Theory (DFT)

DFT remaps the n-body problem into that of minimizing a functional depending on the electron density $n(\boldsymbol{r})$. The electron density $n(\boldsymbol{r})$ is defined as the integral of the square of many-body wave-function over all but one spatial coordinates of all electrons multiplied by the number of electrons.

$$n(\boldsymbol{r}) = N \int \dots \int |\psi(\boldsymbol{r}, \boldsymbol{r}_1, \boldsymbol{r}_2, \dots, \boldsymbol{r}_n)|^2 d\boldsymbol{r}_1, \dots, d\boldsymbol{r}_n. \tag{2.9}$$

This quantity depends only on 3 degrees of freedom. Contrary to the wave function, the electron density $n(\boldsymbol{r})$ is an observable and DFT establishes that this contains all information required to define the system. Thomas and Fermi have been the first to develop a functional theory dependent on the density. Minimizing such a functional with respect to the density returns the ground state density. This approach failed for the many-electron system as exchange and correlation effects were not taken into account and the kinetic energy of the electron was approximated by the kinetic energy of the

non-interacting electrons in a homogeneous electron gas [44].

Hohenberg-Kohn Theorems

Density functional theory is based upon two theorems given by Hohenberg and Kohn [45]-

1. For a system of interacting particle in an external potential $V_{ext}(\boldsymbol{r})$, the potential is determined uniquely, except for a constant, by the ground state electron density $n_o(\mathbf{r})$.

2. A universal energy functional $E[n]$ of the density $n(\boldsymbol{r})$ can be defined, valid for any external potential $V_{ext}(\boldsymbol{r})$.

$$\begin{aligned} E[n] &= T[n] + E_{int}[n] + \int d^3r V_{ext}(\boldsymbol{r}) n(\boldsymbol{r}) + E_{ion-ion}, \\ &\equiv F_{HK}[n] + \int d^3r V_{ext}(\boldsymbol{r}) n(\boldsymbol{r}) + E_{ion-ion}, \end{aligned} \tag{2.10}$$

where: $T[n]$ is the kinetic energy of electrons and $E_{int}[n]$ is the total energy due to the interaction among electrons. For any particular $V_{ext}(\boldsymbol{r})$, the exact ground state energy of the system is the global minimum of the functional, and the density $n(\boldsymbol{r})$ that minimizes the functional is the exact ground state density $n_o(\boldsymbol{r})$ The Functional F_{HK} defined in equation (2.10) includes all internal energy, kinetic and potential of the interacting electron system.

Kohn-Sham Scheme

In the Kohn-Sham approach the density-dependent problem is remapped onto an independent particle problem. This approach assumes that the total density of the original interacting system is equal to that of some non-interacting system subject to an effective potential. The many-body contributions to the potential are incorporated in the exchange-correlation functional of the density $E_{XC}[n]$. The error is thus confined to the approximation of the exchange-correlation functional [46].

The Kohn-Sham ansatz rests upon two assumptions:

1. The exact ground-state density can be represented by the ground-state density of

an auxiliary system of non-interacting particles, which satisfies the equation

$$H_{KS}\varphi_i(\boldsymbol{r}) = \varepsilon_i\varphi_i(\boldsymbol{r}), \tag{2.11}$$

where φ_i is the single particle Kohn-Sham orbital and ε_i are the Lagrange multipliers that ensure the conservation of the number of particles.

2. The auxiliary Hamiltonian is chosen to have the usual kinetic energy operator and an effective potential V_{eff} acting on the electrons,

$$\begin{aligned} H_{KS} &= -\tfrac{1}{2}\nabla^2 + \hat{V}_{ion-el}[n] + V_H[n] + V_{XC}[n], \\ &= -\frac{1}{2}\nabla^2 + V_{eff}[n], \end{aligned} \tag{2.12}$$

where:

$V_H[n] = \int d^3\boldsymbol{r}' \frac{n(\boldsymbol{r}')}{|\boldsymbol{r}-\boldsymbol{r}'|}$, and $V_{eff}[n] = \hat{V}_{ion-el}[n] + V_H[n] + V_{XC}[n]$.

By using the Kohn-Sham approach the full interacting many-body problem can be written in the form

$$E_{KS} = T_e[n] + \int d\boldsymbol{r} V_{ion-el}(\boldsymbol{r})n(\boldsymbol{r}) + E_H[n] + V_{ion-ion} + E_{XC}[n], \tag{2.13}$$

where:

$E_H[n] = \int d^3\boldsymbol{r}' d^3\boldsymbol{r} \frac{n(\boldsymbol{r})n(\boldsymbol{r}')}{|\boldsymbol{r}-\boldsymbol{r}'|}$,

$T_e[n]$ is the total kinetic energy of non interacting electrons and E_{XC} is the exchange correlation energy.

2.1.4 Exchange-Correlation Functionals

A good approximation of $E_{XC}[n]$ is important to obtain reliable results in DFT calculations. Unfortunately the exact exchange-correlation functional can be only found by solving the $3(n+N)$ many-body wave function. The first attempt to find the explicit expression for $E_{XC}[n]$ was for the homogeneous electron gas. The basic assumption was

that the exchange and correlation energy depend on the local value of density. This is called the local density approximation(LDA). The exchange-correlation functional can be written as:

$$E_{XC}^{LDA}[n(\boldsymbol{r})] = \int n(\boldsymbol{r})\epsilon_{XC}(n(\boldsymbol{r}))d\boldsymbol{r}, \tag{2.14}$$

where $\epsilon_{XC}(n(\boldsymbol{r}))$ is the exchange-correlation energy per particle of the homogeneous electron gas [47].

The LDA might look unrealistic but the results obtained with it are surprisingly good. However, LDA usually overestimates the binding energy (often of molecules and solids) and underestimates the bond lengths. The homogeneous electron gas is the only system for which the exchange-correlation functional is known and most of the functionals are based on this approach. One improvement over the LDA is the generalized gradient approximation (GGA), in which a dependence on the first derivative of the electron density is also included in the functional.

$$E_{XC}^{GGA}[n(\boldsymbol{r})] = \int f(n(\boldsymbol{r}), \nabla n(\boldsymbol{r}))d\boldsymbol{r}. \tag{2.15}$$

Including the gradient gives better binding energy compared to the LDA. Many GGA parameterizations exist, differing in the functional form of the exchange and correlation energy. One of the most important functional form of E_{XC}^{GGA} which has been used in this work was developed by Perdew, Burke and Ernzerhof in 1996 (PBE) [48]. Some of the advantages of the PBE over the LDA are :

1. Atomic and molecular total energy are improved.
2. It gives better cohesive energy of solids.
3. Improved description of the relative stability of bulk phases.
4. More realistic for magnetic solids.

The LDA also has some advantages in a few cases over the GGA:

1. The LDA yields good relative bond energies for highly coordinated atoms, e.g. surface energies, diffusion barriers on surfaces.
2. The GGA workfunctions for several metals turn out somewhat smaller than in the

LDA.

2.1.5 The Bloch Theorem

Until now our discussion was centered around dealing with the correlated nature of the electrons within a solid, but this is not the only problem. There are problems due to the large number of electrons in the solid. These can be overcome by considering that the whole electronic Hamiltonian and all the physical quantities describing a periodical system also share the translational invariance of the lattice. The Bloch theorem states that the single particle electronic wave function in a periodic crystal can be expressed in the form

$$\psi_k(\mathbf{r}) = \mathbf{e}^{\mathbf{ik.r}}\mathbf{u_k}(\mathbf{r}), \tag{2.16}$$

where ψ_k is eigen states and $u_k(r)$ is a periodic function with the same periodicity of the crystal e.g. $u_k(\mathbf{r} + \mathbf{T_n}) = \mathbf{u_k}(\mathbf{r})$, where $\mathbf{T_n}$ is the periodic operator.

From the Bloch Theorem one can relate the periodicity in the potential with the periodicity in the wave function, e.g. for an infinitely periodic potential one does not need to solve the wave function over all the space, instead one can relate it to the periodicity in the wave function as shown in equation 2.16.

2.2 Computational Approach

2.2.1 Basis Sets Expansion

In order to solve the KS equations we need to transform the original integro-differential problem into a more tractable algebraic one. This can be achieved by expanding the electronic wavefunctions on a basis set of known functions and using this representation to express the Hamiltonian operator. We used a plane wave basis set and localised orbitals. The most common basis sets are plane waves and localised basis sets, represented by atom like orbitals [49].

2.2.2 Supercells

In a perfect crystal, the atomic arrangement is in the form of a periodically repeated unit cell. Perfect periodicity is absent in many practical physical systems, but the system can be approximated to be periodic by choosing the necessary supercell. A supercell is a cell which consists of multiple units of the unit cell, it can be constructed in many different ways, such as the ones shown in figure 2-1. Few examples of systems where it is necessary to use supercells are point defects in crystals, surfaces and substitutional alloys. All these systems can be simulated by using the periodically repeated fictitious supercell. For example in the simulation of a point defect care should be taken that the defect does not interact with its image in order to simulate accurately the isolated defect. Surfaces are simulated by using crystal slab alternated with the slab of empty space taking care that the bulk behaviour is present in the centre of the slab and surface behaviour is unaffected by the presence of the periodic replica of the crystal slab. Finite systems too can be studied by using supercells. Enough empty space should be present between the periodic replica of the crystal slab so that the interaction between them is weak [7].

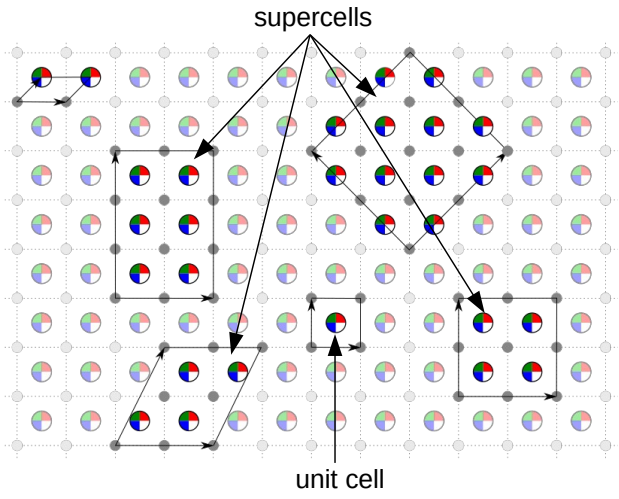

Figure 2-1: Figure showing a unit cell and different types of supercells in a 2D cubic crystal [7].

2.2.3 Pseudopotentials

Valence electrons play a vital role in defining the physical and chemical properties of materials, while the core electrons do not have any significant role in the chemical bond. This fact can be utilized for simplifying the description of the atom. The pseudopotential is an effective potential constructed to substitute the all electron potential such that chemically active valence electrons are described by pseudo-wavefunctions while the core electrons being considered together with the nuclei by a suitably modified potential. The other desired property of pseudopotential is that it should be transferable (applicable to many different systems) [50], and as smooth as possible [51].

2.2.4 Periodic Boundary Conditions (PBC)

PBC enables the macroscopic properties of real systems to be calculated from a finite number of particles. The primary cell is replicated in all directions as image cells, the replica of the cells are called image cells. If the position of an atom in a simulation cell is

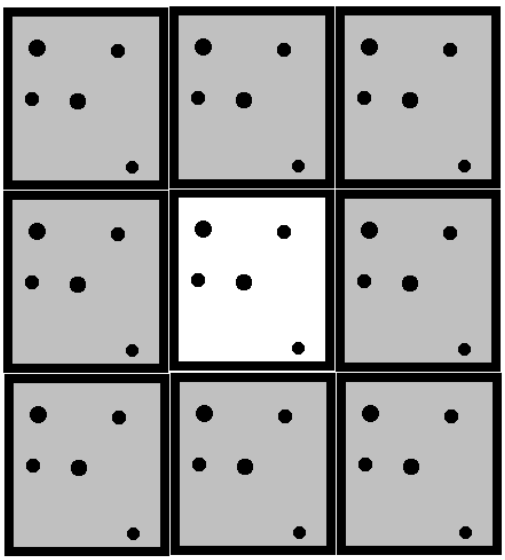

Figure 2-2: Replication of the all atoms of white box throughout the space to form an infinite lattice.

$\boldsymbol{r}_i$, then PBC also produces mirror images of the atoms of positions given by eq. 2.17

$$\bar{\boldsymbol{r}}_i^{image} = \bar{\boldsymbol{r}}_i + l\bar{\boldsymbol{a}} + m\bar{\boldsymbol{b}} + n\bar{\boldsymbol{c}}, \tag{2.17}$$

where $\boldsymbol{a}, \boldsymbol{b}, \boldsymbol{c}$ are vectors that correspond to the edges of the box l, m, n are any integers from -∞ to +∞. Each particle is interacting with the particle in the box as well as the particles in the adjacent boxes. The choice of the origin of the simulation box has no effect on the behavior of the system.

Using the supercell approach and PBC the following rules should be taken into account:

1. The cell size should be sufficiently large to avoid the fictitious interaction of the particles with their periodic images.

2. Any structural feature of the system of interest should be represented within the supercell.

2.2.5 Density of States (DOS)

One important concept in material science is that of the density of states (DOS). The density of states is defined as the number of energy states per unit volume per unit energy available to the system (the available states, which can be occupied by electrons). From the DOS one can understand the number of states available to be occupied by the electrons at a specific energy. For a system with a fixed volume, the DOS at a specific energy corresponds to the number of states available at that energy. The nature of adsorption of a molecule on a surface can be studied by investigating the changes of the DOS accompanied by the adsorption. The unit of the DOS is the number of states per volume of the supercell per eV. The DOS computed using DFT is most often reported in arbitrary units instead of its absolute value, since mostly the relative DOS values are of concern for many studies.

A molecular orbital is occupied by an electron if its energy lies below the Fermi level and is unoccupied if it is above the Fermi level. For many applications the most important molecular orbitals are the highest occupied molecular orbital (HOMO) and lowest

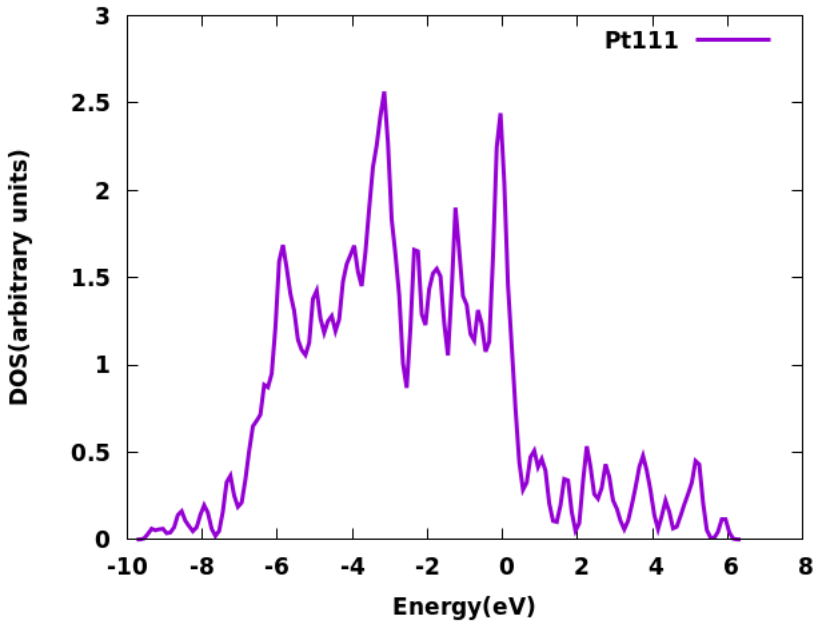

Figure 2-3: DOS of Pt(111) surface,the DOS does not have a HOMO-LUMO as it is a metal. Fermi level aligned with 0 eV.

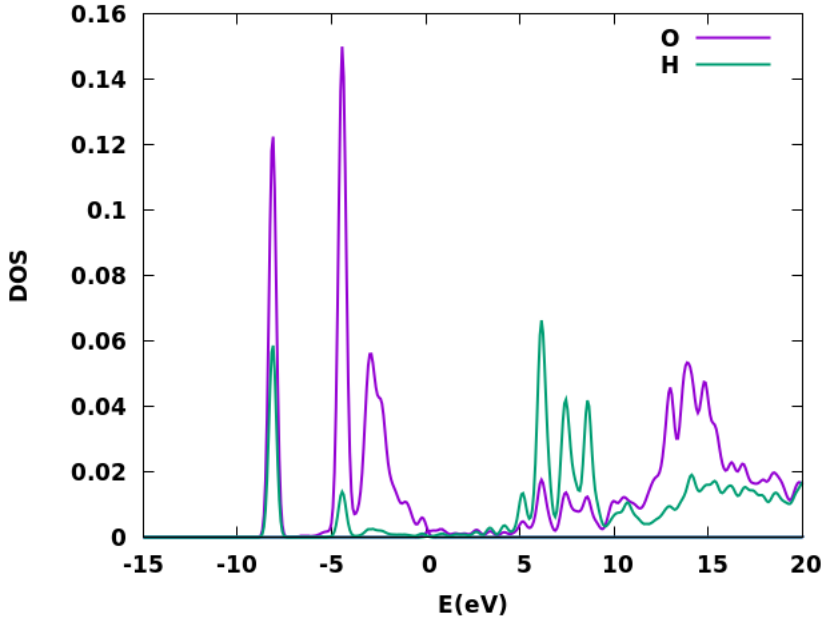

Figure 2-4: PDOS of O and H of liquid water, shows separately the contribution of electron density of O and H. Fermi level aligned with 0 eV.

unoccupied molecular orbital (LUMO). A valence band lies below the Fermi level and a conduction band lies above the Fermi level. The valence and conduction bands form two separate bands for semiconductors and insulators, and the energy gap between them is referred to as a band gap. A metal does not have a band gap and the Fermi level lies inside one band as shown in Fig. 2-3.

As DOS is useful in determining electron occupancy in specific energy level, it is often desirable to gain further insights such as which atom or orbital constitutes a particular energy level. A projected density of states (PDOS) helps one to determine the relative contributions of each orbital/atom to the total density of states at a given energy level. The DOS can be projected onto either an orbital or atom. Figure 2-4 shows the PDOS of O and H in liquid water.

2.2.6 *ab initio* Molecular Dynamics (AIMD)

The AIMD calculates the interatomic forces at a given time instant from the quantum-mechanical perspective within DFT. The system at any given time can be parametrized in terms of the coordinates of all the relevant nuclei and electrons. With the help of Born-Oppenheimer approximation, one can treat the nuclei fixed at the instantaneous positions of the atoms and the time-independent Schrödinger equation for the many-body wave function of the electrons is solved. This Schrödinger equation is then solved using DFT (time-independent) to obtain energy. The energy thus obtained is considered to be a function of the nuclear coordinates, and it can act as the interatomic potential that is needed to compute the forces in Newton's equation of motion for the nuclei. And by computing the gradients of the DFT energy at this fixed point with respect to the nuclear coordinates, the forces are obtained and the nuclei are moved accordingly to get to the next time step and with these new nuclear coordinates, the DFT process is repeated again.

In the case of standard MD, a potential field is used to calculate the instantaneous forces on each atom. Potential function (or, in other words, force field) is generally a function of the atomic coordinates. Most potential models involve a maximum of three-particles terms. Whereas in the case of AIMD, Schrödinger equation for the many-body

wave function of the electrons is solved, so it clearly gives an upper hand to MD in terms of speed but AIMD can also incorporate effects due to bonding, charge transfer, polarization and many-body effects intrinsically, while in standard MD they must be imposed, artificially. In both methods, however, the motions of the atoms are computed by applying Newton's second law to the atomic coordinates (by treating atoms classically). Quantum espresso and CP2K are the two plane wave DFT codes which I have used in my simulations.[1]

Initially, during the initialisation of the system (The initialisation of the system involved, finding the converged lattice parameter, work function, vacuum length on top of the platinum surface and interlayer distance between the layers of platinum surfaces), I have used Quantum espresso. Later for *ab-initio* molecular dynamics, CP2K is used (as ab-initio MD is not possible in Quantum espresso). I have double checked my earlier calculation in CP2K and found the same values as that of Quantum espresso (e.g. values of lattice parameter and work function of Platinum). Timestep and K point density plays a crucial role in DFT calculation, so, now we will discuss them next. Timestep and K point density plays a crucial role in DFT calculation, this will be discussed in detail in Appendix D. In the next section we will discuss QUICKSTEP [52], which is part of freely available computer code (CP2K), it performs accurate and efficient DFT calculations on large, complex systems. It has been used in our simulation to perform AIMD.

QUICKSTEP:

We present here the implementation of DFT method named QUICKSTEP, which is part of the freely available program package CP2K. New GPW (Gaussian Plane wave) method is implemented for fast and accurate calculation of DFT. GPW has been widely used for accurate DFT calculations in gas and condensed phases and can be effectively used for MD simulations. Although, the standard approach to DFT system was efficient and can handle hundreds of atoms. The DFT approach involved computation of the Hartree energy which in turn depends on the orthogonalisation of the wave functions which do not

[1] visit https://www.quantum-espresso.org/ for detailed information about Quantum espresso
visit https://www.cp2k.org/ for detailed information about CP2K

scale linearly with the system size, and hence these terms dominate the computational cost of larger systems. The hybrid GPW which has been used in QUICKSTEP provides an efficient way to treat these terms accurately at a significantly reduced cost. In this method, the electron density is described by an auxiliary plane wave while atom-centred Gaussian type basis set is used to describe wave functions. Representation of density as plane wave improves the efficiency of Fast Fourier Transformation (FFT) as Hartree energy starts scaling linearly with system size. After defining the wave function next part as per the DFT calculation is the choice of pseudopotentials. In QUICKSTEP an extended database (H-Rn) with GTH pseudopotential parameters based on the local density approximation is available for use. It has also been optimised for use with an exchange-correlation potentials of Becke and Perdew (BP) [53], Becke, Lee, Yang, and Parr (BLYP) [53], Tozer and Handy (HCTH/120, HCTH/407) [54] and Perdew, Burke and Ernzerhof (PBE) [55].

Next part is the calculation of electrostatic energy which consists of contribution from electrons and nuclei. This is solved by using the Ewald sum method which treats all terms of electrostatic energy simultaneously (i.e. long range part of all electrostatic interactions is treated in Fourier space, whereas the short range is treated in real space). In the area of exchange and correlation, they did not find any method fully satisfactory, as a balance between the different accuracy goals is difficult to achieve. At last the accuracy of the system was tested by performing a test run on molecules (i.e. H_2, Li_2, LiH etc) to calculate the bond distance and the results were compared with NUMOL (which L is a purely numerical DFT code and thus considered to be free of basis set effects). Results show a satisfactory agreement for all bond distances.

In summary, it can be said that the dual representation of charge density allows for an efficient treatment of Hartree energy terms in QUICKSTEP. Furthermore, the linear scaling of the Kohn-Sham matrix was obtained by the description of the wave function as a completely localised basis.

In the next sections, we will be discussing some computational approach which has been used in the construction of our model system and its analysis. These are- radial distribution function, work function, band alignment and ion imbalance model. Solvation

shell has been discussed in the appendix C.

2.2.7 Radial Distribution Function

In a system of particles, it can be simply defined as the variation of density as a function of distance from a reference point or particle. It is usually represented by G(r). It helps in understanding the probability distribution at a particular distance r away from a reference point. The general algorithm involves counting the number of particles within a distance of r and $r + dr$ away from the particle, as shown in the figure 2-5, here the blue particle is the reference particle, green particles are those whose centres are within the circular shell, shown in pink [8]. The radial distribution function then finally plotted by binning all such points together in a histogram.

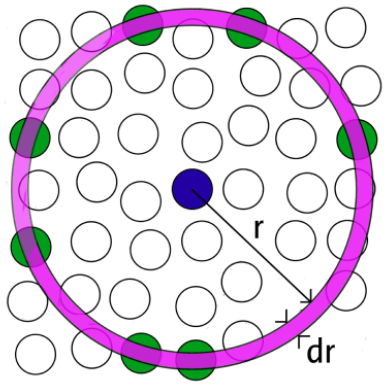

Figure 2-5: Figure shows the number of particles within a distance of r and $r + dr$ (shown in green colour) away from the reference point (shown in blue colour) [8].

2.2.8 Work Function

It is defined as the minimum amount of energy required to remove an electron from a metal surface to a point in the vacuum immediately outside the solid surface. This energy is the characteristic of the metal surface, which depends on the orientation of the crystal as well as the contamination. Experimentally thermionic emission and photoemission methods are majorly used to find the work function of materials. Theoretically, it can be found

by the energy difference between the electrostatic potential in the vacuum and the Fermi level of the material (see figure 2-6).

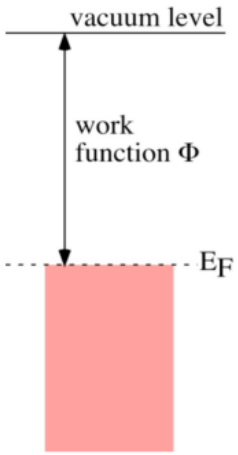

Figure 2-6: Figure shows the schematic energy level diagram for the calculation of work function in a metal. It is defined as the energy difference between the electrostatic potential in the vacuum and the Fermi level of the material (E_F) [9].

2.2.9 Band Alignment

Whenever a molecule comes in contact with a surface there is a change in the energy alignment of the molecule with respect to the surface. The Fermi level equilibration is fundamental to any electrical interface. Since in our model we will be seeing the effect of application of potential on the structure of double layer by introducing different numbers of sodium and chlorine atoms in electrolyte, being an electrical interface it is necessary to check the energy level alignment and is good to see how are they going to respond in contact with platinum surface. Already a lot of studies has been carried out to study the level alignment, a study by Ayelet Vilan and David Cahen shows different scenarios of energy alignment of the substrate and the molecule [10]. In this work they have compared different scenarios considering the substrates of high work function and low work function with the molecule, starting from vacuum level alignment to hybrid states and finally to ionization of substrate-molecule have been considered as shown in figure 2-7. In the next

section, we will be discussing the energy alignment in our model (the ion unbalance model), where we will be introducing an unbalanced population of Na and Cl ions in the electrolyte solution to give a different status of charge to the electrodes.

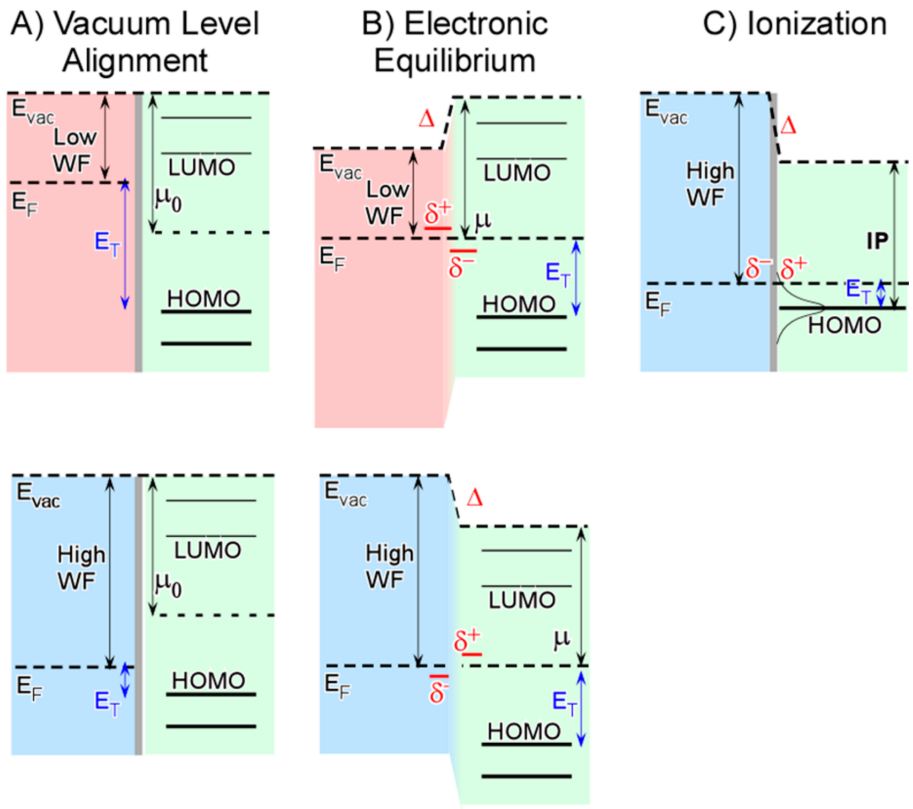

Figure 2-7: Figure shows different scenarios for substrate-molecule energy alignment. The solid substrate is depicted by red and blue colour for low and high work function respectively. The molecule is depicted by green colour and molecular levels are depicted by horizontal lines (two for HOMO and two for LUMO). Gray line at the intrerface represents lack of interface states, Δ and E_T are interface potential step and the tunneling barrier (defined as the distance between the metal Fermi level and the molecular HOMO level) respectively. (A) Vacuum level alignment in the state of non electrical equilibrium. (B) Hybrid states (bonding groups) localised at the substrate-molecule interface, the interface can be polarised in order to maintain a net equilibrium between the electron chemical potential of the molecule (μ) and the fermi level of the solid (E_F), this results in an extremely sharp induced potential energy step (Δ). (C) In cases where the substrate's Fermi level is outside the molecular gap, (In this example IP$<$WF) the charging of the moleule takes place. However, the low interface permittivity enforces a nonzero E_T [10].

2.2.10 The *ion unbalance* model

Different charging states of the electrode are obtained by introducing in the electrolyte solution different unbalanced populations of neutral atoms of different type (e.g. Na and Cl). This will lead to the formation of cations and anions in solution and a charged electrode.

In *ab initio* simulations, the density functional theory (DFT) approach determines self consistently the charge of each species by filling the Kohn-Sham electron states according to their relative energy with respect to the system's Fermi energy. This in turn is determined by the metal. If the metal electrode is large enough to act as a suitable charge reservoir, the charge of each ion will be determined by the transfer of electrons to/from the electrode, whose final charging state will be such to maintain overall charge neutrality. The introduction of different, moderate, imbalances in the number of cations and anions in the solution will thus result in the transfer of different amounts of charge between the electrolyte and the electrode. For instance, adding to the solution a proportion of atomic species leading to the formation of more cations than anions will result into a more negatively charged electrode and an excess of cations in solution. These in turn will contribute to the DL screening of the electrode.

The validity of the proposed methodology relies on the correct DFT description of the single electron energy levels' alignment, which may change for different approximations of the exchange and correlation functional. In particular the levels' alignment should reflect the ordering shown in Fig. 2-8. Notably, this is achieved already by the generalised gradient approximation at the level of the Perdew-Burke-Ernzerhof (PBE) potential [35] despite the fact that other properties, such as the water band gap and the band gap of quite a few semiconductor may be severely underestimated [56].

Importantly, the bulk electrolyte energy level (located in the middle of each electrolyte region) represents a common reference for the differently charged systems under consideration and can be used to align the respective electronic structures, without artificially introducing any vacuum slabs within the cell [57]. The electrostatic potential drop (with

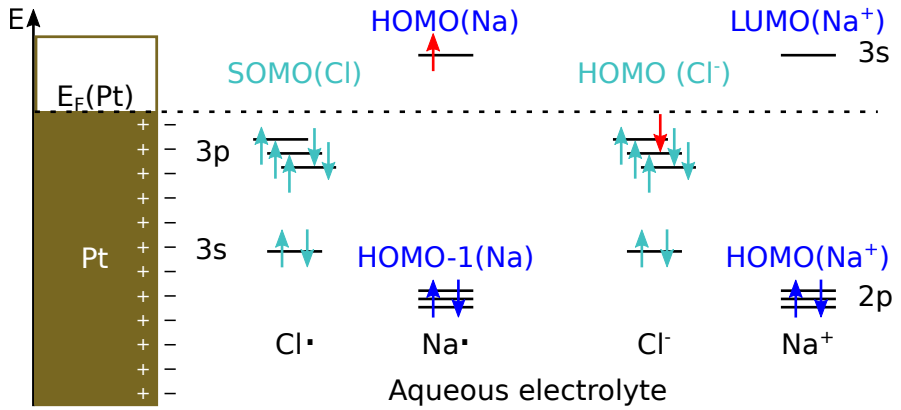

Figure 2-8: Single electron energy levels alignment and schematic picture of a Pt/electrolyte half-cell. E_F(Pt) separates filled and empty electronic states. Filled and empty water molecular states lay well below and above E_F, respectively. The highest occupied state for Na (here HOMO(Na), by analogy with the nomenclature for highest occupied molecular orbitals) is above E_F, and thus this species is expected to be fully ionised in solution. Correspondingly, the lowest unoccupied state for Cl, (namely, the degenerate Semi Occupied Molecular Orbital, SOMO(Cl)), is below E_F, therefore it becomes filled in the system under consideration. Notably, a frozen picture of the single electron energy levels in our system is adopted here.

respect to this bulk electrolyte level) for each electrode charging state (i.e. each ions' population) will be obtained *a posteriori*, from the corresponding equilibrium charge density distribution. Different potential drops can be associated to electrodes at different absolute potentials, measurable e.g. with respect to the SHE. Notably, system size and the simulation times are very relevant in our model, as to exploit our scheme we assume that the system is at equilibrium and that the centre of the aqueous electrolyte approaches bulk conditions.

Finally, our approach coupled to PBC, has also the advantage of producing a single type of interface (the *half-cell*) even in the case of the charged electrodes, since the screening between the two electrode surfaces in the cell will decouple them and the excess of ions will be equally partitioned between the two electrode surfaces. This allows us to disentangle at the same time the role of the anode and the cathode, and to improve the statistics by averaging over the two interfaces present in the simulation cell.

Chapter 3

Models and Convergency Tests

Before starting the simulation of metal/water interface one needs to determine the suitable parameters to be used. The theoretical obtained values may differ slightly from the experimentally observed values depending upon the type of potential file used (refer chapter 2 for more details) and the type of calculation which is going to be performed. One important part of this thesis is the study of the Platinum/water interface (as it is the most widely experimentally studied system), so first we will address the modelling of water and Pt explicitly. For the water it is important to find the proper box size, which will help in finding the appropriate distance for non-interacting water molecules. Therefore the convergency test will be done by varying the box size. Refer to appendix A for modelling of water. For the platinum the first task to perform was to find the appropriate K-point (the minimum number of points in K space at which the Brillouin zone is to be sampled), then using that K-point find the lattice parameter. Finally the converged lattice parameter used in subsequent models. Since the final aim of the thesis is to model the electrode-electrolyte interface, differently oriented platinum surfaces (001) and (111) are modeled. Most important to these are the variations in the interlayer distance with the K-points and the variation in work function as well. Finally selecting the appropriate K-point, the density of states(DOS) of symmetric layers was compared, to check whether the physically symmetric layer are electronically symmetric or not.

All the calculations are performed by using Quantum espresso code and the generalized

gradient approximation (GGA) to describe the exchange correlation effects within the exchange-correlation functional by Perdew, Burke and Ernzerhof (PBE) [55].

3.1 Bulk Platinum and Surface

Platinum crystallises in the FCC structure. Convergence tests on total energy versus energy cut-off and K-points grid sampling of the Brillouin zone was performed. We represent the surface by using a supercell approach as described in section 2.2.2. The surface in the unit cell interacts with its mirror images. In order to avoid this interaction, enough vacuum gap should be introduced to the top of the slab. The right amount of vacuum is found out by performing a convergency test by varying the vacuum length. The convergence of the work function and the interlayer distance versus the K-point grid sampling was studied for the (001) and (111) platinum surfaces. This will help in understanding the charge on the surface of the metal in an electrolytic cell.

3.1.1 Platinum Bulk

The first convergence test on bulk platinum is carried out by studying the total energy versus K-points (Fig: 3-1). Then we optimized the lattice parameter (Fig: 3-2) using the equation of states 3.1 [58] and calculated bulk modulus.

$$[H]E_{tot}(V) = \frac{B_O V}{B'_O}[\frac{(V_O/V)^{B'_O}}{B'_O - 1} + 1], \tag{3.1}$$

In equation 3.1, B_O and B'_O are the bulk modulus and its pressure derivative at the equilibrium volume V_O, while $E_{tot}(V)$ represents the variation of total energy with volume. The experimentally obtained [59] lattice parameter is 3.92Å and the bulk modulus is 278 GPa. By using a 8x8x8 K-points grid we have obtained lattice parameter of 3.99Å and bulk modulus of 283.85 GPa as shown in table 3.1. Theoretically [60] 3.99Å was obtained using 16X16X16 K-points grid and using PBE functional.

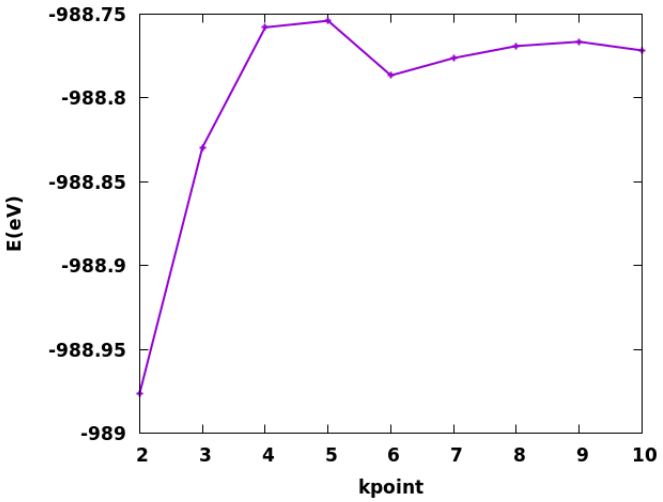

Figure 3-1: Figure showing energy vs K points grid for bulk platinum showing the variation of total energy with variation in K points.

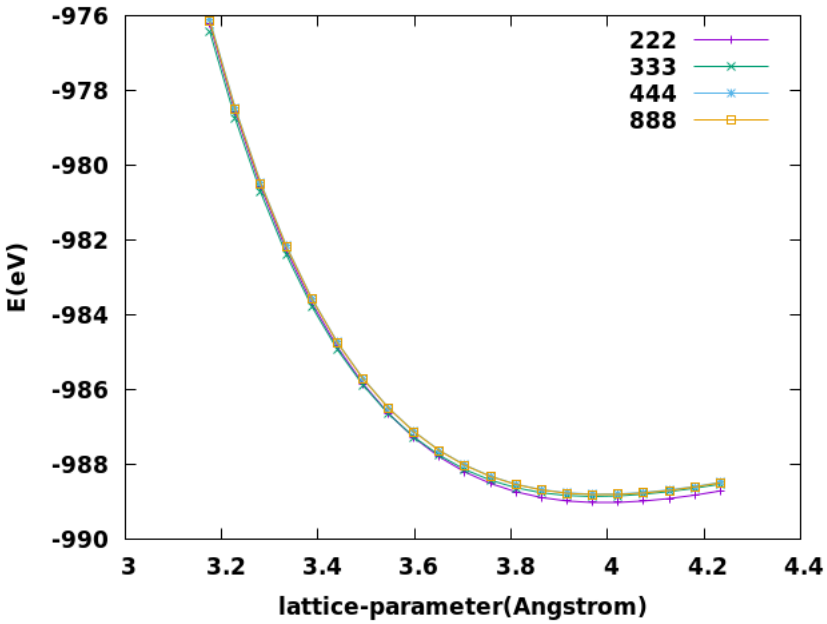

Figure 3-2: Figure showing energy vs lattice parameter at different K points grid for bulk platinum, used for optimizing the lattice parameter using the equation of states.

3.1.2 Platinum Surface

The study of the (001) and the (111) surface was carried out by varying the vacuum size in the supercell as shown in table 3.2 [1] and 3.3 respectively. In order to simulate a Pt

[1] ΔE is calculated by subtracting the energy of the consecutive vacuum gap.

surface we used a periodically separated supercell approach, where the periodic crystal slabs alternates with slabs of empty space. The crystal slab must be large enough that bulk behavior is reached in the middle. The vacuum slab must be large enough that a bulk behavior is unaffected by the presence of periodic replica. We selected a relevant quantity for our further calculations and studied the total energy of our system and its dependence on the vacuum and crystal slab size. When the total energy as a function of these two quantities does not change any more (within the accepted error) there is no more interaction between the replica. At this point using a larger vacuum gap would only be a computational burden. Similarly, we need to find the minimum number of layers in the crystal slab, able to reproduce in the middle the bulk properties e.g. density of states(DOS). A large number of layers would make the calculation too demanding. Notably using the supercell approach for a finite slab, we will have two surfaces and then its properties must be symmetrised with respect to the middle layer. From the size of the system one can get an idea about the computational resources and the time required to perform this calculation. After the convergence test we found that the 8x8x1 K point grid effectively describes both the Pt(001) and the Pt(111) surfaces, this K point grid will be used throughout this section. Supercells so obtained are shown in Fig: 3-3.

The numbering of the different layers is given with respect to vacuum surfaces shown in figure 3-4[2]. To understand the nature of interlayer spacing in the platinum surfaces, we studied the variation of interlayer spacing as a function of K points. In figures 3-5 and 3-6 it can be seen that as one moves from the surface to the center of the slab the

[2]This numbering will be used extensively in this chapter for referring different layers of platinum surface.

Table 3.1: Table showing the platinum lattice parameter and bulk modulus obtained by varying the K points grid.

K-points grid	Lattice parameter(Å)	Bulk modulus (GPa)
1	4.32	117.32
2	3.99	288.05
3	3.98	285.23
4	3.99	284.23
8	3.99	283.85

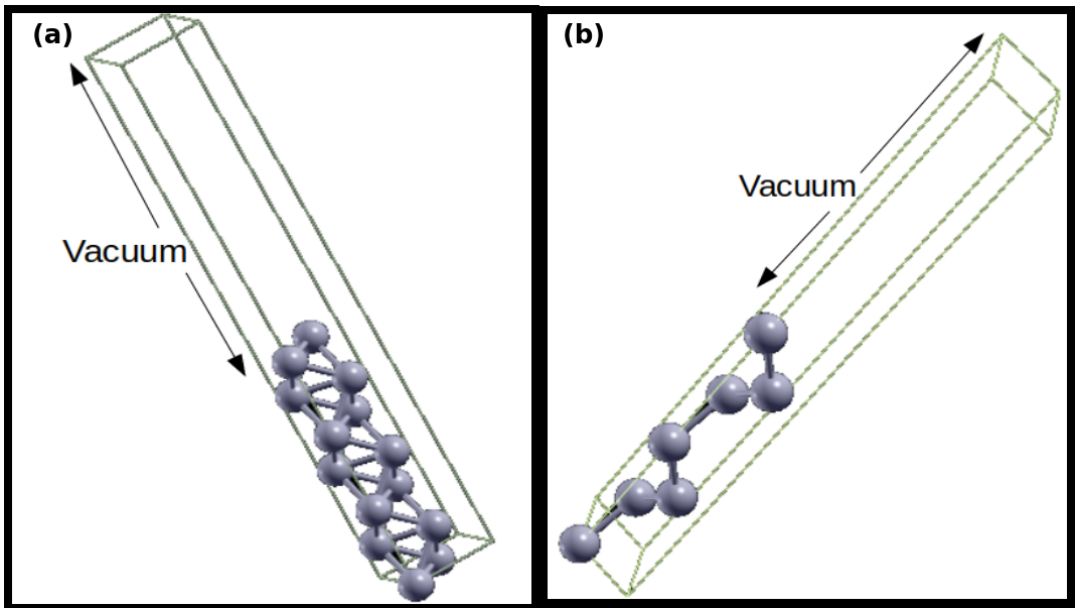

Figure 3-3: Figure shows the supercell of platinum used for modelling the 7 layers slab (a) (001) surface and (b) (111) surface.

Table 3.2: Total energy E and ΔE with variation in vacuum gap in 7 layers Pt(001). The '$*$' marks the vacuum gap sufficient for modelling the surface.

Gap(Angstrom)	E(eV)	ΔE(eV)
3.99	-13839.8676602	-
7.98	-13839.5452061	0.3224541
$*$11.97	-13839.5448132	0.0003929
15.96	-13839.5448315	-0.0000183
19.95	-13839.5448107	0.0000208
23.94	-13839.5447979	0.0000128

inter-spacing is more close to that of the bulk as expected.

From figures 3-5 and 3-6 one can see that Pt(001) and Pt(111) have different response to inter-spacing with increasing K points. The trend is similar to the result obtained by J.L.F. Da Silva et al [61]. It can also be noticed that the 8X8X1 K points are sufficient enough to model the Pt (001) and (111) surfaces.

In order to verify that the middle layer of the two differently oriented surfaces has the property similar to bulk Pt the projected density of states (PDOS) of the middle layer with two surface orientations was compared with that of bulk Pt (see Fig: 3-7). From the figure it can be seen that the PDOS are all very similar so we conclude that they are able

Table 3.3: Total energy E and ΔE with variation in vacuum gap in 7 layers Pt(111). The '$*$' marks the vacuum gap sufficient for modelling the surface.

Gap(Angstrom)	E(eV)	ΔE(eV)
3.10	-6921.0718292	-
5.93	-6920.3804373	0.6913918
8.75	-6920.3761047	0.0043326
$*$11.57	-6920.3760758	0.0000289
14.39	-6920.3760655	0.0000103
17.22	-6920.3760574	0.0000081
20.04	-6920.3760431	0.0000143

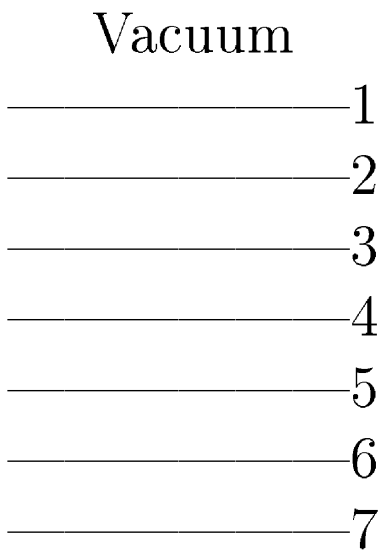

Figure 3-4: The numbering of different layers of platinum with respect to vacuum, starting with layer 1 from top to 7 at the bottom.

to mimic the property of the bulk to a large extent.

Analysing figures 3-9 and 3-8 it can be seen that the PDOS of symmetric layers(e.g 1 and 7, 2 and 6, 3 and 5) are identical to each other. Based on this we conclude that 7 layers are adequate to model the Pt(111) and Pt(001) surfaces. We then studied the structure of our surfaces and their dependence on simulation parameters. The ($*$) asterisk marked values (see table 3.3 and 3.2) are used for the further calculations.

From table 3.4 it can be seen that in the Pt(001) interlayer-distance between the layers

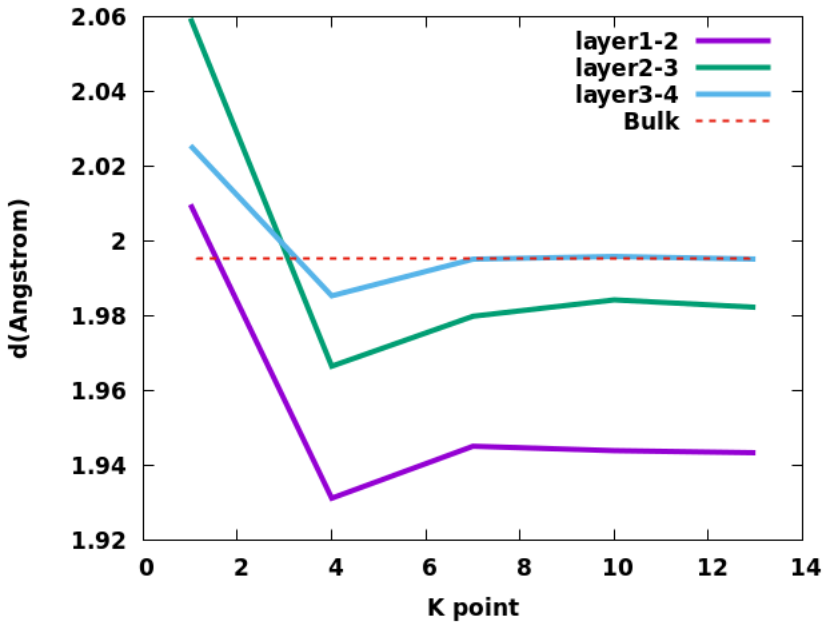

Figure 3-5: Figure shows the interlayer distance as a function of the K-points grid (XxXx1) in Pt (001), it can be seen that as one moves from surface to centre the interlayer spacing comes closer to that of bulk. The convergence of the curves with increase in K points can also be seen.

is smaller than that of bulk Pt. By contrast in Pt(111) (table 3.5) the distance between the external layer and the subsurface layer is slightly larger than the ideal bulk value.

Trasatti [62] has shown in his remarkable work that the electron work functions, electronegativity, and potentials of zero charge of metals are linearly interrelated. So we also studied the convergence of the work function. In figure 3-10 the work functions of the slabs Pt(111) and Pt(001) have been plotted as a function of the K-points grid. The work function of Pt(111) slab converges to 5.70 eV compared to Pt(001) slab, which is 5.69 eV. Experimentally the work function of Pt(001) [63] and Pt(111) [63] are found to be 5.82 ± 0.15eV and 6.08 ± 0.15eV respectively. By using DFT PBE potential the value of the work-function of Pt(111) [61] was found to be 5.69eV, while using the Quantum espresso code and using K-points grid of 16X16X1 and PBE potential the value of the work function was found to be 5.66eV and 5.69eV for Pt(001) and Pt(111) respectively [60], which is very close to our obtained result.

Since a Pt slab comprising seven layers in combination with water is very expensive

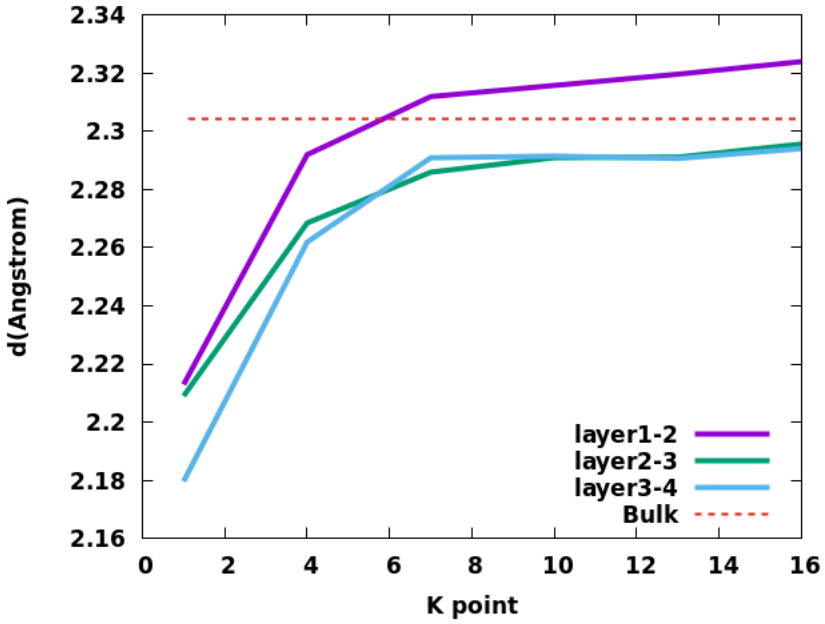

Figure 3-6: Interlayer distance as a function of K-points grid in Pt (111), it can be seen that as one moves from surface to centre the interlayer spacing comes closer to that of bulk. The convergence of the curves with increase in K points can also be seen.

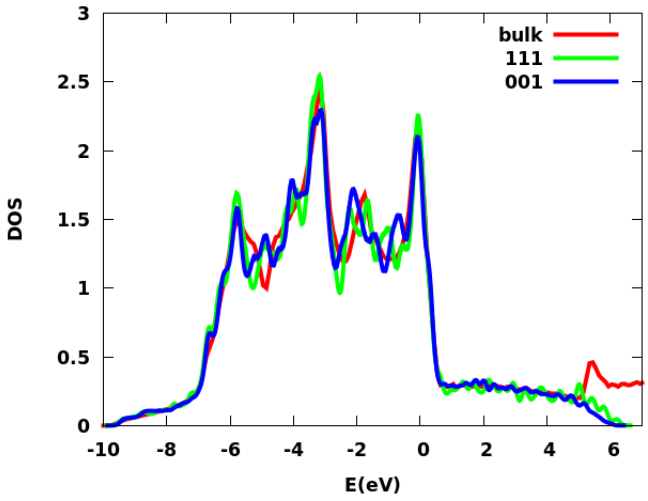

Figure 3-7: PDOS of middle layer of 7 layers platinum surfaces (001) and (111) compared with bulk (surfaces calculated using 8X8X1 K points while bulk using 8X8X8 K points). It can be seen that the PDOS of (001) and (111) are all very similar to the bulk, so we conclude that they are able to mimic the property of the bulk to a large extent.

computationally, alternatively four-layers slabs were tested. The first test was conducted by varying the vacuum length in the supercell, as shown in the table 3.6 and 3.7. From

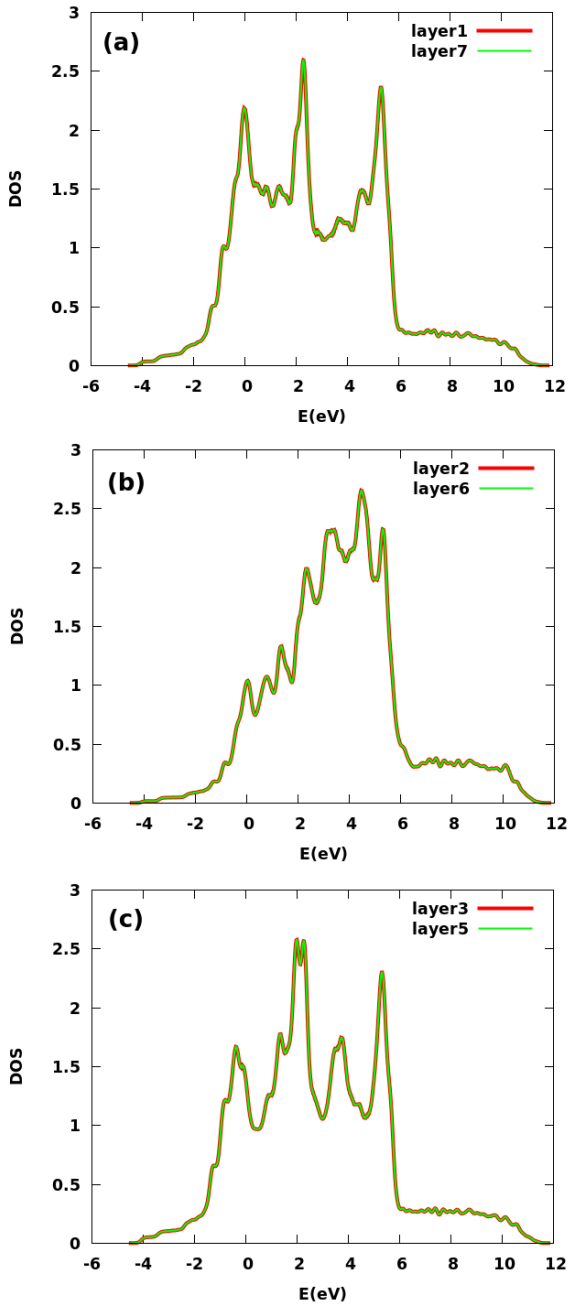

Figure 3-8: PDOS of symmetric layers(e.g 1 and 7, 2 and 6, 3 and 5 shown in figure (a), (b) and (c)) of the 7 layers Pt (001) slab compared with each other, the symmetric layers superimpose each other, confirming the same density of states (calculated with 8X8X1 K points grid).

this we conclude that any length greater than 12.5 Angstrom vacuum seems to be good enough for the simulation of the Pt(001) and Pt(111) surface.

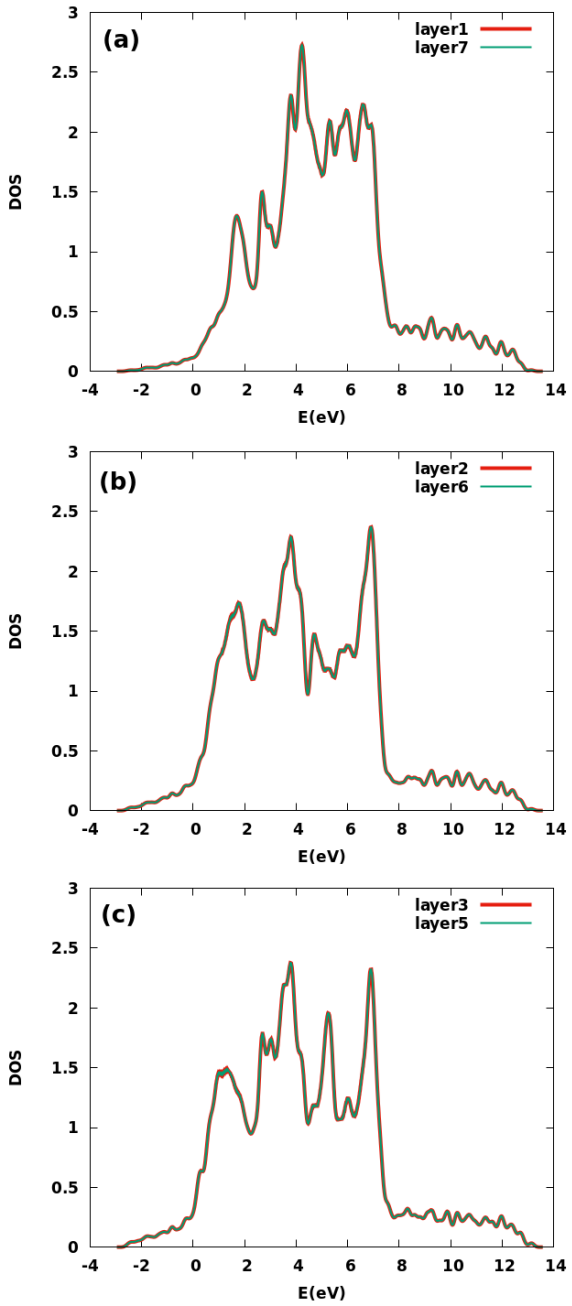

Figure 3-9: PDOS of symmetric layer(e.g 1 and 7, 2 and 6, 3 and 5 shown in figure (a), (b) and (c)) of the 7 layers Pt (111) slab compared with each other, the symmetric layers superimpose each other, confirming the same density of states (calculated with 8X8X1 K points grid).

The density of states (DOS) of the 4-layer platinum was compared with that of the bulk to see if it can be used to represent the bulk layer. From the Fig: 3-11 it can be

Table 3.4: Interlayer distance in Platinum(001) using a 8x8x1 k point grid [(bulk =1.995 Å)], it can be seen that symmetric layers have same interlayer distance.

Layer	Interlayer distance(Å)
Layer1-2	1.952
Layer2-3	2.005
Layer3-4	2.002
Layer4-5	2.002
Layer5-6	2.005
Layer6-7	1.952

Table 3.5: Interlayer distance in Platinum(111) using a 8x8x1 k point grid [(bulk =2.304 Å)], it can be seen that symmetric layers have same interlayer distance.

Layer	Interlayer distance(Å)
Layer1-2	2.326
Layer2-3	2.294
Layer3-4	2.299
Layer4-5	2.299
Layer5-6	2.294
Layer6-7	2.326

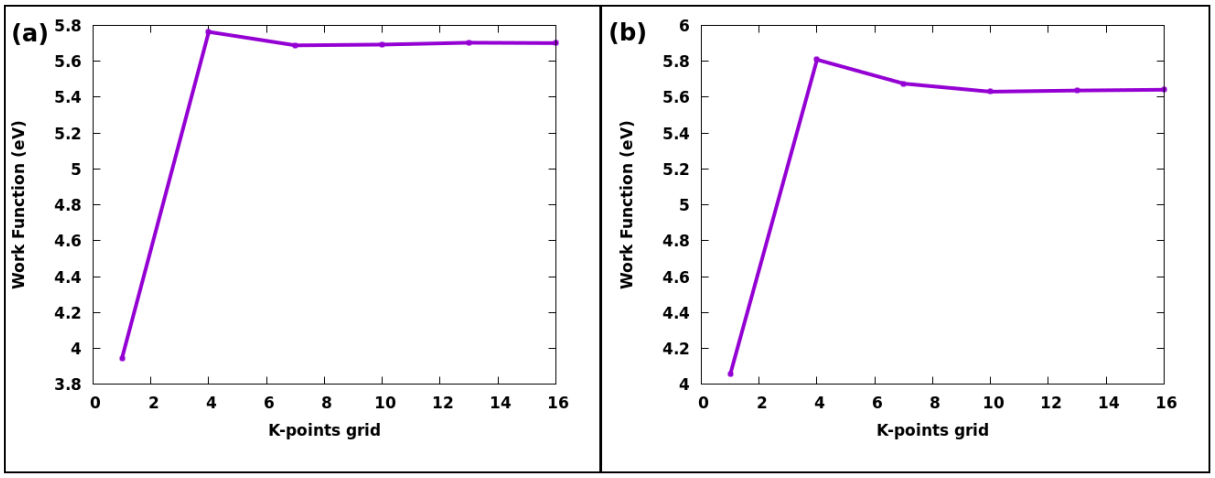

Figure 3-10: Work function vs K-points density Figure shows the work function as a function of the K-points grid (XxXx1) in 7 layers Pt (a) (111) slab and (b) (001) slab. The convergence of the curves with increase in K points grid can be observed.

concluded that 4 layers sufficient to model platinum surface.

After comparing the DOS, the interlayer distance was compared as shown in Fig: 3-12 and 3-13. These quantities have the same trend as that shown for the 7 layer system,

Table 3.6: Total energy E and Δ E as a function of the vacuum gap in a 4 layers Pt(111) slab.

Gap(Angstrom)	E(eV)	Δ E(eV)
5	-3953.977924	-
7.5	-3953.974427	-0.003498
10	-3953.974124	-0.000302
12.5	-3953.974099	-0.000025
15	-3953.974080	-0.000019
17.5	-3953.974080	0.000000
20	-3953.974090	0.000010
22.5	-3953.974079	-0.000011
25	-3953.974074	-0.000005

Table 3.7: Total energy E and Δ E as a function of the vacuum gap in a 4 layers Pt(001) slab.

Gap(Angstrom)	E(eV)	Δ E(eV)
5	-7906.879165	-
7.5	-7906.845855	-0.033310
10	-7906.844177	-0.001678
12.5	-7906.844104	-0.000073
15	-7906.844098	-0.000006
17.5	-7906.844084	-0.000014
20	-7906.844081	-0.000003
22.5	-7906.844088	0.000007
25	-7906.844070	-0.000018

except layer 2-3. The problem can be fixed by fixing the middle layers equivalent to the bulk interlayer distance in the simulation and letting the surface layers relax by itself. For 4 layers Pt(001) slab the interlayer distance between layers 1 and 2 is 1.935 Å, between 2 and 3 is 1.967 Å while that of bulk is 1.995 Å (slab is calculated using 8X8X1 K points while the bulk calculated using 8X8X8 K points grid). For 4 layers Pt(111) slab the interlayer distance between layers 1 and 2 is 2.306 Å, between 2 and 3 is 2.274 Å while that of bulk is 2.304 Å (slab is calculated using 8X8X1 K points while that of bulk calculated using 8X8X8 K points grid).

After comparing the interlayer distances the PDOS of symmetric layers plotted together as shown in the Fig: 3-14 and 3-15. It can be seen that the PDOS are completely

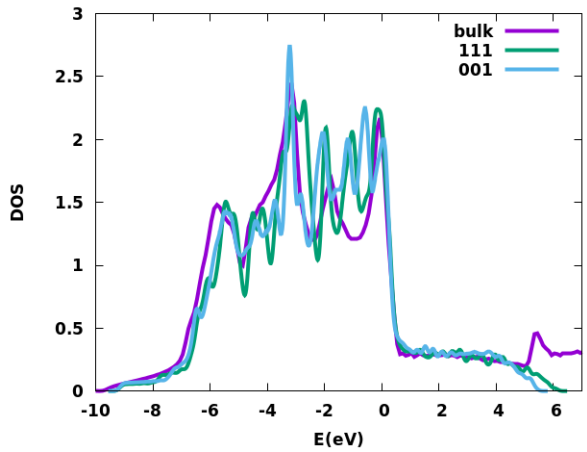

Figure 3-11: PDOS of middle layer of 4 layers platinum surfaces (001) and (111) compared with bulk Pt (surfaces calculated using 8X8X1 K points while bulk using 8X8X8 K points grid).

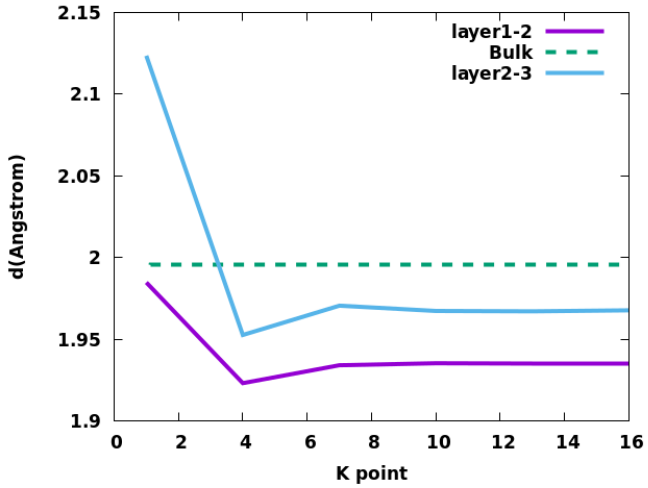

Figure 3-12: Interlayer distance as a function of K-points grid in Pt(001) 4 layers slab (calculated using 8X8X1 K points grid). Both the curves are showing a convergence behaviour with increasing K points grid.

overlapping, which confirms the symmetry.

Finally the work function is plotted as a function of K points grid, shown in the Fig: 3-16. It also has similar trend as that of the 7 layers Pt slab. For the 4 layers Pt(001) the work function is 5.63eV, while that of 7 layers Pt(001) is 5.69 eV. For 4 layers Pt(111) the work function is 5.69 eV while that of 7 layers Pt(111) it is 5.70 eV. In Pt(001) as well as in Pt(111) a reduction in the number of layers in the slab has produced a slight

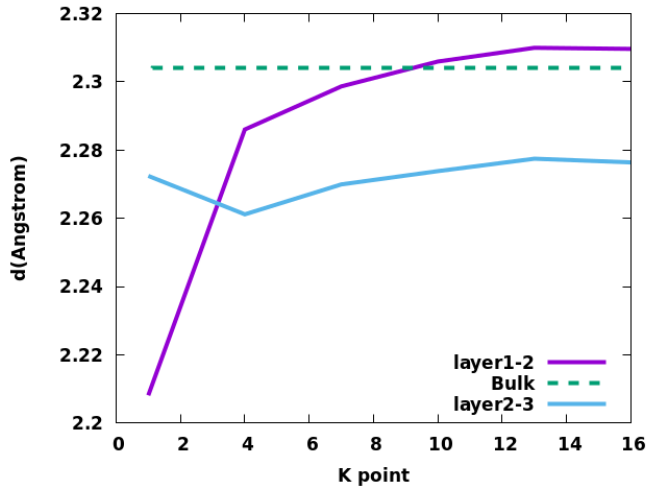

Figure 3-13: Interlayer distance as a function of K-points grid in Pt(111) 4 layers slab (calculated using 8X8X1 K points grid). layer 1-2 is showing a consistent convergence behavior while layer 2-3 has yet not converged.

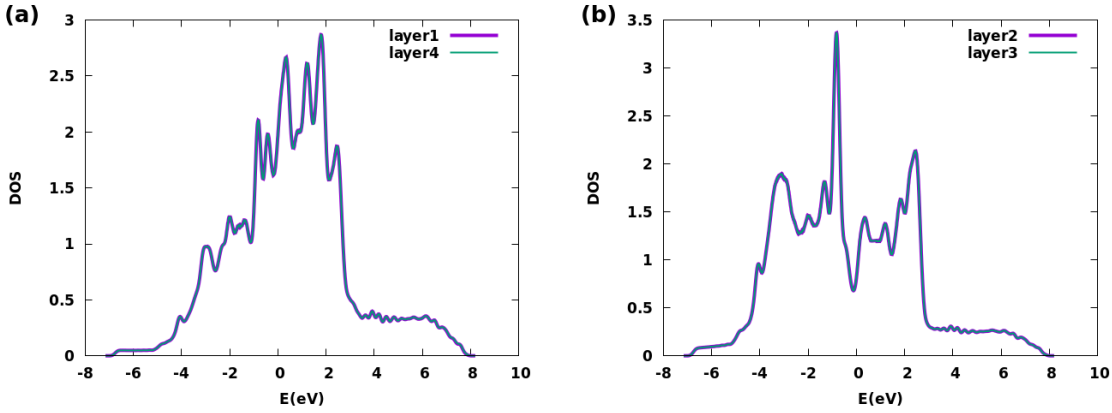

Figure 3-14: PDOS of symmetric layers(e.g 1 and 4, 2 and 3) of Pt(001) 4 layers slab compared with each other (a) PDOS of top and bottom layer (b) PDOS of both middle layer (both calculated using 8X8X1 K points grid). All the symmetric layers are superimposing on each other, confirming the symmetry.

decrease in the value of the work function. From all the tests it can be concluded that 4 layer platinum slab is sufficient for studying the interface. It should be used with 8X8X1 K points grid or higer.

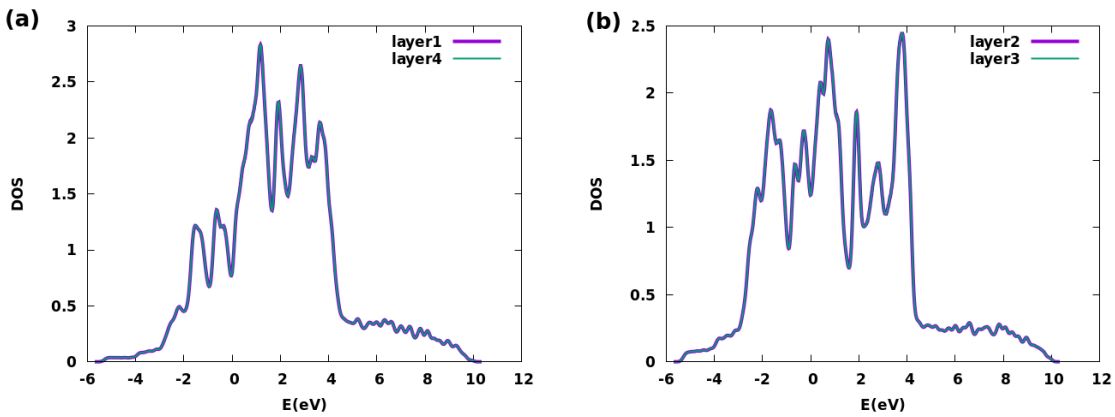

Figure 3-15: PDOS of symmetric layer(e.g 1 and 4, 2 and 3) of 4 layers Pt(111) compared with each other (a) PDOS of top and bottom layer (b) PDOS of both middle layer (both calculated using 8X8X1 K points grid). All the symmetric layers are superimposing on each other, confirming the symmetry.

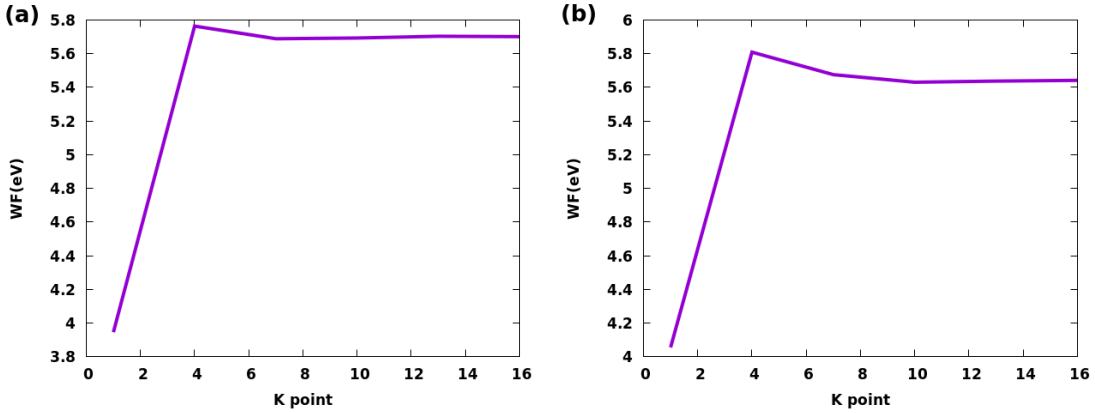

Figure 3-16: Work function vs K-points density of a 4 layers Pt slab (a) for 4 layers Pt(111) slab (b) for 4 layers Pt(001) slab (both calculated using 8X8X1 K points grid). Both the curves are showing a convergence behaviour with increasing K points grid.

3.2 Starting Pt-Water Simulation

Before starting the simulation with unbalanced population of ions in solution we carried out a 20 ps Born-Oppenheimer molecular dynamics simulation of a benchmark system, where no ions are dissolved in solution. In our system we have a Pt slab in contact with water (see figure 3-17), we named it 0Na:0Cl as there are no ions in the solution. MD based on DFT is performed for all systems using the Quickstep module of the CP2K package [52]. The electronic structure is obtained at the PBE level.Tether, Goedecker and Hutter (GTH) pseudopotentials [64, 65], valence triple-zeta TZV basis set for Pt, TZVP (TZV polarisation) basis sets for the other atoms and a cutoff energy of 300 Ry for the plane waves are used. We will be discussing the methodology in detail in next chapter in which we are introducing unbalanced population of ions in solution to charge the electrodes differently.

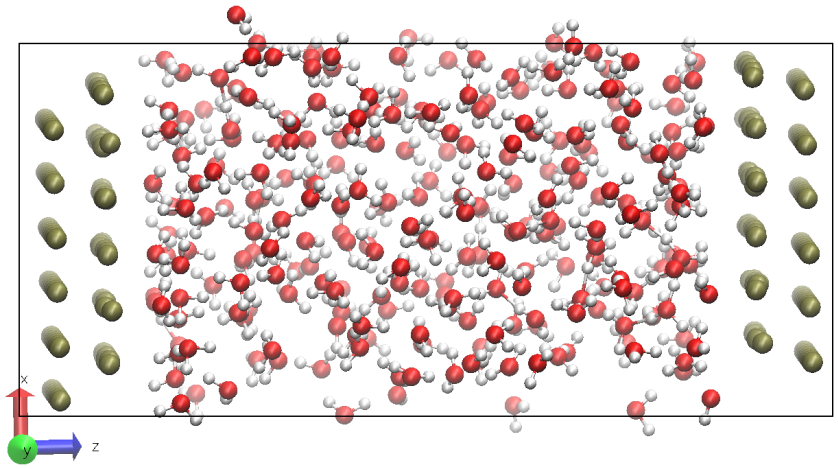

Figure 3-17: Figure shows Pt/water solution model system. Here we present a snapshot of the trajectory of the 0Na:0Cl system. Red, white and olive-green colour represent oxygen, hydrogen and platinum respectively.

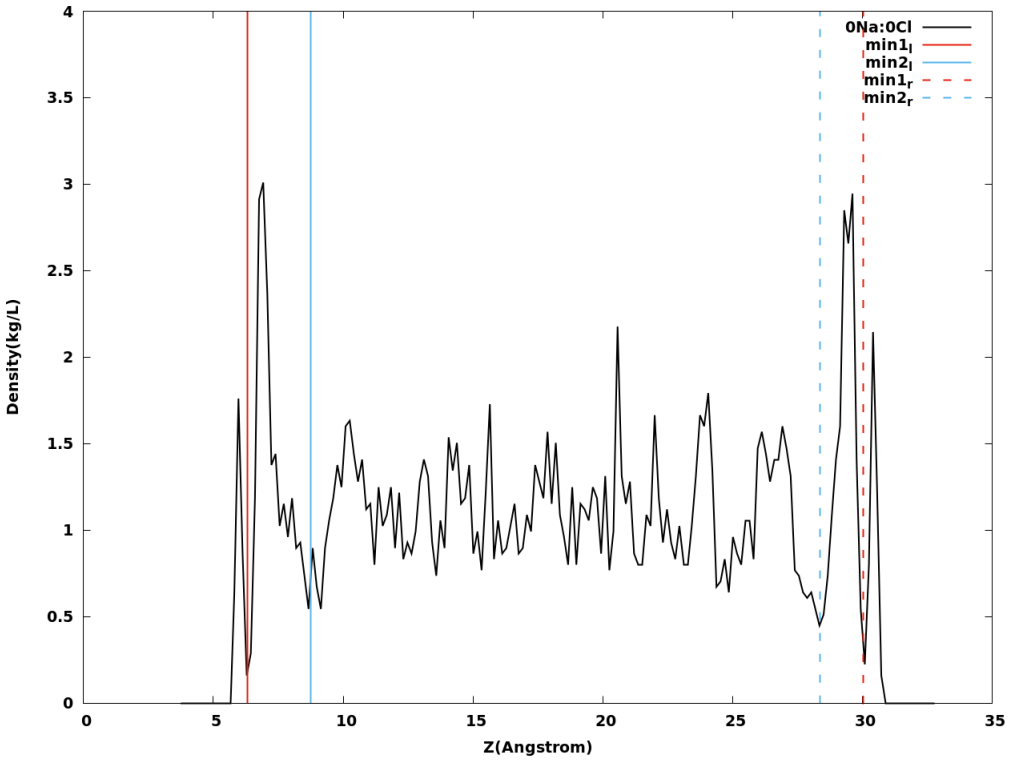

Figure 3-18: 0Na:0Cl system: graph of water density variation throughout the electrolyte, it shows different region of water layers near the electrode i.g. first (min1) and second (min2) minimum of the water density profile. The subscript 'l' and 'r' represent the left and right position of the respective minima.

Over here we will be discussing the structural analysis of this system. After running the simulation we plotted the density variation of the water molecules to see the behaviour of water in contact with platinum (see figure 3-18). The density of water is calculated as time average density (which is the average of density calculated at intervals of 0.5 ps). This density was plotted as a function of distance from the electrode surface, formation of two water layers near the electrode can be seen in the figure. The two layers were defined by the respective minima one encounters moving away from the electrode in the density distribution curve. The first and second minima are represented by 'min1' and 'min2' respectively. In the middle of the slab, the density fluctuates around 1, which brings it closer to the actual value. Then we analysed the distribution of water in the first and second layers and found an average of 3.42 and 20 water molecules in the first and second layers respectively. Next to understand the orientation of water molecules in these layers

time average atomic density profiles for the O and H atoms belonging to the aqueous electrolyte in contact with the electrode (in units of atoms per Å) was plotted (see figure 3-19). In figure 3-19(a) one can observe the overlap of 'O' and 'H' curve implying 'H' molecules are in the same plan as that of O atoms. It can be concluded that the water molecule are oriented parallel to the electrode surface. In figure 3-19(b) we can observe pick of 'H' before that of 'O' implying water molecules are oriented perpendicular to the surface. This finishes structural analysis of Pt in contact with water, we will be discussing the charges of these layers in great detail in the next chapter.

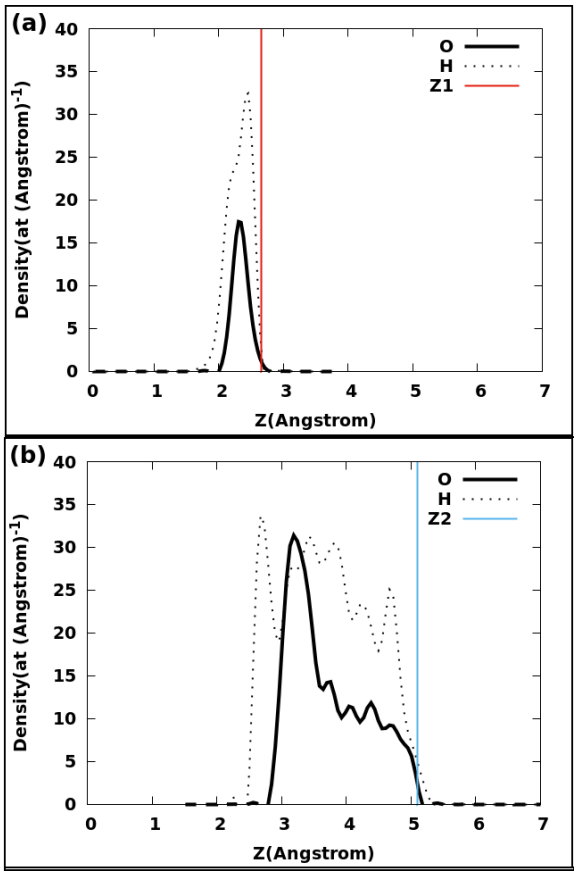

Figure 3-19: Figure shows average atomic density profiles for the O and H atoms belonging to the aqueous electrolyte in contact with the electrode (in units of atoms per Å) for 0Na:0Cl system. Here (a) represents the water molecules belonging to the first water layer, in contact with the electrode. In (b) the water molecules of the second water layer. The plain and dashed lines stand for the O and H atoms' contributions, respectively. Z1 and Z2 mark the end of the first and second layer.

Chapter 4

Platinum/water interface under bias

This work was done in collaboration with Rémi Khatib and Marialore Sulpizi (both from the Department of Physics, Johannes Gutenberg University). Earlier in chapter 1 we discussed the modelling of metal/water interface under bias. Starting with models developed by Filhol and Neurock [5], further advancement by Rossmeisl [6] and ending with modern simulation methods which explicitly addresses the description of the electrode potential, typically resort to supercell geometries and periodic boundary conditions (PBC) in three dimensions to speed up the calculations and minimise the effect of finite sample sizes. Since in this case it is difficult to apply an electric field across the cell, the effect of the application of an electrostatic potential is modelled by imposing charges on the electrodes. In these schemes cell neutrality is achieved by adding a distribution of fixed counter-charges to the cell, which can have the form of a homogeneous background filling the simulation cell [5], of charged planes [66] or hydronium ions placed at a fixed distance from the electrode surface [67]. Most of these approaches reproduce the localised electric field and the potential energy drop within a microscopic distance from the metal surface [5]. However, none of them provides a comprehensive view of interface structure, solvent composition and charge polarisation within the DL under applied potential. This is due to the small size of the samples used and the lack of an extended dynamic description of its formation based on first principles, able to capture the subtle interplay of electronic, ionic and thermal effects. A realistic modelling of the electrochemical environment overcoming these

simplified models for the DL, in combination with well controlled experiment, is crucial to understand and control electrodes' activity [42, 68].

An alternative computational SHE method, devised to investigate coupled proton-electron transfer reactions was developed by Sprik and co-workers [39, 40, 41, 35]. This approach allows one to refer the computed potential to the SHE by using the solvation free energy of the proton. The method is sophisticated and powerful, but its downside is the high computational cost, which jeopardise the straightforward study of realistic metal/electrolyte interfaces. Furthermore, it does not provide the description of the over-potential associated to the transfer of species to, from or across the interface under bias and does not include explicit description of ions in solution or address the problem of controlling the charge on electrode.

For these reasons here we abandon part of the theoretical sophistications of the previous methods and adopt a simpler and intuitive description of the metal/electrolyte interface. In practice, we use molecular dynamics (MD) simulations to reproduce the reality of an electrified interface under an applied potential and to carry out a virtual experiment.

We develop an extremely realistic first principles model, which accounts explicitly for charge polarisation effects at both sides of the interface, the full dynamics of solvent rearrangement and the electronic structures details. By simulating and comparing systems with different electrodes charging states, we unravel for the first time how the application of a potential affects the DL structure and the charge distribution in this system. We directly evaluate the capacitance, the zero point charge and the absolute electrode potential for each interface.

More in general, our approach provides the realistic framework that enables the estimation, from first principles, of the internal energy, the entropy and the free energy along the reaction paths simulated in a realistic charged environment. This information is, for instance, needed to develop and tune semi-empirical models, to simulate the steady state of large systems over time scales longer than those currently achievable with fully *ab initio* simulations.

4.1 The model system

In our model (see Fig. 4-1) a Pt slab in contact with a NaCl aqueous solution is realistically represented by about 1500 atoms and 5250 electrons. We simulate the *ab initio* dynamics of three systems of nearly equivalent solvent's composition (≈2 M[1]), differing for the slightly different relative number of Na and Cl ions included in the solution. We name these systems after their solvent composition 10Na:10Cl, 12Na:10Cl and 10Na:12Cl, respectively. The entire system is neutral and there is no charge background.

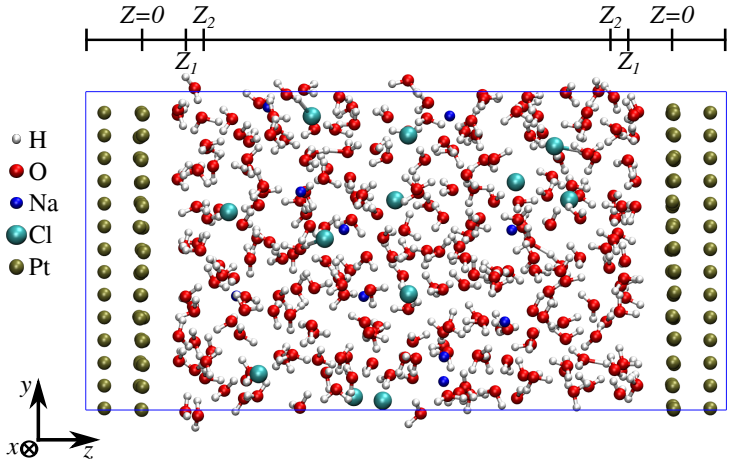

Figure 4-1: Our Pt/water solution model system. Here we present a snapshot of the trajectory of the 10Na:12Cl system (with 10 Na and 12 Cl ions in solution). The horizontal bar on top of the snapshot marks the external boundary of the first and second water layer (Z_1 and Z_2, respectively). $Z = 0$ labels the average position of the surface Pt layers in contact with the aqueous electrolyte. Red, white, olive green, cyan and blue spheres represent O, H, Pt, Cl and Na atoms, respectively.

The system size is adequate for our purposes for a number of reasons. Firstly, at the electrolyte concentration considered (≈2 M of NaCl in water) the separation between the two electrode surfaces (d=28 Å) corresponds to ≈8 Debye screening lengths. This reduced Debye length ensures that the 'bulk' condition is reached in the centre of the cell, i.e. at a relatively small distance from the surface of the electrode. Secondly, the large cell cross section (286 Å^2) reduces the effects of the 2D periodicity along the electrode surface, justifying the minimal k-point sampling (Γ-point only) of the system Brillouin

[1]Here M stands for molarity which is defined as the number of moles of solute per liter of solution.

zone. Thirdly, the Pt slab alone contains nearly 3000 electrons. Thus it represents a sizeable charge reservoir able to correctly position the system Fermi energy and to stabilise its value even upon the transfer of charges from the electrolyte to the electrodes. Finally, the overall size of the system allows us to accumulate sufficient statistics even during the relatively short timescales accessible to *ab initio* simulations. We have simulated each of the charged systems for ≈50 ps after equilibration.

This relatively simple model represents a substantial challenge to our computational approaches, which could only be managed thanks to the efficient CP2K implementation of DFT [52].

4.2 Methodology Used

MD based on DFT is performed for all systems using the Quickstep module of the CP2K package [52]. The electronic structure is obtained at the PBE level [69]. Tether, Goedecker and Hutter (GTH) pseudopotentials [64, 65], valence triple-zeta TZV basis set for Pt, TZVP (TZV polarisation) basis sets for the other atoms and a cutoff energy of 300 Ry for the plane waves are used. For every atomic configuration the potential energy of the systems of interest is computed by minimising the electronic DFT functional, while the time evolution is simulated by Born-Oppenheimer molecular dynamics, using the gradients of the DFT potential energy surface to provide the forces entering Newton's equations of motion. The time-step used to integrate the equations of motion is 0.7 fs within the NVT ensemble. The temperature is controlled by using a Langevin thermostat [70, 71, 56, 72] set at 340 K.

For all systems PBC are used. The in-plane cell parameters are $a = 14.568$ Å and $b = 19.626$ Å. In order to keep the density of the aqueous solution consistent with the studied system (≈1 kg·L^{-1} or slightly higher, depending on the salt concentration), the normal axis, c changes in the interval 35.942 Å $\leq c \leq 39.603$ Å.

The Pt/water half-cell is realistically modelled with nearly 1000 atoms. In particular, we have 768 Pt atoms, 250 water molecules, a variable number of Na^+ and Cl^- ions,

depending on composition, and about 5250 electrons. The Pt(111) electrode surface is modelled by using a 4-layer slab (42 Pt atoms per layer). The coordinates of the central layers of the Pt slab are constrained to the bulk electrode values. Using a four layer slab introduces an error in the evaluation of the Pt work function of less than 0.04 eV. This is acceptable in view of the reduced computational cost. Extensive tests have been performed over the slab size against sampling of the Brillouin zone.

We will be dividing this study into two major parts-

- Electronic analysis (Dealing with Bader charges, PDOS, potential drop and capacitance)
- Structural analysis (Dealing with structure and orientation of molecules)

4.3 Electronic analysis

4.3.1 Bader charges

We evaluated the charge across our system using Bader analysis [73, 74, 75]. This method allows to define volumes around each atom [76] separated by a zero-flux surfaces ($\nabla\rho = 0$), where the electronic density is minimal along the normal to the surface [77]. Since the electronic density is correlated with the nuclei positions, one can assign a charge to any atom. The absolute value of such charge without any reference has to be taken with caution since the definition of the atomic volume is arbitrary. Only the comparison between charges obtained with consistent methods is relevant. For this reason, due to the simplified definition of atomic volume adopted by the Bader scheme part of the charge localised around Cl^- ions is accounted to the H atoms of the first water solvation shell pointing toward it. Indeed, these H atoms are more negatively charged than the other H atoms (namely, those in the ions' first solvation shells and those belonging to water molecules far from the electrode surface, refer to appendix C for more details).

In the following, a detailed analysis of the excess Bader charges around selected regions of the three interfaces are studied. The excess charge is evaluated as the difference between

nominal and calculated charges around each atom. All the average here means time average, which means their values saved at different time interval were used for averaging except the initial 5 picoseconds (as the molecules were not equilibrated in that time).

Table 4.1: Excess Bader charges within the first solvation shell of Cl ion. Water No., O, H-away and H-towards and Water average represent the average number of water molecules, the average charge on O and H atoms - pointing away or towards the ion - and on each water molecule in the first solvation shell around Cl atom, respectively. Cl+Water and Cl represent the total average charge in each solvation shell and on Cl ion, respectively

System	Water No.	O	H-away	H-towards	Water Average	Cl+Water	Cl
12Cl:10Na-Pt	4.4±0.2	-1.27±0.01	0.633±0.010	0.620±0.008	-0.022±0.003	-0.83±0.01	-0.738±0.001
10Cl:10Na-Pt	3.1±0.1	-1.27±0.02	0.660±0.011	0.620±0.014	-0.022±0.002	-0.80±0.01	-0.735±0.002
10Cl:12Na-Pt	4.0±0.2	-1.26±0.01	0.634±0.007	0.616±0.011	-0.021±0.003	-0.81±0.01	-0.720±0.002

Table 4.2: Excess Bader charges within the first solvation shell of Na ion. Water No., O, H and Water average represent the average number of water molecules, the average charge on O and H atoms, and on each water molecule in the first solvation shell around Na atom, respectively. Na+Water and Na represent the total average charge in each solvation shell and on Na ion, respectively.

System	Water No.	O	H	Water Average	Na+water	Na
12Cl:10Na-Pt	4.46±0.24	-1.28±0.01	0.627±0.007	-0.026±0.002	0.800±0.014	0.9109±0.0004
10Cl:10Na-Pt	3.60±0.17	-1.29±0.02	0.630±0.012	-0.027±0.003	0.814±0.009	0.9049±0.0007
10Cl:12Na-Pt	4.23±0.20	-1.28±0.01	0.629±0.007	-0.026±0.002	0.800±0.010	0.9090±0.0002

In table 4.1 and 4.2 it can be observed that the solvation shell charge is independent of the type and number of ions dissolved as well as the type of electrode used. The number of molecules in the solvation shell is in between 4-5 We can also be seen that the solvation shell of 10Cl-10Na-Pt has comparatively less number of water atom in the solvation shell compared to the other system on analysis it was found that it couples with the Na atom. For all system the absolute value of the charge depends weekly on the solvated ions amounting to o.8|e| in both cases.

The analysis of the excess Bader charges in the water layers in close proximity with the electrode, averaged along the trajectory and among the two interfaces, is reported in Tab. 4.4 et seq. Boundaries and average positions of first and second water layers in contact with the electrodes are defined using the position of peaks and minima of the O density profile shown in Fig. 4-2, and corresponding table defining position and boundaries is 4.3.

The charges on the other water molecules, neither part of first or second water layer, nor of any solvation shells in our system is reported in Tab. 4.6.

In table 4.4 we expect the first layer of water to be oppositely charged from that of electrode, it is but not in the same magnitude, it's varies as electrode becomes more positive, there are more water molecules in the first layer and therefore there is more charge in the first layer. At the same time we note that the average charge on water is very similar in all system, thus differently charged electrode induce a charge in the first layer of water in contact with the electrode. The charge distribution in the water molecule is more polarised in case of the Ag electrode. In first layer the water is polarisedsuch a way that the O atoms are slightly less negatively charged and the H atoms are slightly more positively charged than the average free water molecule. Overall the water molecules are positively charged.

In 4.5 we expect it to be of opposite sign to that of metal electrode to maintain the balance, instead the nature of the charge is more dependent on the nature of the charge of the first layer as it is opposite in nature to that of the first layer, and as the electrode turns more negative so is total charge of the second layer in case of Pt electrode.

Table 4.3: Cartesian coordinates in Å used to define position and boundaries of first and second water layer. Z_i mark the external boundary of layer i and correspond to the density minima of the O mass density profile. z_{Mi} mark the position of the i^{th} peak in the O mass density profile. All distances are measured from the Pt external surface layer

System	z_{M1} (Å)	Z_1 (Å)	z_{M2} (Å)	Z_2 (Å)
12Na:10Cl	2.3	2.7	3.2	5.0
10Na:10Cl	2.3	2.7	3.3	5.5
10Na:12Cl	2.3	2.7	3.3	4.7

In table4.6 we expect the free water molecule to be completely neutral, the charge on the water molecule with it's polarisation will be used as reference for that system although it has a very small magnitude. We also expected the 10Cl:10Na system to have more free water molecules than the other system so the results are in accordance to our expectation.

In Tab. 4.7 et seq. we compare the Water number density of water and excess Bader charges in the water layers near the electrodes, as defined using the position of the mini-

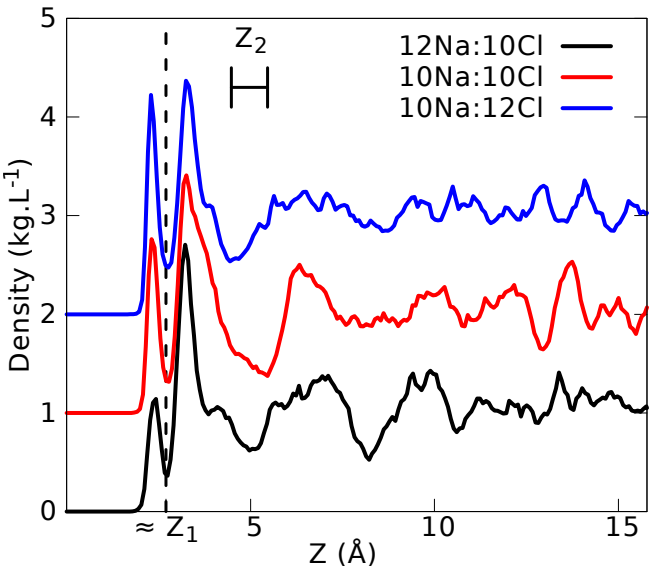

Figure 4-2: Average density profile of the O atom in the aqueous solution. To facilitate the reading, the results are vertically shifted. The separation between first and second water layer is identified by Z_1, while the separation between the second region and the rest (bulk) of the solution is marked by the Z_2 interval, as the coordinate is not the same for the three interfaces. The zero of the Z scale is aligned to the position of the centre of the metal slab.

Table 4.4: Excess Bader charges in the first layer of water near the electrode. Water No., Total-Water, Avg.-Water, O and H represent the average number of water molecules, the total charge on the water layer, the average charge per water molecule, average charge per O and H atoms, respectively.

System	Water No.	Total-Water	Avg.-Water	O	H
12Cl:10Na-Pt	7.7±0.5	0.77±0.05	0.100±0.005	-1.19±0.10	0.65±0.05
10Cl:10Na-Pt	5.0±0.4	0.49±0.05	0.10±0.01	-1.20±0.12	0.65±0.05
10Cl:12Na-Pt	2.8±0.4	0.29±0.04	0.10±0.01	-1.17±0.06	0.63±0.02

Table 4.5: Excess Bader charges in the second layer of water near the electrode. Water No., Total-Water, Avg.-Water, O and H represent the average number of water molecules, the total charge on the water layer, the average charge per water molecule, average charge per O and H atoms, respectively.

Sys.	Water No.	Total-Water	Avg.-Water	O	H
12Cl:10Na-Pt	13.2±1.4	-0.09±0.04	-0.007±0.004	-1.24±0.11	0.61±0.06
10Cl:10Na-Pt	16.0±0.8	-0.16±0.04	-0.010±0.002	-1.24±0.04	0.61±0.02
10Cl:12Na-Pt	16.1±0.8	-0.23±0.04	-0.015±0.003	-1.21±0.04	0.59±0.02

Table 4.6: Excess Bader charges in free water. Free water is the water which is neither part of solvation shells nor of first or second water layers. Water No., Total-Water, Avg.-Water, O and H represent the average number of water molecules, the total charge on free water, the average charge per water molecule and average charge per O and H atoms, respectively.

Sys	Water No.	Total-Water	Avg.-Water	O	H
12Cl:10Na-Pt	133.9±3.0	0.088±0.140	0.0007±0.0010	-1.272±0.007	0.637±0.004
10Cl:10Na-Pt	167.7±3.3	0.122±0.147	0.0007±0.0009	-1.267±0.006	0.634±0.003
10Cl:12Na-Pt	143.5±4.0	0.055±0.142	0.0004±0.0010	-1.269±0.008	0.635±0.004

mum or that of the shoulder of the O density distribution in the direction perpendicular to the electrode surface. The corresponding figures for the tables (4.7, 4.8 and 4.9) are 4-3, 4-4 and 4-5. It can be easily seen in the figure the presence of first minima (which defines the end of first layer of water), shoulder and the second minima (which defines the end of second layer). While doing the charge analysis we found out that the first layer of water is positively charged, while that of from first minima to shoulder is negatively charged, as we move away from the shoulder to second minima there is gradual increase in positively charged water molecules resulting in mix charged water molecules but overall they are slightly positive in case of 10Na:12Cl, 10Na:10Cl and 12Na:10Cl. The charge in first and second layers of water is dependent on the unbalanced population of ion. We found that the shoulder is a region where the transition occurs from layered to the bulk property (in the layers charge and mass density are very large compared to the bulk) It can be seen from the figures that 10Na:10Cl has the largest shoulder region while 10Na:12Cl has the smallest. Presence of unbalanced population of ions affects the shoulder region as increases in unbalanced ions shrink the shoulder region. Shoulder region has positively as well as negatively charged water molecules so we did not find any relation between the unbalanced population of ions and charge in the regions as it can be seen from the tables.

Table 4.7: 10Na:12Cl system: comparison of water number density (per unit of cell surface) and excess Bader charges in the water layers near the electrode as calculated using either the minimum or the shoulder of the O density profile. Water No., Total-Water, Avg.-Water, O, H represent the average number of water in the first layer, total excess charge in the layer, average charge per water molecule, per oxygen and hydrogen atoms, respectively.

System	Water No.	Total-Water	Avg.-Water	O	H
Avg:layer1:min	7.7±1.3	0.77±0.11	0.101±0.009	-1.19±0.09	0.65±0.05
Avg:layer2:min	21.0±1.3	-0.04±0.07	-0.002±0.003	-1.22±0.10	0.60±0.05
Avg:layer2:shoulder	13.2±1.8	-0.08±0.06	-0.007±0.005	-1.23±0.1	0.61±0.05
Inbtwn	7.8±1.0	0.04±0.03	0.005±0.004	-1.26±0.07	0.63±0.04

Table 4.8: 10Na:10Cl system: comparison of water density and excess Bader charges in the water layers near the electrode as calculated using either the minimum or the shoulder of the O density profile. Water No., Total-Water, Avg.-Water, O, H represent the average number of water in the first layer, total excess charge in the layer, average charge per water molecule, per oxygen and hydrogen atoms, respectively.

System	Water No.	Total-Water	Avg.-Water	O	H
Avg:layer1:min	5.0±2.1	0.49±0.19	0.098±0.016	-1.20±0.12	0.65±0.05
Avg:layer2:min	28.3±1.1	-0.12±0.07	-0.004±0.002	-1.24±0.04	0.61±0.02
Avg:layer2:shoulder	16.0±4.3	-0.16±0.74	-0.010±0.007	-1.24±0.04	0.61±0.02
Avg:Inbtwn	12.3±0.6	0.04±0.04	0.003±0.003	-1.24±0.05	0.63±0.02

Table 4.9: 12Na:10Cl system: comparison of water density and excess Bader charges in the water layers near the electrode as calculated using either the minimum or the shoulder of the O density profile. Water No., Total-Water, Avg.-Water, O, H represent the average number of water in the first layer, total excess charge in the layer, average charge per water molecule, per oxygen and hydrogen atoms, respectively.

System	Water No.	Total-Water	Avg.-Water	O	H
Avg:layer1:min	2.8±1.0	0.29±0.10	0.102±0.017	-1.16±0.06	0.64±0.02
Avg:layer2:min	26.6±1.2	-0.23±0.07	-0.009±0.002	-1.21±0.04	0.59±0.02
Avg:layer2:shoulder	16.1±1.5	-0.23±0.06	-0.015±0.004	-1.21±0.04	0.59±0.02
Avg:Inbtwn	10.4±1.1	0.001±0.03	0.000±0.003	-1.28±0.1	0.64±0.05

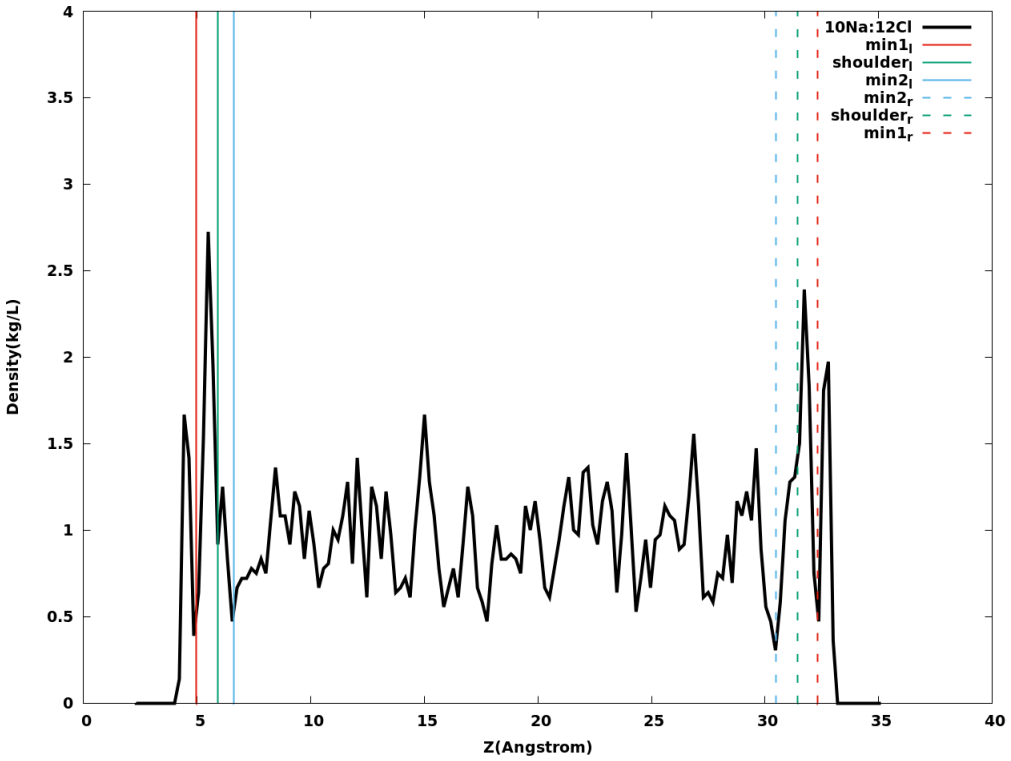

Figure 4-3: 10Na:12Cl system: graph of water density variation throughout the electrolyte, it shows different region of water layers near the electrode i.g. first minimum (min1), second minimum (min2) and shoulder of the water density profile. The subscript 'l' and 'r' represent the left and right position of the respective label. It has the highest density of water in first layer compared to other two systems.

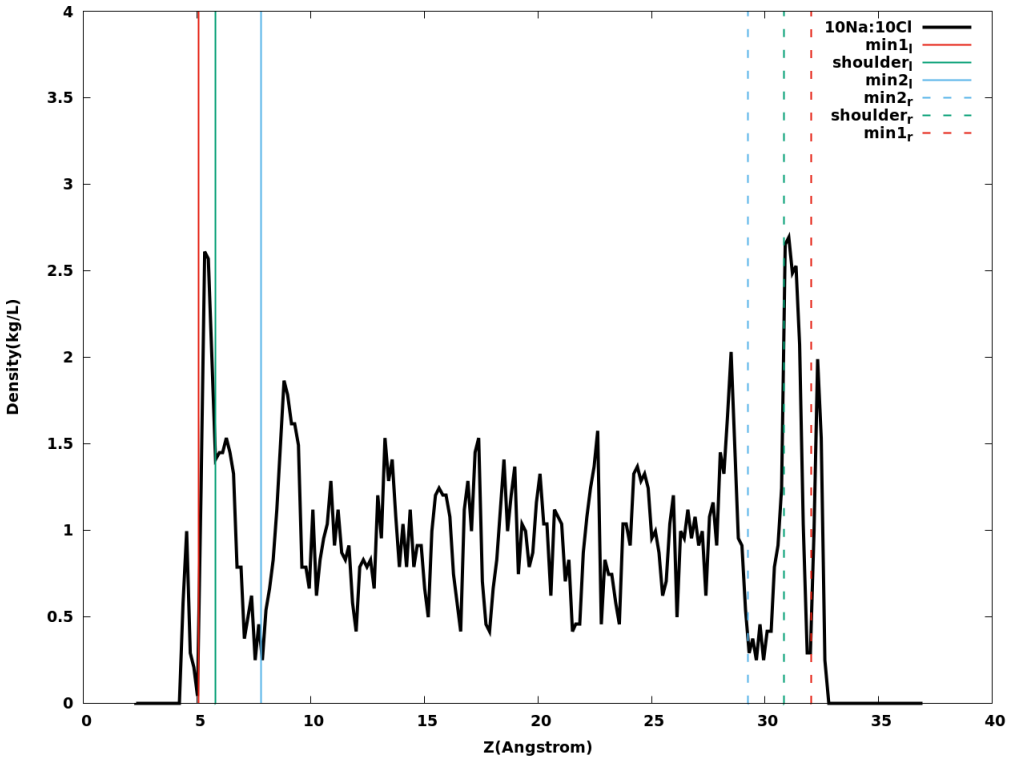

Figure 4-4: 10Na:10Cl system: graph of water density variation throughout the electrolyte, it shows different region of water layers near the electrode i.g. first minimum (min1), second minimum (min2) and shoulder of the water density profile. The subscript 'l' and 'r' represent the left and right position of the respective label.

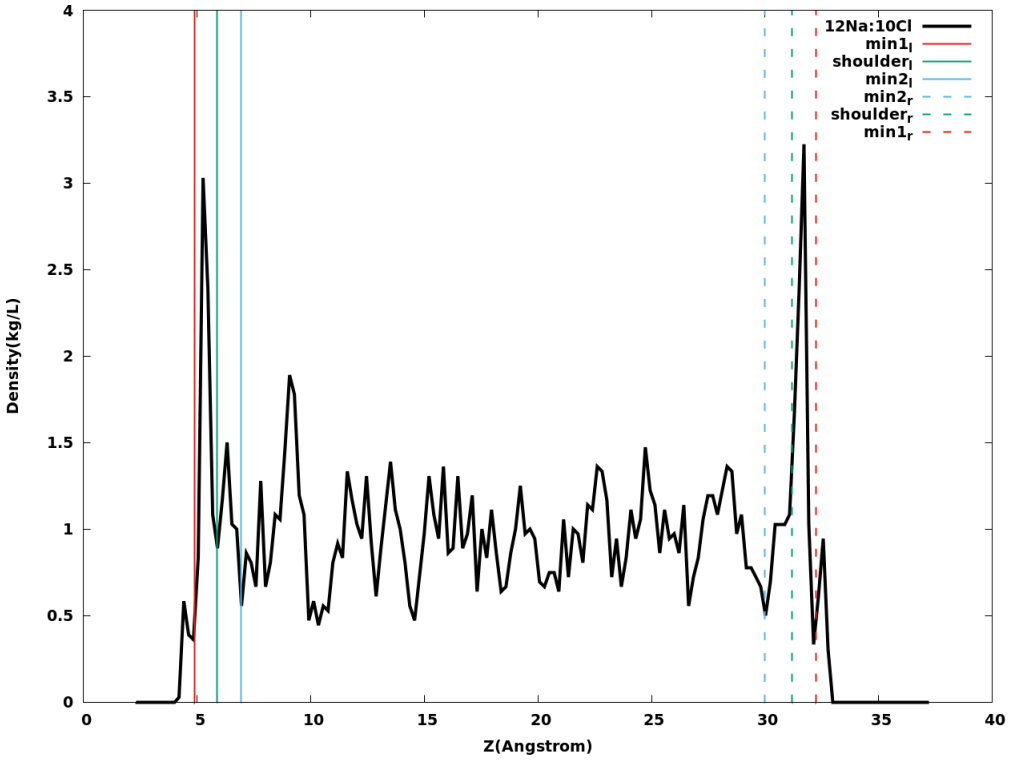

Figure 4-5: 12Na:10Cl system: graph of water density variation throughout the electrolyte, it shows different region of water layers near the electrode i.g. first minimum (min1), second minimum (min2) and shoulder of the water density profile. The subscript 'l' and 'r' represent the left and right position of the respective label. It has the least density of water in first layer clearly showing density dependense of water near the electrodes on the concentration of ions in solution.

4.3.2 The charge at the electrode-electrolyte interface

The first feature of the Pt/water DL revealed by our model is that the surface charging at the metal/water interface cannot be described by using a simple capacitor model and strongly depends on the applied potential.

In the conventional Gouy-Chapman-Stern picture of the DL, the notion of electrode charge is identified with the charge strictly localised at the metal electrode, counterbalanced by that of the ions on the surface and in the diffuse layer, the area with a gradient in concentration of counter ions. The more complex picture emerging from our calculations shows that (1) electrode charge spills over the water molecules in contact with the metal (the charge on the electrolyte side of the DL is not determined uniquely by the ions, as per traditional models); (2) an oscillating charge distributes at the metal/water interface; (3) there is a strong dependence of the interfacial charge on the applied potential. This picture provides the computational foundation for the more general thermodynamic definition of electrode charge as the amount of electricity to be supplied to the electrode when its surface is increased by a surface unit with the concentration of the solution components remaining constant [78].

Table 4.10: Bader excess (nominal-calculated) valence charges in units of $|e|$. In column 'system', the name of the system under consideration, defined by the number of Na^+ and Cl^- ions in solution and the type of metal electrode. In columns 2-6 the total, subsurface and external surface charge and the charge on first and second layer of water in contact with the electrode, respectively. These values are averaged along the trajectory and between the two interfaces present in our cell. Columns "Cl + H" and "Na" report the charge localised around Cl and Na ions. Due to the crude definition of the boundary of the volume defining the Bader charge around each atom, part of the charge actually localised on Cl was accounted by the Bader scheme to the charge of the H atoms pointing towards it. In this table the sum of Cl and this *artificial* H charges are reported. In the last two columns, "Solvation Shells" and "DL", we report the total charge in the first solvation shells of Na and Cl ions and the total charge on the double layer, DL, including electrode, first and second water layer.

System	Metallic electrode			Interfacial water		Ions		Solvation Shells	DL
	Total	Subsurface	Surface	Layer 1	Layer 2	Cl+H	Na		
10Na:12Cl-Pt	-0.03±0.08	1.67±0.05	-1.70±0.06	0.77±0.12	-0.08±0.06	-0.83±0.01	0.9109±0.0004	-1.96	0.65
10Na:10Cl-Pt	-0.61±0.12	1.68±0.05	-2.29±0.08	0.49±0.18	-0.16±0.74	-0.80±0.01	0.9049±0.0007	0.14	-0.28
12Na:10Cl-Pt	-1.10±0.07	1.70±0.04	-2.80±0.05	0.29±0.10	-0.23±0.06	-0.81±0.01	0.9090±0.0002	1.50	-1.04
0Na:0Cl-Pt	-0.56±0.08	1.65±0.05	-2.21±0.08	0.62±0.08	-0.09±0.07	0	0	0	0

The analysis of the excess (nominal-calculated) Bader charges distribution across the system quantifies the new perspective emerging from our calculations. First of all, Bader analysis confirms the viability of our approach, i.e. that the electrode state can be effectively controlled by the relative imbalance in the population of anions and cations in solution. Indeed, a larger excess of positive (negative) ions in solution corresponds in our calculations to a more negatively (positively) charged electrode (see Tab. 4.10).

We also observe that overall the negative charge on the electrode and at the DL is larger than what could be expected from traditional models [79]. In particular, the charge on the electrode side of the DL amounts to -1.1 $|e|$, -0.6 $|e|$ and -0.03 $|e|$ and the overall charge on the DL amounts to 0.65 $|e|$, -0.28 $|e|$ and 1.5 $|e|$, for the 12Na:10Cl, 10Na:10Cl and 10Na:12Cl systems, respectively (see Tab. 4.10). The absolute charge around every ion is on average 0.8 $|e|$, rather than exactly 1 $|e|$ (see first paragraph of 4.5 for a discussion of this point). As expected, the charge variation on the electrode moiety of the DL localises on the electrode's surface, whilst the charge in the inner layers of the Pt slabs is always the same for all interfaces studied (see "Surface" and "Subsurface" in Tab. 4.10) and zero in the centre of every metal slab. Moving from the negatively charged metal surfaces we encounter a net positive electronic excess charge in the first water layer in contact with the electrode and a negative charge again in the second water layer, before reaching again neutrality in the bulk electrolyte, in the central part of the cell (see Tab. 4.10 and Fig. 4-6).

The observed electronic charge spillover to the water layers in contact with the electrode is strongly dependent on the applied potential and occurs in such a way that each molecule in the first water layer always carries the same amount of positive charge ($\approx$ 0.1 $|e|$), irrespective of the electrode state. Correspondingly, the overall charge on the water layers in contact with the differently charged electrodes is determined by the different number of (equally charged) molecules composing these layers (see Tab. 4.10 and next paragraph), with the number of molecules composing the first water layer progressively increasing when the electrode becomes more positive (see Tab. 4.11). This means that the electrode charge is screened by changing the water density at the interface.

Notably, a negatively charged electrode and a charged water layer is observed also in

the presence of nominally neutral electrolyte, i.e. when a balanced population of ions (10Na:10Cl) or no ion (0Na:0Cl) are present in solution. This is in clear contrast with the assumption in standard computational approaches that the electrode remains neutral in the presence of a neutral electrolyte. This is one of the key findings of this work.

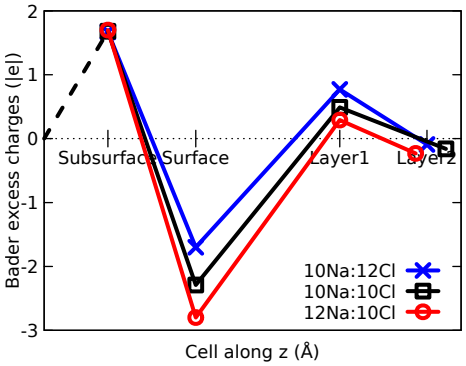

Figure 4-6: Graphical representation of the overall excess (nominal-calculated) Bader valence charge distribution along the double layer. The charge is averaged along the trajectory and between the two surfaces present in our cell. The black dashed line (joining the Pt subsurface layers and the region in their middle) signals that in the middle of the metal slab the actual charge is 0 (see Fig. 4-10).

In the following section we will complement the emerging new picture with a detailed analysis of the structure of the water layers in contact with the electrode.

4.3.3 Evaluation of the electrode/electrolyte potential drop

The potential drops between the electrode and the electrolyte at our three charged interfaces can be evaluated in different ways, in principle equivalent.

An *effective* way of evaluating the potential drop, currently accepted in the literature [6], has been adopted in our study. The *effective* potential drop (ΔV) is obtained by subtracting from the electrostatic potential of the total charged system (with a charged electrode and electrolyte) that of its neutral separate components (i.e. the neutral electrode and electrolyte, both surrounded by vacuum) in the same atomic configuration as in the charged system. The bulk potential of the electrode is equated to zero and the value in the middle of the cell is taken as ΔV. As shown in Fig. 4-7 the potential drops associated to different electrode charges are clearly distinguishable along the simulation.

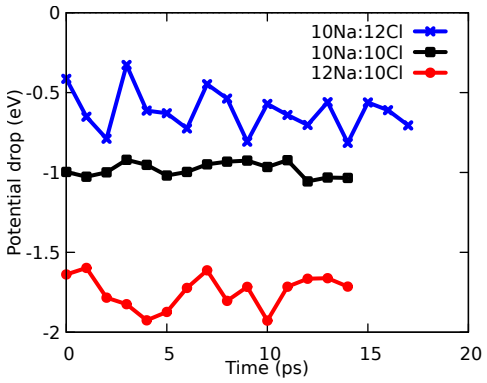

Figure 4-7: *Effective* potential drop, ΔV, versus time for the three interfaces studied. The *effective* ΔV is obtained by subtracting from the electrostatic potential of the total system (with charged electrode and electrolyte) that of its neutral separate components (i.e. the neutral electrode and the electrolyte, both surrounded by vacuum) in the same atomic configuration assumed in the charged system.

The potential drop can also be evaluated by directly relating the Fermi energies of each system to the vacuum level. The vacuum level can be consistently obtained for every system inserting a vacuum slab in the middle of the water layer and measuring the vacuum potential in the centre of the cell [57]. Using this approach naturally allows to define at the same time an absolute energy scale and evaluate the potential of zero charge, PZC, by aligning the vacuum level to the SHE. As shown in Fig. 4-8, the potential drops

corresponding to different electrode states are clearly distinguishable along the trajectory. However, the potential / charge relation, calculated in this way, is non-linear, with the system 10Na:10Cl at a lower potential than both 12Na:10Cl (higher negative charge on the electrode) and 10Na:12Cl (lower negative charge on the electrode) systems. Notably, the evaluation of the vacuum potential using this approach is uncertain, due to the reduced size of our system and the limited statistics (≈15ps, as shown in Fig. 4-8), not enough to compensate the dipole which got created by inserting some vacuum in the middle of the system.[2]

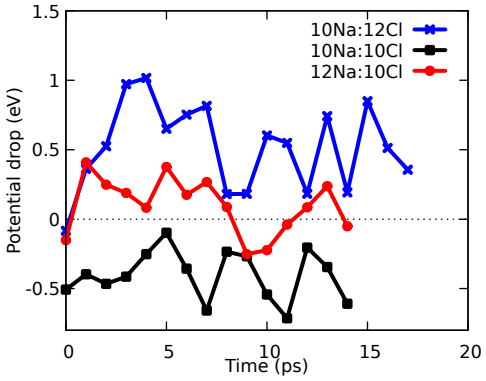

Figure 4-8: *Absolute* potential drop, ΔV, versus time, for the three interfaces studied. The *absolute* ΔV is obtained as the difference between vacuum potential energy and the Fermi level.

Finally, the potential drop could be also straightforwardly calculated by relating the interfacial Fermi level to the bulk electrolyte energy level, as evaluated in the centre of the cell. The potential of neutral bulk water could be in turn aligned to the vacuum level. Further alignment of this to the standard hydrogen electrode (SHE) level from experimental data would allow to define an absolute scale for the redox potential. However, the error on the evaluation of this quantity (e.g. the variance of the potential drop data versus time – see Fig. 4-9) resulted too big to extract a meaningful capacitance. This error could be reduced by increasing the sampling time.

[2]The simulation was done for ≈15ps due to the limitation of computation time.

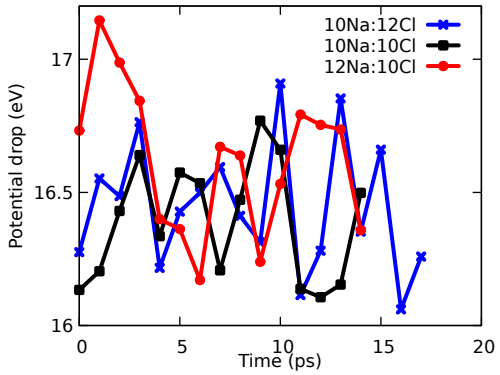

Figure 4-9: Standard potential drop for the three interfaces studied, calculated as the difference between the potential energy in the bulk electrolyte and the potential energy in the bulk electrode.

4.3.4 The Interface Capacitance

The study of the relation between the interfacial potential drop, ΔV, and the DL charge, ΔQ, allows us to evaluate *a posteriori* the interface capacitance $C = \Delta Q/\Delta V$. ΔQ, is here evaluated from Bader analysis and includes the charge on the electrode and in the charged water layers in its proximity.

Far from the electrodes, in the middle of the electrolyte region of each system, the bulk electrolyte condition is reached. This condition is clearly marked by the locally flat average electrostatic potential energy and density profiles; and by a locally neutral electrolyte solution in the centre of each cell (see Fig. 4-10). The potential drops ΔV associated to the three different electrode states under consideration can be compared by aligning their common bulk electrolyte levels. The charge modulation in the system (shown in bottom inset Fig. 4-10) can be easily compared to the potential modulation (shown in top inset Fig. 4-10), for ease of comparison the system (10Na:10Cl) itself has been shown in the middle. As we move from subsurface to surface we can see the peaks in charge modulation (shown in bottom inset Fig. 4-10).

As shown in Fig. 4-11, the potential drops associated to different electrode charges are clearly distinguishable during the simulation time and they depend linearly on the interfacial charge. The capacitance is calculated as the slope of the linear fit of the potential/charge relation (see Fig. 4-11) and amounts to $C = 8.29\ \mu\text{F}\cdot\text{cm}^{-2}$. This is close to

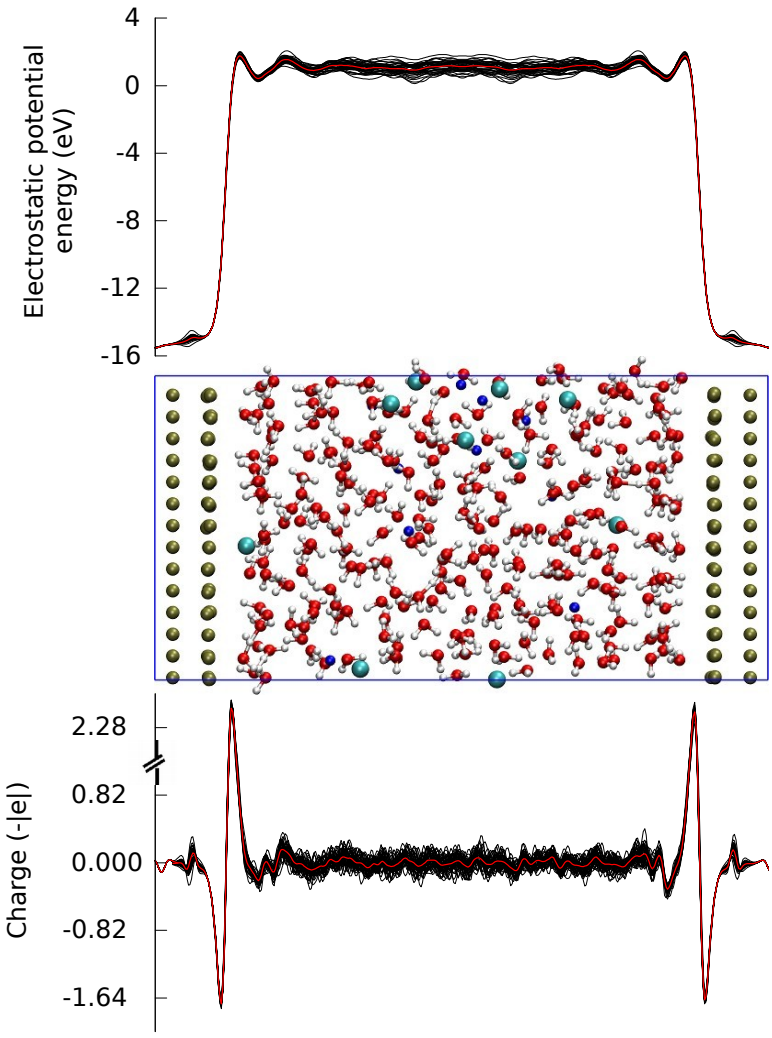

Figure 4-10: Macroscopic total (ionic cores + valence electrons) charge (inset at the bottom, representation not to the scale) and electrostatic potential energy (top inset) profiles along z (perpendicularly to the electrode surface), for the representative 10Na:10Cl system (represented in the central inset). These profiles are calculated along the trajectory every 1 ps (black lines). The average of these profiles is represented with a red line. Similar charge and potential drop trends are observed for all the systems.

the experimental value [80] for the capacitance of a Pt/water electrolyte solution interface at high frequency and low NaCl concentration, expected to be lower than 10 μF·cm^{-2}. Such value does not include the low frequency modes determined by the presence of the diffused layer [81]. However, due to the high ions concentration in our model, the diffused layer – the area with a gradient in concentration of counter ions – is very narrow and only

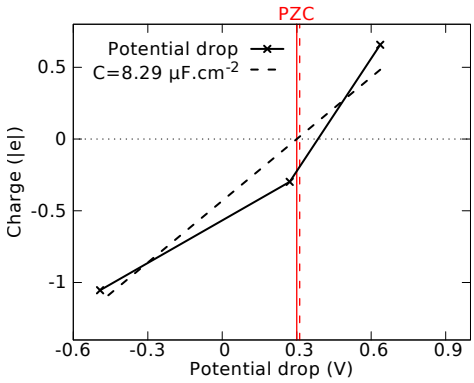

Figure 4-11: Double layer charge versus potential drop ΔV , as averaged along the trajectory for 12Na:10Cl (electrode charge -1.1 $|e|$), 10Na:10Cl (electrode charge -0.6 $|e|$) and 10Na:12Cl (electrode charge -0.03 $|e|$) systems. Charge and potential drop are provided in units of $|e|$ and Volts, respectively. Also reported, the system's capacitance ($C = 8.29\ \mu\text{F}\cdot\text{cm}^{-2}$), evaluated from the slope of the charge/potential linear fit (dashed black line). The continuous vertical red line represents the experimental PZC. Aligning this potential to the point where the linear fit crosses zero charge, allowed to define ad absolute potential scale for our electrodes, referred to the standard hydrogen electrode potential. The dashed vertical red line represents our evaluation of the PZC, where ΔV is evaluated relating the interfacial Fermi energy in every system to the vacuum level, and this latter to the SHE.

extends to the water layers region at interface.

No specific ion adsorption has been modelled on the surface. Therefore, from the calculated potential drop trends, it is possible to evaluate the *potential of zero (total) charge (PZC)* for the Pt electrode, as measured immediately after the electrode – previously cleaned in ultra high vacuum – is immersed in solution. This is straightforwardly obtained by finding the potential corresponding to the zero charge point on the line fitting our data.

Notably, in order to evaluate the capacitance with our method there is no need to place the electrode potential on an absolute scale, as only differences between the potential drops corresponding to different electrode charges are needed. However, by aligning the calculated and the experimental PZC for a Pt(111)/water interface ($PZC_{\text{exp}} = 0.3$ V with respect to the SHE) [35, 82] we can define an absolute scale for the redox potential at our interfaces. In this way the absolute electrode potentials with respect to the SHE of the 12Na:10Cl, 10Na:10Cl and 10Na:12Cl systems are calculated at -0.48, 0.27 and 0.64

V, respectively.

Notably, the potential drop ΔV can be evaluated for each state of the electrode charge in different ways, in principle. For instance, the potential drop can also be evaluated by directly relating the Fermi energies of each system to the vacuum level. This last procedure can be consistently applied for every system inserting a vacuum slab in the middle of the water layer and measuring the potential drop with respect to the vacuum potential in the centre of the cell [57]. This approach naturally allows us to define at the same time an absolute energy scale – by aligning the vacuum level to the SHE – and to evaluate the PZC - using the linear fit of the potential charge relation at zero charge (see figure 4-11). The PZC with respect to the SHE calculated in this way amounts to $PZC = 0.31$ V, a value extremely close to the experimental one [35, 82].

4.4 Structural analysis

4.4.1 Water structure and orientation

Current models describe the metal/water interface [83, 84, 85] by having every second water molecule oriented parallel to the surface and the other pointing one H atom either toward or away from the surface. In these models one assumes that the electrode polarisation is not associated to any mass redistribution in the water layer in contact with the metal electrode [67, 79, 86]. In this study we find that the electrode polarisation is closely associated with the mass distribution in the water layer in contact with the metal electrode, which is exactly the opposite of earlier studies. The most remarkable finding revealed by our approach is the strong dependence on the applied potential of the density of first and second water layers in contact with the electrode (see table 4.11).

The electrolyte mass density profile along the direction perpendicular to the electrode surface, exhibits in all systems two well-defined peaks, which unequivocally individuate the first and the second water layer in contact with the electrode (see Fig. 4-2). Fig. 4-12 shows that the intensities of the first O and H density peaks increase as the metal electrode becomes more positively charged, namely as we move from system 12Na:10Cl, to 10Na:10Cl, to 10Na:12Cl. We also learn that all the water molecules in the first layer have, on average, almost the same orientation (and charge), with the O atom closer to the metal (in an atop site position), and the H atoms slightly pointing towards the bulk water.

The mass density of the second water layer (see the intensity of the second peak in the electrolyte density profile in Fig. 4-12 (b)) is less affected by the electrode charging state. However, its orientation strongly depends on it. The water molecules in this layer, are characterised by broader density peaks and a different orientation depending on the electrode state, with one H located almost in the same plane of O (actually pointing slightly outwards) and one pointing towards the Pt surface (our electrodes are all negative) and with more H atoms progressively pointing towards the surface as the electrode becomes more negatively charged.

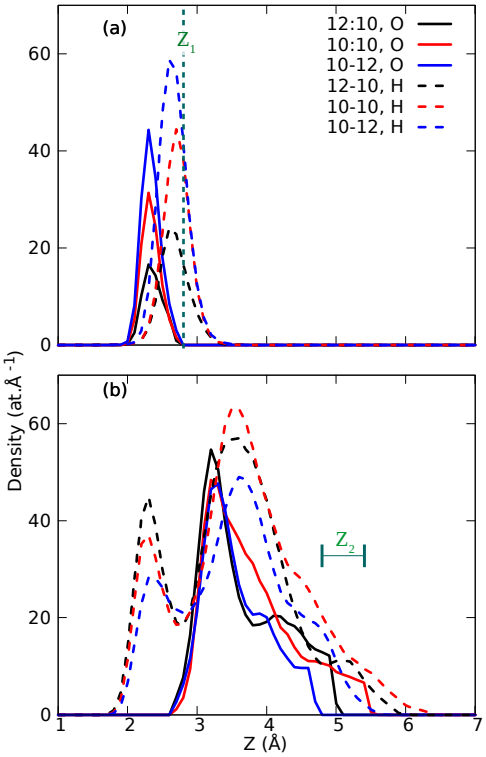

Figure 4-12: Average atomic density profiles for the O and H atoms belonging to the aqueous electrolyte in contact with the electrode (in units of atoms per Å). 12Na:10Cl, 10Na:10Cl, and 10Na:12Cl systems are represented in black, red and blue, respectively. Differently unbalanced ion populations in solution lead to differently charged electrodes. The charge on the metal moiety of the interface is reported in the brackets next to each label (in units of $|e|$). For each system, the atomic density profiles are averaged over 50 ps long trajectories obtained performing DFT based Born Oppenheimer molecular dynamics. First and second water layers are defined as described in Tab. 4.3. Here (a) represents the water molecules belonging to the first water layer, in contact with the electrode. In (b) the water molecules of the second water layer. The plain and dashed lines stand for the O and H atoms' contributions, respectively. The separation between first and second water layer is identified by Z_1, while the separation between the second region and the rest (bulk) of the solution is marked by the Z_2 interval.

Fig. 4-13 shows that the O atoms in the first layer form intra-layer chemical bonds with the H atoms and interlayer H bonding, whose density depends on the electrode state, as highlighted by a coordination number n=2 under 1.5 Å and n=2.2-2.8 at larger distances, up to 3 Å.

Finally, we study the dynamic behaviour of the water molecules in contact with the electrode at different potentials. The positions of the O atoms belonging to first and sec-

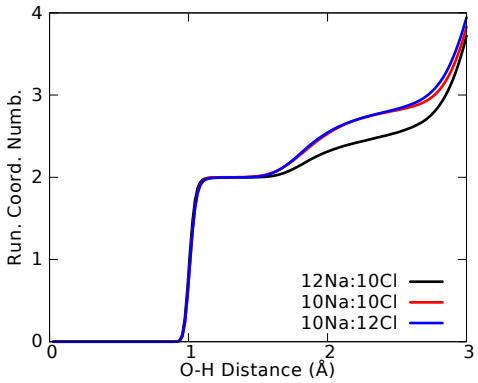

Figure 4-13: Integrated O-H radial distribution profile ("Running" Coordination number), where O belongs to the molecules of the first water layer in contact with the electrode. Black, red and blue lines represent the profiles relative to 12Na:10Cl, 10Na:10Cl and 10Na:12Cl systems, respectively.

Table 4.11: Average number density of water molecules per surface in the cell and per system, in the first and second layer in contact with the electrode. The cross section of our cell is (A=286 $Å^2$), corresponding to 42 surface Pt atoms.

System	Layer 1	Layer 2:shoulder
12Na:10Cl	2.8	16.1
10Na:10Cl	5.0	16.0
10Na:12Cl	7.7	13.2

ond water layers are reported as a function of time in Fig. 4-14(a). This picture clearly shows that the water molecules belonging to the first layer do not diffuse (within a ≈50 ps time scale) and remain on the atop sites of the Pt(111) surface (red traces in Fig. 4-14). In contrast, the water molecules belonging to the second water layer are more mobile, as shown by the blue traces in Fig. 4-14. The observed interfacial water structure is in agreement with other works [29, 34, 87, 88, 89]. Interestingly, even if the supercell used is not compatible in all directions with a closely packed hexagonal (or pentagonal) arrangement on the surface, hexagonal and pentagonal motives are observed at the interface over the simulation time. This is consistent with experimental observations of hexagonal and pentagonal water arrangements on Pt(111) [87, 84, 90]. Such water rings are formed by water molecules belonging to the first and second layer above the surface and their structure and density depends on the density of the first water layer, so it is again potential dependent (see Fig. 4-14(a)).

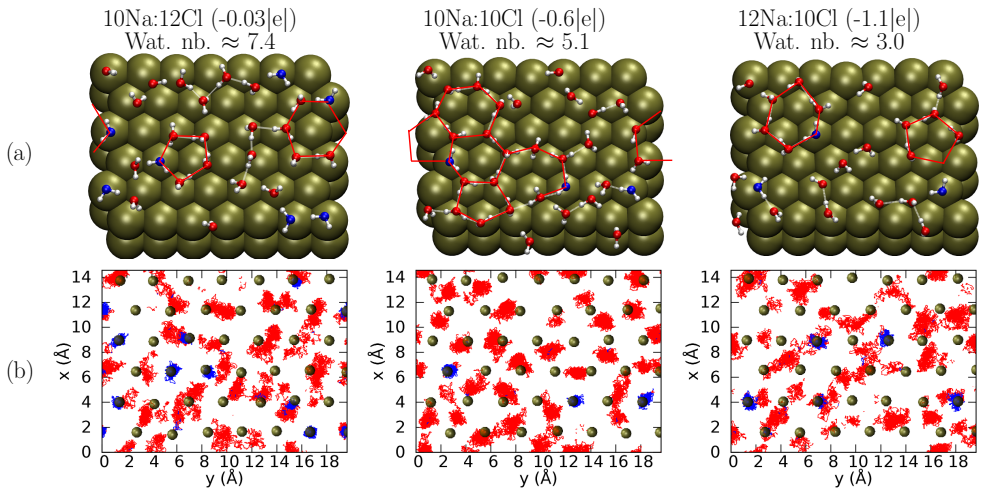

Figure 4-14: (a) Prototypical configuration of first and second water layer for 10Na:12Cl, 10Na:10Cl and 12Na:10Cl systems, respectively. Red lines highlight hexagonal and pentagonal motives. (b) Trajectories of O atoms belonging to first and second water layer in contact with the electrode, marked with blue and red lines, respectively. The charge on the metal electrode is also reported (units of $|e|$). Wat. nb. indicates the average number of molecules in the first water layer.

The peculiar potential-dependent structure of the water layers in contact with the Pt electrode results from the balance between the mass density of the first charged water layer and the orientation of the second one (Fig. 4-15). The results presented above demonstrate a new model for the DL at metal/water interfaces which goes beyond the standard Gouy-Chapman-Stern picture. We unveiled a complex dependence of interfacial charge screening and polarisation as well as atomic structure and dynamics on the applied potential, which will likely affect reaction rates and the catalytic processes therein. We expect that our approach will represent the baseline for future self-consistent evaluations of kinetic overpotentials associated with electrocatalytic transformation within the DL of metal water interfaces.

Our model is consistent with the experimental observation of key electrochemical quantities such as the interface capacitance and the potential of zero charge. In the following,

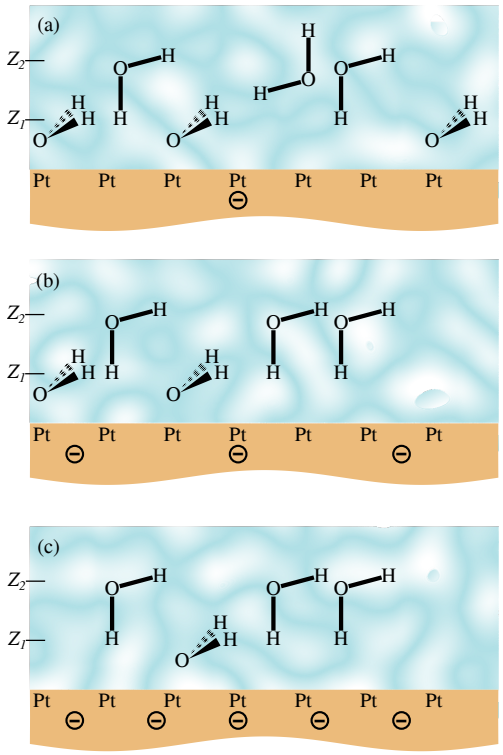

Figure 4-15: Schematic view of the water bilayer at the Pt/H_2O interface for different state of charges (this is a cartoon showing the trend in the result, it's not to the scale.). (a) Poorly charged Pt, typically with 10 Na and 12 Cl in solution, (b) negatively charge Pt, typically with 10 Na and 10 Cl in solution, (c) highly negatively charged Pt, typically with 12 Na and 10 Cl in solution.

we will illustrate how we used our approach to evaluate such electrochemical quantities and to predict SFG spectra, which cannot be easily extracted experimentally.

4.4.2 Computational SFG spectra

The water orientation at the interface could be insightfully probed by interfaces sensitive spectroscopy, such as Sum-Frequency-Generation (SFG). Despite a couple of pioneering attempt to investigate the Pt/water interface with SFG, the experimental investigation is made challenging by the presence of a strong non-resonant signal from the metal, which prevents to directly access the water structure and orientation [91]. However, calculating the resonant SFG spectra at the Pt/water interface is computationally possible, and this is here obtained with surface sensitive Vibrational Density of States (VDOS) [92, 93] (see appendix B for details). Using this approach, we observe in the first adsorbed layer (upper panel in Fig. 4-16) a single positive band located at around 2800–3000 cm^{-1}, whose intensity increases as the positive charge on the electrode increases. The more intense x the signal is, the higher is the density of the water molecules pointing towards the water bulk (outside the Pt surface). The surface sensitive VDOS for the second adsorbed water layer (lower panel in Fig. 4-16) presents a completely different behaviour. For all the systems studied, a positive and a negative band are present. As the positive charge on the electrode increases, the intensity of the positive band at lower frequencies increases, indicating a higher density of the dipoles oriented as in the first adsorbed layer. At the same time, the negative band is reduced, also signalling water reorientation. Our VDOS results are consistent with the observed density distribution and molecular orientation under bias (illustrated in Fig. 4-12) and provide a useful instrument to experimentalists to distinguish and interpret the interfacial geometric structures of water at Pt interfaces under a bias potential.

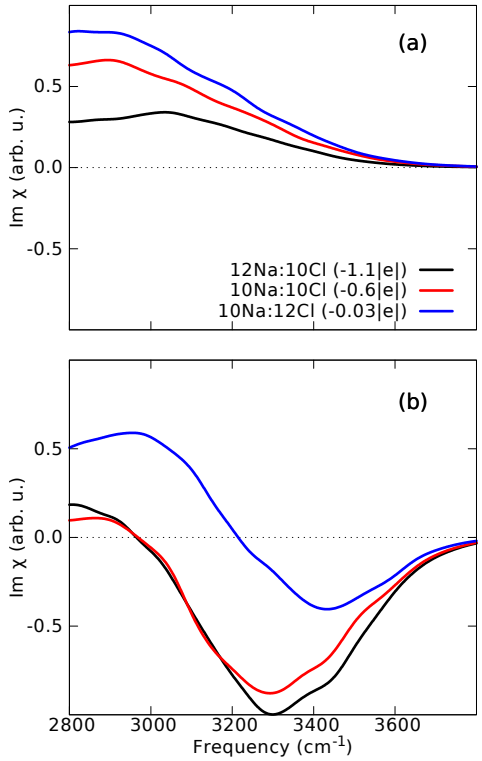

Figure 4-16: Layer resolved surface sensitive vibrational density of states (VDOS), for 12Na:10Cl, 10Na:10Cl and 10Na:12Cl systems, represented with black, red and blue lines, respectively. The charge on the metal moiety of each DL is also reported in brackets, in units of $|e|$. In (a) the VDOS obtained from the water molecules of layer 1, an increasing number of which points towards the bulk of the electrolyte, as the electrode becomes more positive. In (b) the VDOS obtained taking into account only water molecules of the second layer, where the number of water molecules reorienting their dipole towards the electrode becomes increasingly larger, as the electrode becomes more negative.

4.5 Methodology assessment

An analysis of the Kohn-Sham density of states projected (PDOS) on the metal moiety and the different species, namely water, Na, Cl and the metal slab (see Fig. 4-17) confirms that the position of the ions' centred energy levels with respect to the Pt Fermi level, E_{F}, is qualitatively correct, namely it reproduces the one schematically presented in Fig. 2-8. In particular, the lowest unoccupied state on Cl is below the Pt Fermi level, while the highest occupied energy level centred on Na is above it. This indicates that electrons localise around the Cl atom, giving rise to a Cl^- anion and leave Na^+ in the cationic form. It can be also seen that the PDOS on Cl (and Na) ions in the three systems we studied

(12Na:10Cl, 10Na:10Cl and 10Na:12Cl) are aligned. Thus, even if the three interfaces have slightly different ionic composition, their ions in solution have a common status of charge and can be considered three expressions of the Pt/water interface under different bias conditions.

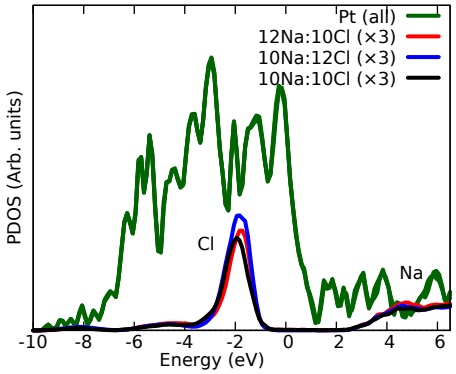

Figure 4-17: PDOS. Average projected density of states on Pt, Na and Cl species along the trajectory. The zero of the energy scale is aligned to the Fermi level. The PDOS on Pt atoms is represented in green. The PDOS on ions in 12Na:10Cl, 10Na:10Cl and 10Na:12Cl systems are magnified (× 3) and represented by a red, blue and black line, respectively. In every system, the same colour code is used to represent both PDOS on Na and Cl, however there is no ambiguity, as they do not overlap.

Consistently, the structure and the charge of the ions' solvation shells only depend on the nature of the solvated ions, and not on their number. This further confirms that adding or subtracting ions to the solution can be used to model different electrodes' states and only affects the charge on the electrode. Interestingly, in every system studied the overall charge associated to first solvation shells around Na and Cl ions is nearly equal in magnitude, but opposite in sign (refer for a full picture of Bader charges in our system). Thus, when an equal population of anions and cations is present in solution their overall charge almost cancels out (see Tab. 4.10).

In Summary, Bader analysis confirms the viability of our approach, i.e. that the electrode state can be effectively controlled by the relative imbalance in the population of anions and cations in solution. Thus we have the first feature of the Pt/water DL revealed by our model is that the surface charging at the metal/water interface cannot be described by using a simple capacitor model and strongly depends on the applied potential. The

charge on the electrode side of the DL amounts to -1.1 $|e|$, -0.6 $|e|$ and -0.03 $|e|$ and the overall charge on the DL amounts to 0.65 $|e|$, -0.28 $|e|$ and 1.5 $|e|$, for the 12Na:10Cl, 10Na:10Cl and 10Na:12Cl systems, respectively. The absolute charge around every ion is on average 0.8 $|e|$, rather than exactly 1 $|e|$. As expected, the charge variation on the electrode moiety of the DL localises on the electrode's surface, whilst the charge in the inner layers of the Pt slabs is always the same for all interfaces studied and zero in the centre of every metal slab. The observed electronic charge spillover to the water layers in contact with the electrode is strongly dependent on the applied potential and occurs in such a way that each molecule in the first water layer always carries the same amount of positive charge (≈ 0.1 $|e|$), irrespective of the electrode state. Notably, a negatively charged electrode and a charged water layer is observed also in the presence of nominally neutral electrolyte, i.e. when a balanced population of ions (10Na:10Cl) or no ion (0Na:0Cl) are present in solution. This is in clear contrast with the assumption in standard computational approaches that the electrode remains neutral in the presence of a neutral electrolyte. We provided an intuitive approach to evaluate key electrochemical quantities such as the potential of zero charge and the capacitance of the electrified interface.

In this study we also find that the electrode polarisation is closely associated with the mass distribution in the water layer in contact with the metal electrode, which is exactly the opposite of earlier studies. The most remarkable finding revealed by our approach is the strong dependence on the applied potential of the density of first and second water layers in contact with the electrode The electrolyte mass density profile along the direction perpendicular to the electrode surface, exhibits in all systems two well-defined peaks, which unequivocally individuate the first and the second water layer in contact with the electrode. The intensities of the first O and H density peaks increase as the metal electrode becomes more positively charged, namely as we move from system 12Na:10Cl, to 10Na:10Cl, to 10Na:12Cl. We also learn that all the water molecules in the first layer have, on average, almost the same orientation (and charge), with the O atom closer to the metal (in an atop site position), and the H atoms slightly pointing towards the bulk water.

The mass density of the second water layer is less affected by the electrode charging

state. However, its orientation strongly depends on it. The water molecules in this layer, are characterised by broader density peaks and a different orientation depending on the electrode state, with one H located almost in the same plane of O (actually pointing slightly outwards) and one pointing towards the Pt surface (our electrodes are all negative) and with more H atoms progressively pointing towards the surface as the electrode becomes more negatively charged. The water molecules belonging to the first layer do not diffuse and remain on the atop sites of the Pt(111) surface, in contrast, the water molecules belonging to the second water layer are more mobile. Hexagonal and pentagonal motives are observed at the interface over the simulation time, such water rings are formed by water molecules belonging to the first and second layer above the surface and their structure and density depends on the density of the first water layer, so it is again potential dependent.

Chapter 5

A Comparative Study of Pt/Water And The Ag/Water Interfaces

If we combine our model with the traditional picture for the DL, the 12Na:10Cl, 10Na:10Cl and 10Na:12Cl systems are expected to generate a charge of -1, 0 and +1 |e| on each electrode surface, respectively. Correspondingly, a net +2, 0 and -2 |e| charge would be localised on the excess ions in solution (our system is globally charge neutral). However, deviations from this idealised picture are observed consisting in a charge transfer between the electrolyte solution and the Pt electrode. In particular, the charge on the electrode side of the DL amounts to -1.1, -0.6 and -0.03 |e|, the overall charge on DL amounts to 0.65, -0.28 and 1.5 |e|, for the 12Na:10Cl, 10Na:10Cl and 10Na:12Cl systems, respectively (see Tab. 4.1 and 4.2) and the absolute charge around the ions' is on average 0.8 |e|, rather than exactly 1 |e|.

The deviation of the charge on ions and electrode from the expected ideal behaviour in our model could either reflect a real feature of the Pt(111)/electrolyte solution interface or be the result of a limitation of the employed DFT potential, such as the self-interaction problem [94, 95] and the related known tendency of standard exchange and correlation functionals to delocalise the Kohn-Sham states.

From an electronic point of view the charge spillover to the metal from the water is due by the modification of the electronic structure of the water molecules chemically

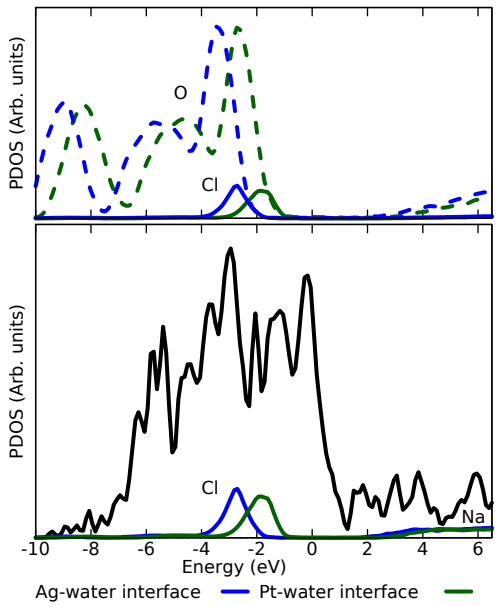

Figure 5-1: Comparison of the projected density of states (PDOS) on O, Cl and Na atomic species, for the 10Na:12Cl-Ag (blue) and 10Na:12Cl-Pt (green) systems. The zero of the energy scale in these graphs is aligned to the Fermi level of the interface under consideration, so Cl and O PDOSes in Ag/water interface (upper inset) are lower in energy with respect to the Fermi level than those in Pt/water interface. This marks the lower value of Pt Fermi level with respect to vacuum. In the lower inset, the PDOS on Pt and the ions. A larger gap between Cl LUMO and Na HOMO is observed in the Ag/water interface.

interacting with the Pt surface. The notion of charge spillover at a metal/water and semiconductor/water interface is currently accepted in the literature [96, 97]. Here we provide for the first time a comprehensive model of how this occur at the Pt electrode under bias. In support to the adequacy of PBE functional for describing such phenomenon, the knowledge that the interface dipole potentials predicted by PBE is extremely close to those calculated at the HSE06 level [96]. The robustness of this property is attributed to the electrostatic nature of the dipole effect in the double layer.

In general the transfer of electron charge to the Pt side of the interface may be ascribed to the chemical properties of Pt, in which relativistic effects lower the energy of the uppermost occupied states [98] thus increasing the metal work function and returning an unusual electronegative character to the surface.

Correspondingly, at a short distance from the electrode described in our calculations we also do not necessarily expect fully ionised atomic species in solution. The accuracy of the EC measurements is not sufficient to confirm or exclude such a charge transfer to Pt, thus there is a margin of uncertainty. However, in favour of this hypothesis, recent DFT calculations [99] on the change in the platinum work function induced by halide adsorption find a similar transfer of electrons from highly electronegative species to metallic Pt, and attributes it to the large work function of Pt(111), which is equivalent to a high electron affinity.

To evaluate the suitability of PBE functional to describe the metallic moiety of the Pt/water interface (and charge transfer to and from the electrolyte), we modelled an additional system by replacing in the 10Na:12Cl system Pt with Ag metal, which is more free-electrons like than Pt and whose work function for the (111) surface is 1.5 eV lower than that of the platinum.

Now we will be discussing the structural analysis of this system. After running the simulation we plotted the density variation of the water molecules to see the behaviour of water in contact with platinum (see figure 5-2). The density of water is calculated as time average density (which is the average of density calculated at intervals of 0.5 ps). This density was plotted as a function of distance from the electrode surface, presence

of first minima (Z1), shoulder and second minima (Z2) are clearly visible. Z1, shoulder and Z2 were clearly visible in case of platinum electrode systems and silver system closely resembles to the density distribution of its platinum counterpart. In the middle of the slab, the density fluctuates around 1, which brings it closer to the actual value. Then we analysed the distribution of water in the first and second layers and found an average of 4.9 and 12.4 water molecules in the first and second layers respectively. While its Pt counterpart has 7.7 and 13.2 respectively in first and second layers of water, we can conclude that the electronegativity of the electrodes are playing a big role in water density near electrodes. The density of second layer is not affected much. Next to understand the orientation of water molecules in these layers time average atomic density profiles for the O and H atoms belonging to the aqueous electrolyte in contact with the electrode (in units of atoms per Å) was plotted (see figure 5-3). In figure 5-3(a) one can observe the overlap of 'O' and 'H' curve implying 'H' molecules are in the same plan as that of O atoms. It can be concluded that the water molecule are oriented parallel to the electrode surface. In figure 5-3(b) we can observe pick of 'H' before that of 'O' implying water molecules are oriented perpendicular to the surface. We observe a very close resemblance in the distribution and orientation of 'O' and 'H' atoms in the two layers to that of its Pt counterpart. This finishes structural analysis of Ag in contact with water, we will be discussing the charges of these layers in great detail in the next chapter.

Table 5.1: Excess Bader charges within the first solvation shell of Cl ion. Water No., O, H-away and H-towards and Water average represent the average number of water molecules, the average charge on O and H atoms - pointing away or towards the ion - and on each water molecule in the first solvation shell around Cl atom, respectively. Cl+Water and Cl represent the total average charge in each solvation shell and on Cl ion, respectively

System	Water No.	O	H-away	H-towards	Water Average	Cl+Water	Cl
12Cl:10Na-Pt	4.4±0.2	-1.27±0.01	0.633±0.010	0.620±0.008	-0.022±0.003	-0.83±0.01	-0.738±0.001
12Cl:10Na-Ag	4.6±0.3	-1.28±0.01	0.641±0.009	0.620±0.008	-0.023±0.003	-0.83±0.01	-0.731±0.002

We did the Bader chrage analysis of the system and compared the data with its platinum counterpart. Firstly we compared the solvation shell of Cl and Na as shown in the table 5.1 and 5.2 and it can be seen that they have almost the same value in every re-

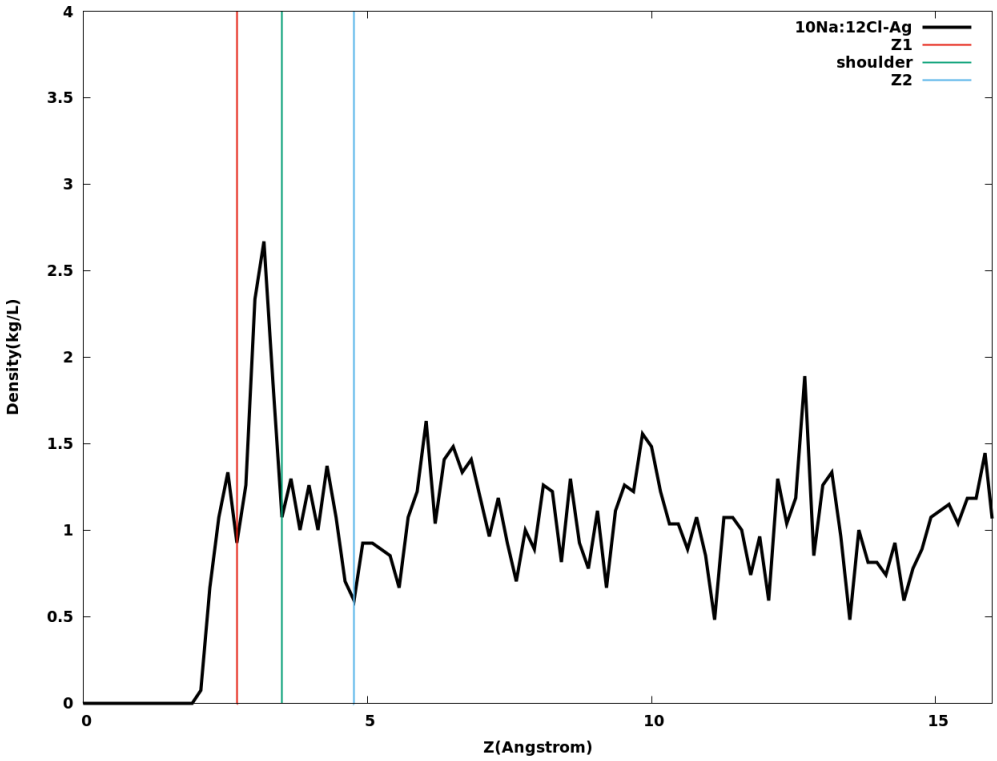

Figure 5-2: Average density profile of the water in the electrolytic solution. The separation between first and second water layer is identified by Z1, while the separation between the second region and the rest (bulk) of the solution is marked by the Z2 interval. The shoulder is also clearly visible here similar to that of platinum electrode systems. The zero of the Z scale is aligned to the position of the centre of the metal slab.

spect.[1] Interestingly, the solvation shell charge is independent of the type and number of ions dissolved as well as the type of electrode used. The number of molecules in the solvation shell is in between 4-5. For all system the absolute value of the charge depends weekly on the solvated ions amounting to o.8|e| in both cases.

In table 5.3 we expect the first layer of water to be oppositely charged from that of the electrode, it is in case of Pt but not in the case of Ag. It clearly indicates the electronegativity of the electrode has a bigger influence on the induced charge in the first layer of water instead of the charge on the electrode. Comparing the Pt and Ag electrodes, it can be seen that the Pt has more number of water molecules in the first layer compared to the Ag as the Pt is more electronegative. At the same time we note that the average

[1]Refer to appendix C for more information about the solvation shell and there comparisons.

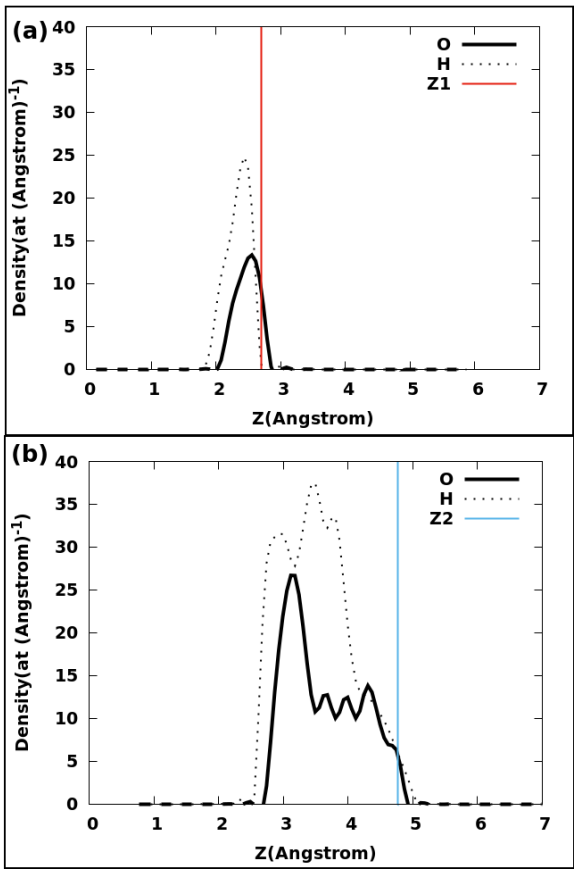

Figure 5-3: Figure shows average atomic density profiles for the O and H atoms belonging to the aqueous electrolyte in contact with the electrode (in units of atoms per Å) for 10Na:12Cl-Ag system. Here (a) represents the water molecules belonging to the first water layer, in contact with the electrode. In (b) the water molecules of the second water layer. The plain and dashed lines stand for the O and H atoms' contributions, respectively. Z1 and Z2 mark the end of the first and second layer.

charge on water were very similar in all Pt systems, for Ag charge per water molecule has been reduced by a factor of 10 in the first layer. The charge distribution in the water molecule is more polarised in case of the Ag electrode. In first layer the water is polarised in such a way that the O atoms are slightly less negatively charged and the H atoms are slightly more positively charged than the average free water molecule.

On analysing the charge distribution in second layer of water we found that electrode has significant effect on the number of water molecule and charge of layers (see table 5.4). There are 12.4 water molecule in the second layer for silver electrode while there

Table 5.2: Excess Bader charges within the first solvation shell of Na ion. Water No., O, H and Water average represent the average number of water molecules, the average charge on O and H atoms, and on each water molecule in the first solvation shell around Na atom, respectively. Na+Water and Na represent the total average charge in each solvation shell and on Na ion, respectively.

System	Water No.	O	H	Water Average	Na+water	Na
12Cl:10Na-Pt	4.46±0.24	-1.28±0.01	0.627±0.007	-0.026±0.002	0.800±0.014	0.9109±0.0004
12Cl:10Na-Ag	4.61±0.17	-1.29±0.02	0.633±0.007	-0.026±0.002	0.790±0.009	0.9101±0.0003

Table 5.3: Excess Bader charges in the first layer of water near the electrode. Water No., Total-Water, Avg.-Water, O and H represent the average number of water molecules, the total charge on the water layer, the average charge per water molecule, average charge per O and H atoms, respectively.

System	Water No.	Total-Water	Avg.-Water	O	H
12Cl:10Na-Pt	7.7±0.5	0.77±0.05	0.100±0.005	-1.19±0.10	0.65±0.05
12Cl:10Na-Ag	4.9±0.5	0.05±0.01	0.011±0.004	-1.30±0.13	0.66±0.07

are approximately 13.2 in case of its platinum counterpart. Charge per water molecule has been increased by a factor of 3 compared to its Pt counterpart. So we can conclude that density of second layer is not affected by the electronegativity of the electrode while charge per water molecule does get affected by it.

In table 5.5 we expect the free water molecule to be completely neutral, the charge on the water molecule with it's polarisation will be used as reference for that system although it has a very small magnitude (slightly negative in case of Ag while slightly positive in case of Pt). We also expected the balanced system to have more free water molecules than the other system so the results are in accordance to our expectation.

The charge on the electrode was analysed in table 5.6, the total charge on silver is 1.0|e| while that of platinum is -0.03|e|. We can conclude that electronegativity has a big role to play in the distribution of charge on the electrode as well as the water layers. The orientation of molecule within first and second layer is same as that of platinum system.

The analysis of the charge transfer to the electrolyte solution and the band structure of the system show that PBE is able in this case to capture the difference in electronegativity between the two metals and shows that the transferred charge on the silver surfaces exactly amounts to the ideal value of 1 |e|. A lowering in Pt of the energy of the uppermost

Table 5.4: Excess Bader charges in the second layer of water near the electrode. Water No., Total-Water, Avg.-Water, O and H represent the average number of water molecules, the total charge on the water layer, the average charge per water molecule, average charge per O and H atoms, respectively.

Sys.	Water No.	Total-Water	Avg.-Water	O	H
12Cl:10Na-Pt	13.2±1.4	-0.09±0.04	-0.007±0.004	-1.24±0.11	0.61±0.06
12Cl:10Na-Ag	12.4±0.6	-0.30±0.07	-0.024±0.005	-1.20±0.05	0.59±0.03

Table 5.5: Excess Bader charges in free water. Free water is the water which is neither part of solvation shells nor of first or second water layers. Water No., Total-Water, Avg.-Water, O and H represent the average number of water molecules, the total charge on free water, the average charge per water molecule and average charge per O and H atoms, respectively.

Sys	Water No.	Total-Water	Avg.-Water	O	H
12Cl:10Na-Pt	133.9±3.0	0.088±0.140	0.0007±0.0010	-1.272±0.007	0.637±0.004
12Cl:10Na-Ag	156.6±2.6	-0.297±0.127	-0.0019±0.0008	-1.281±0.006	0.640±0.003

occupied states, is indeed observed in Pt. Correspondingly, the projected density of states on O, Cl and Na atomic species, for the 10Na:12Cl-Ag (blue) result downshifted by -1.5 eV (Fig. 5-1).

Observing a charge transfer from the electrolyte solution to the Ag surface similar to that observed on the Pt surface, would have pointed to the inability of the selected DFT functional to describe the role of the metal band structure, and of the Fermi energy/work function.

Table 5.6: Bader excess (nominal-calculated) valence charges in units of $|e|$. In column 'system', the name of the system under consideration, defined by the number of Na^+ and Cl^- ions in solution and the type of metal electrode. In columns 2-6 the total, subsurface and external surface charge and the charge on first and second layer of water in contact with the electrode, respectively. These values are averaged along the trajectory and between the two interfaces present in our cell. Columns "Cl + H" and "Na" report the charge localised around Cl and Na ions. Due to the crude definition of the boundary of the volume defining the Bader charge around each atom, part of the charge actually localised on Cl was accounted by the Bader scheme to the charge of the H atoms pointing towards it. In this table the sum of Cl and this *artificial* H charges are reported. In the last two columns, "Solvation Shells" and "DL", we report the total charge in the first solvation shells of Na and Cl ions and the total charge on the double layer, DL, including electrode, first and second water layer.

System	Metallic electrode			Interfacial water		Ions		Solvation Shells	DL
	Total	Subsurface	Surface	Layer 1	Layer 2	Cl+H	Na		
10Na:12Cl-Pt	-0.03±0.08	1.67±0.05	-1.70±0.06	0.77±0.12	-0.08±0.06	-0.83±0.01	0.9109±0.0004	-1.96	0.65
10Na:12Cl-Ag	1.00±0.06	0.44±0.02	0.56±0.07	0.05±0.01	-0.30±0.07	-0.83±0.01	0.9101±0.0003	-2.06	0.75

Chapter 6

Smaller Simulation Cell

In the chapter 4, we studied a Pt/water interface under bias. We studied the application of a potential by introducing an unbalanced population of ions in the system. We succeeded in that, and then we studied the charge density in the system, water density in solution, the variation of potential inside the electrolytic system, effect on the orientation of water molecule under bias and many other things. In this chapter, we will simulate a smaller system as the larger system was computationally very expensive (It took almost a year to get the 50 ps trajectory and 3 Million hours in terms of CPU hours). We will try to find a small system which can replicate the bigger system so as to save time and increase the efficiency. If we are successful in this endeavour, then reaction pathways and energy profiles for water splitting, modelling explicitly the double layer where this reaction occurs can be done easily and within a very short span of time. Effects of electrode coverage, surface defects on catalytic activity can be done with much ease and with a large number of variations. In the next few sections some convergence test will be done to finalize the size of the system to simulate, then we will start the *ab initio* MD simulation of the smaller system.

6.1 Platinum/Water interface

We start the simulation by finalising a 4 layer system after doing convergency tests. After the basic tests concerning the variation of the energy with the vacuum length above the Pt(111) surface, 15 Angstrom vacuum seemed sufficient to simulate the Pt(111) surface with water. Figure 6-1 shows the comparison of the DOS for the symmetric layers of the slab, it can be seen that for the symmetric layers PDOS superimpose to each other. Then the PDOS[1] of the middle layers of the platinum slab compared with the bulk, in order to verify if the material can mimic the property of the bulk (see figure6-2). The middle layer mimics the property of bulk to a large extent (see figure 6-2), so it can be used for further calculation.

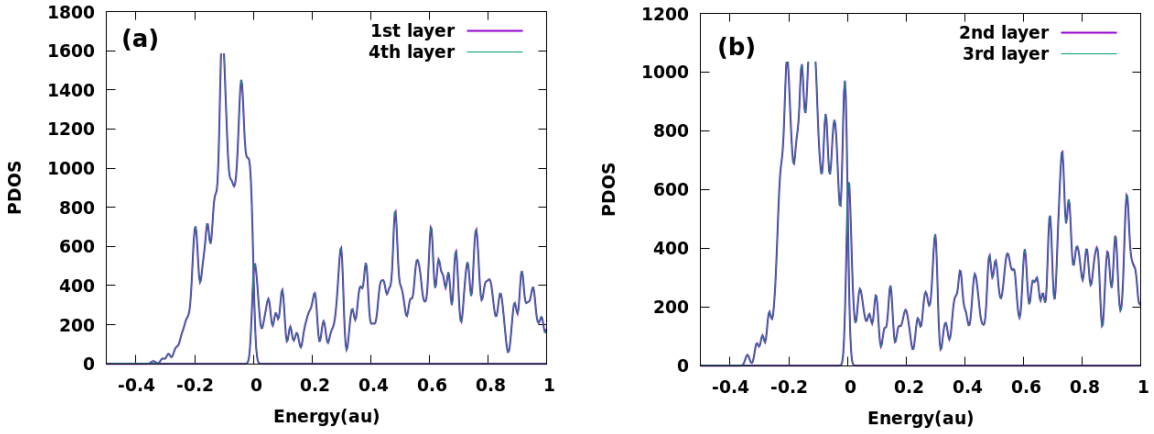

Figure 6-1: Figure shows both the symmetric layer of the smaller system have symmetric PDOS. In (a) PDOS of 1st and 4th layer of the smaller system is comapred and in (b) PDOS of 2nd and 3rd layer of the smaller system is compared.

Few more tests were carried out with a 4 layers Pt(111) slab and H_2O. Four different system were considered using 1, 2, 13 and 26 water molecules on the Pt surface with 15 Angstrom vacuum. Periodic boundary condition (PBC) have been used to avoid finite size effects. First of all the systems were relaxed. Then the potential profile was analysed to see the effect of the water molecules. Then the work function was calculated to observe the effects of the water molecules as well as their orientation on the surface of the material. As

[1]refer 2.2.5 last paragraph for PDOS

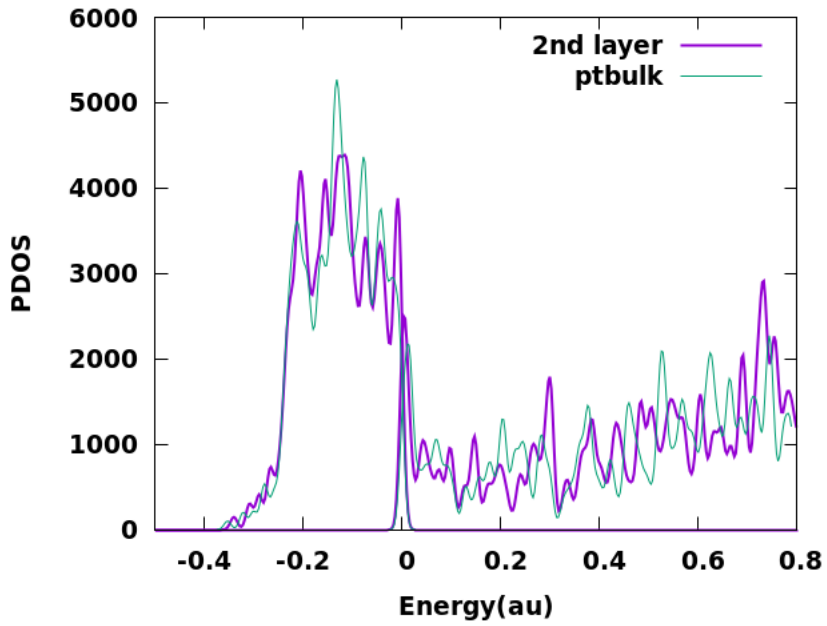

Figure 6-2: Comparison of 2nd layer DOS of the smaller system, with that of the bulk platinum.

it has been already found, the orientation of the water molecules affect the work function of the material[100]. For all the calculations, the top view and side view of the starting configuration as well as the final configuration has been shown in figure 6-3, 6-4, 6-5 and 6-6. The distance of the water molecule from the surface was calculated at the end of the calculation.

Table 6.1 shows the average distance of water molecules in various systems. In $1H_2O$, $2H_2O$, $13H_2O$ system it can be observed that the average distance of the water molecule from the surface is ≈ 3Å, while in $26H_2O$ system due to the large spread of water molecules the average distance from the surface is 4.55Å. Figure6-7 shows graphically the potential profile in different systems, it can be easily seen there is a large drop in the potential when there are more water molecules. In the next part of the study the work function of different systems was analysed as shown in figure 6-8. The figure shows decreasing trend with increasing water molecule number except for the case of 26 water molecules, which shows an increase in work function as compared to 13 water molecules situation. The reason for this behavior is the net dipole moment as shown in the study of Sheng

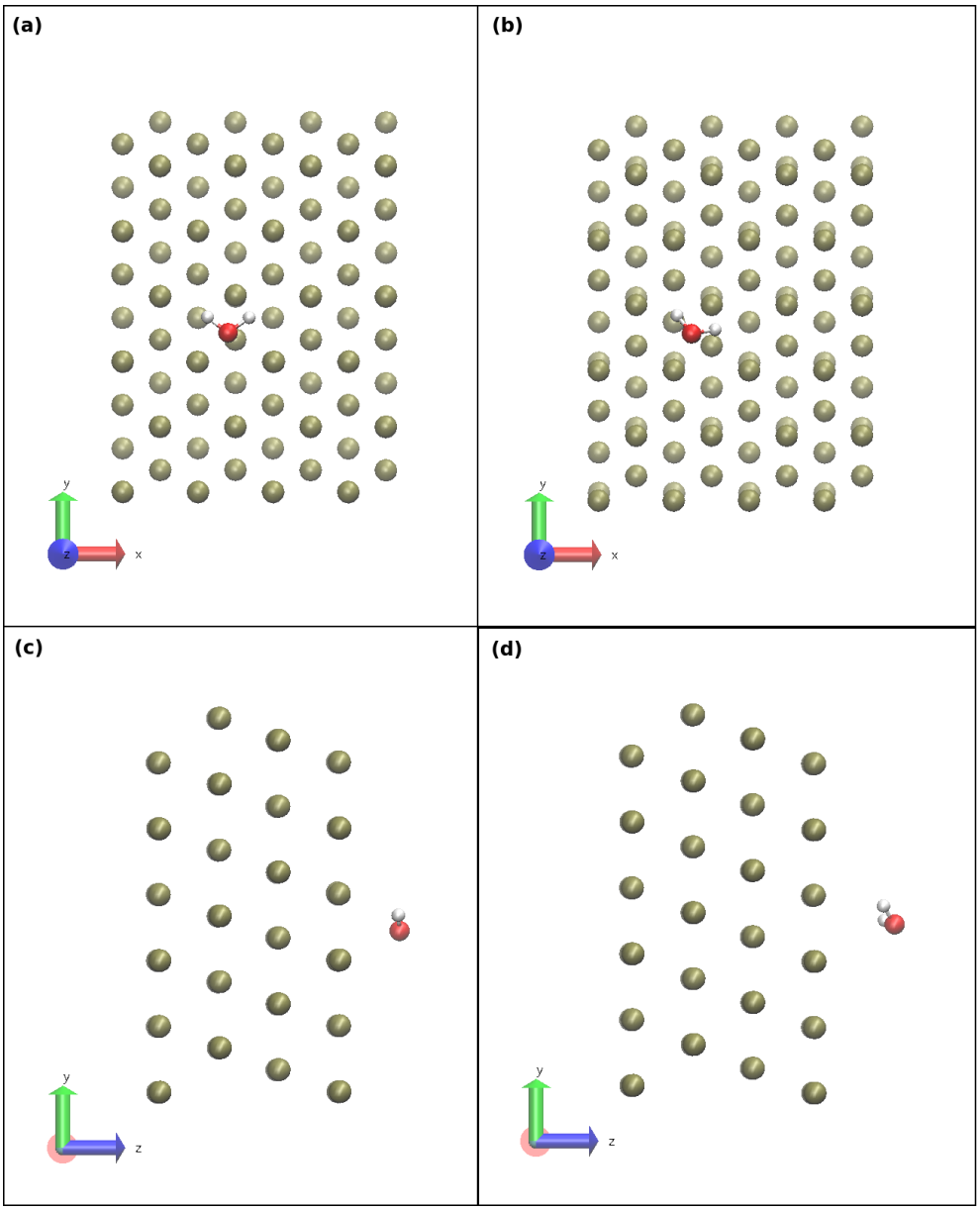

Figure 6-3: Figure shows the relaxation process of a 4 layer platinum (111) slab with 1 water molecule. It shows the orientation of the molecule at the beginning and end of the simulation (after relaxation), (a) shows top view of initial configuration, (b) shows top view of final configuration, (c) shows sideview of initial configuration and (d) shows sideview of final configuration. The red sphere represent the 'Oxygen', white 'Hydrogen' and olive green 'Platinum'.

Meng[100]. We conclude that the orientation of the water molecule has an effect on the work function of the metal as it is related to dipole moment of the molecule on the metal

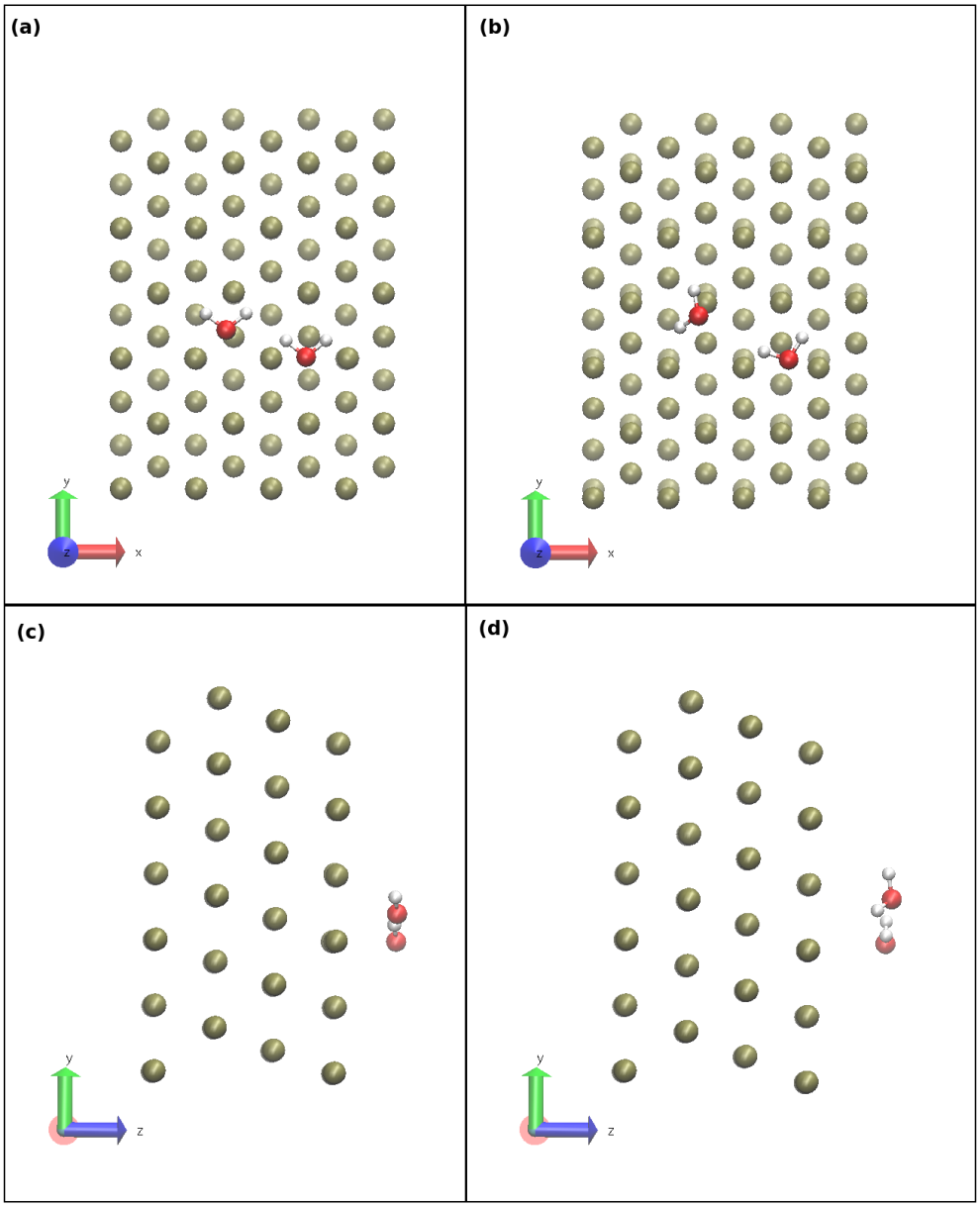

Figure 6-4: Figure shows the relaxation process of 4 layer platinum (111) slab with 2 water molecule, it shows the orientation of the molecule at the beginning and end of the simulation (after relaxation), (a) shows top view of initial configuration, (b) shows top view of final configuration, (c) shows sideview of initial configuration and (d) shows sideview of final configuration. The red sphere represent the 'Oxygen', white 'Hydrogen' and olive green 'Platinum'.

surface.

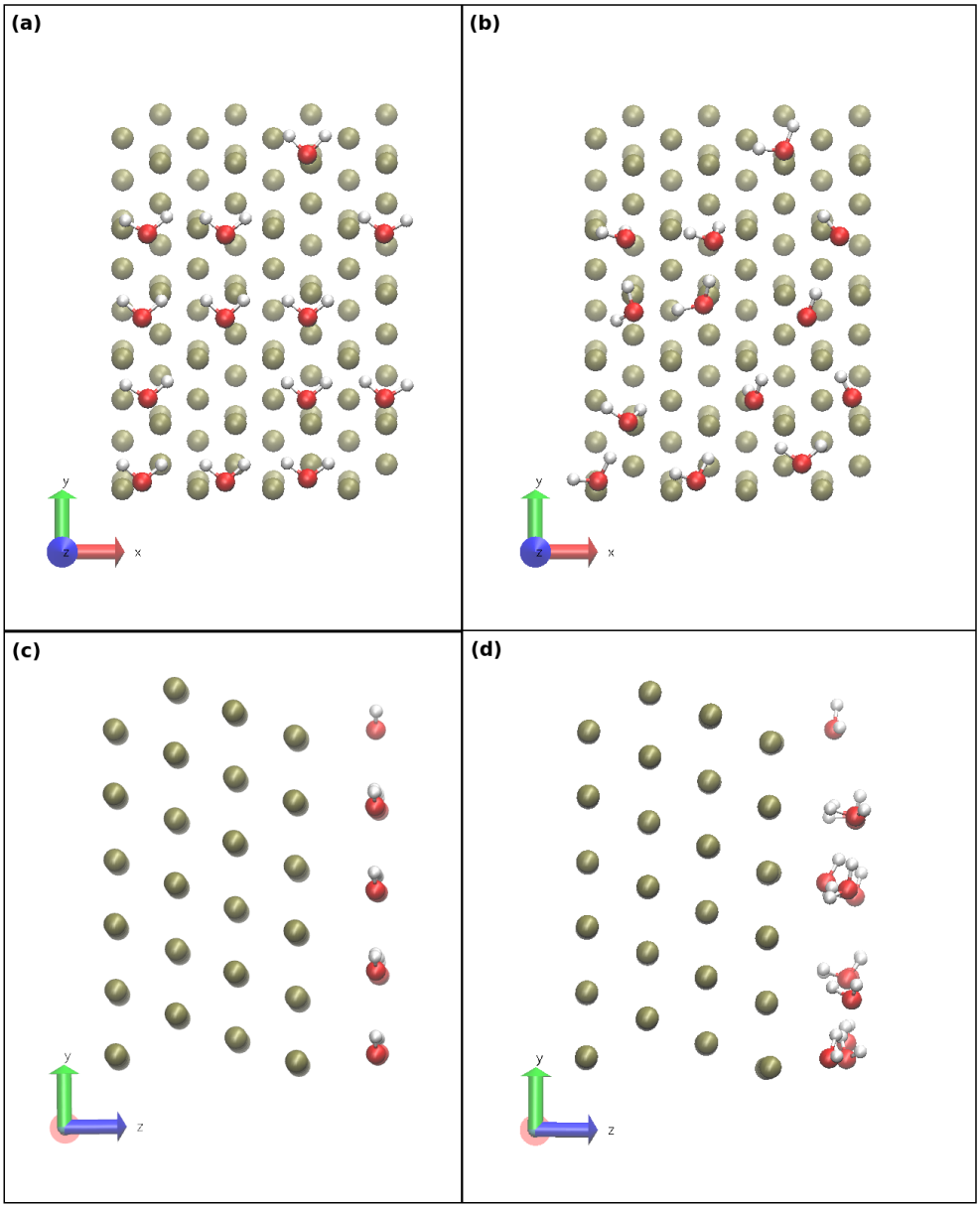

Figure 6-5: Figure shows the relaxation process of 4 layer platinum (111) slab with 13 water molecule, it shows the orientation of the molecule at the beginning and end of the simulation (after relaxation), (a) shows top view of initial configuration, (b) shows top view of final configuration, (c) shows sideview of initial configuration and (d) shows sideview of final configuration. The red sphere represent the 'Oxygen', white 'Hydrogen' and olive green 'Platinum'.

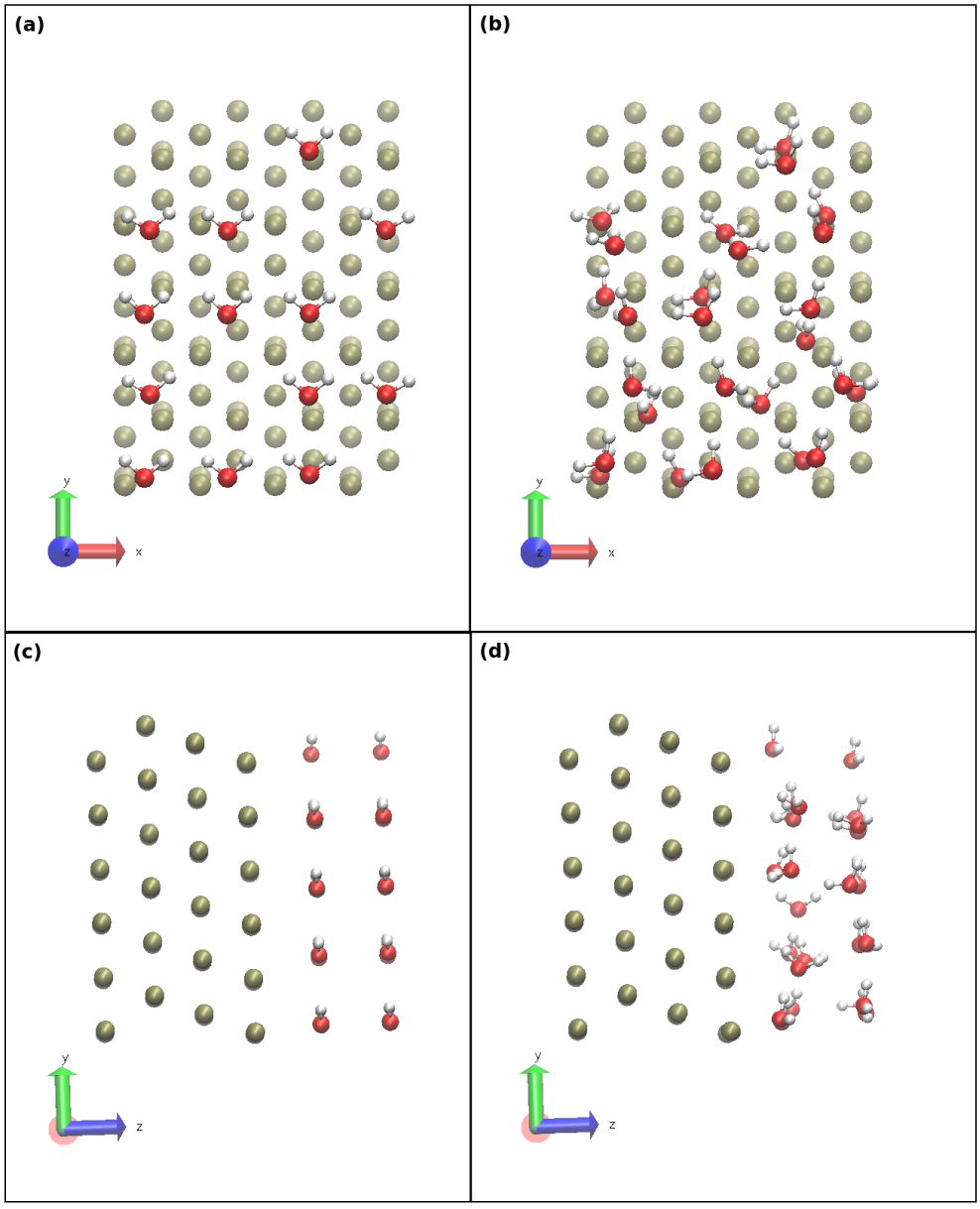

Figure 6-6: Figure shows the relaxation process of 4 layer platinum (111) slab with 26 water molecule, it shows the orientation of the molecule at the beginning and end of the simulation (after relaxation), (a) shows top view of initial configuration, (b) shows top view of final configuration, (c) shows sideview of initial configuration and (d) shows sideview of final configuration. The red sphere represent the 'Oxygen', white 'Hydrogen' and olive green 'Platinum'.

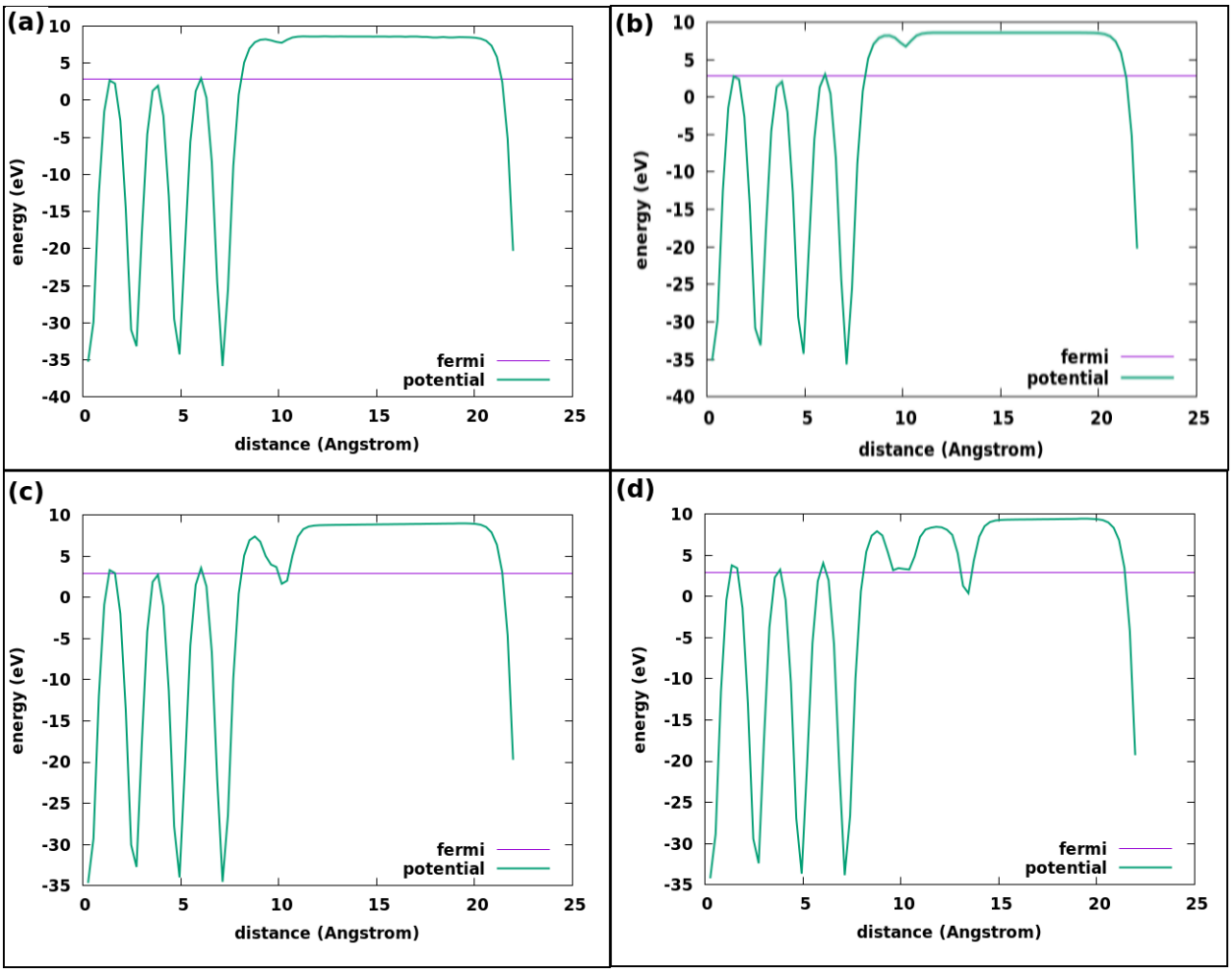

Figure 6-7: Figure shows the average potential profile of 4 layers platinum (111) surface on interaction with different number of water molecules- (a) potential profile of platinum with 1 water molecule on its surface, (b) potential profile of platinum with 2 water molecule on its surface, (c) potential profile of platinum with 13 water molecule on its surface and (d) Potential profile of platinum with 26 water molecule on its surface.

Table 6.1: Average distance of water molecules from Pt(111) surface in various sytem before and after relaxation

System	Initial Distance(Å)	Final Distance(Å)
$1H_2O$	2.27	3.01
$2H_2O$	2.30	3.01
$13H_2O$	3.03	2.97
$26H_2O$	4.57	4.55

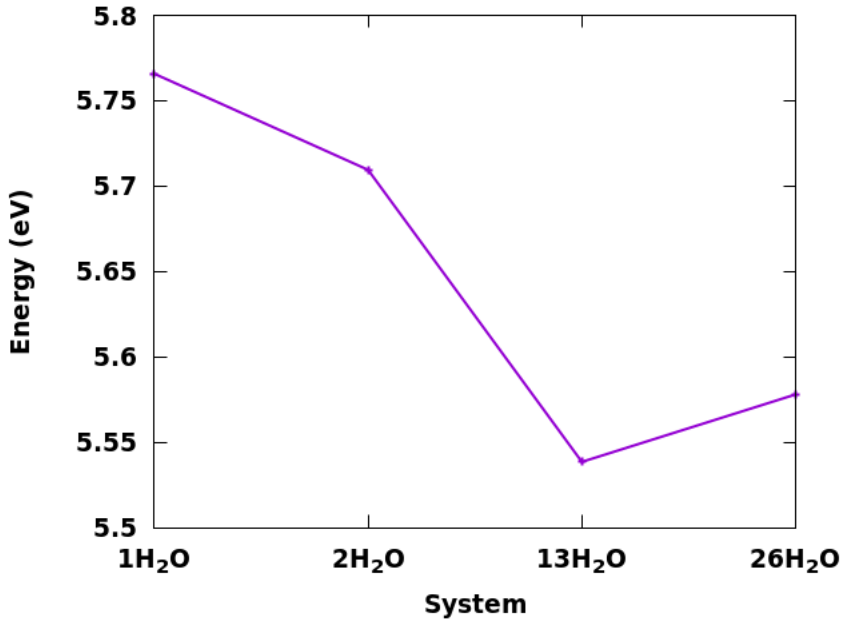

Figure 6-8: Variation of work function of Pt(111) with increasing number of water molecule on its surface.

6.2 *ab initio* MD of smaller Pt/water system

After this initial analysis, we created our final system with 96 Pt atom distributed into 4 layers and 88 H_2O molecules, shown in the figure 6-9 to start the *ab initio* MD. The water is distributed on both sides to cancel the effect of dipole moments. Data here show the simulation for a time of ≈12ps. The density profile of the system was analysed after the simulation as shown in figure 6-10. The density has been measured from the surface. The figure clearly shows two distinct peaks corresponding to the first and second layer of water, the peak distribution on the left has distinct peaks compared to the right side which is diffused. We analysed the potential profile of the system as shown in the figure 6-11, it clearly shows uniformity in distribution of the potential across the surface as it can be seen a similar type of potential profile on both side of the surface reaching a constant value far from the surface.

Table 6.2: Excess of Bader charges in the first layer of the water near the electrode. Water No., Total-Water, Avg.-Water, O and H represent the average number of water molecules, the total charge on the water layer, the average charge per water molecule, the average charge per O and H atoms, respectively (for the small system).

Water layer	Water No.	Total-Water	Avg.-Water	O	H
1^{st} Layer	2.6±0.4	0.30±0.04	0.12±0.01	-1.22±0.11	0.66±0.06
2^{nd} Layer	7.5±0.8	0.02±0.05	0.003±0.006	-1.28±0.17	0.65±0.09
Rest of water	33.8±0.6	-0.01±0.03	-0.0002±0.0009	-1.27±0.09	0.63±0.05

Table 6.3: Bader excess (nominal-calculated) valence charges in units of $|e|$ per unit area of electrode in units of Å ^{2}, for electrode is compared under the section of Metallic electrode, then Interfacial water. Finally the number of interfacial water molecules per unit area in units of Å ^{2}, under the Water No. (see figure 6-12 for more detail).

System	Metallic electrode			Interfacial water		Water No.	
	Total	Subsurface	Surface	Layer 1	Layer 2	Layer 1	Layer 2
Bigger System	-0.0020	0.0058	-0.0078	0.0022	-0.00031	0.021	0.088
Smaller System	-0.0020	0.0060	-0.0080	0.0018	0.00015	0.016	0.044

Finally, Bader charge analysis was performed and the results are shown in the table 6.2, and the graph corresponding the table, figure 6-12. By comparing this curve to the correspondingly larger system analysed in section 4.3.2, only difference which can be

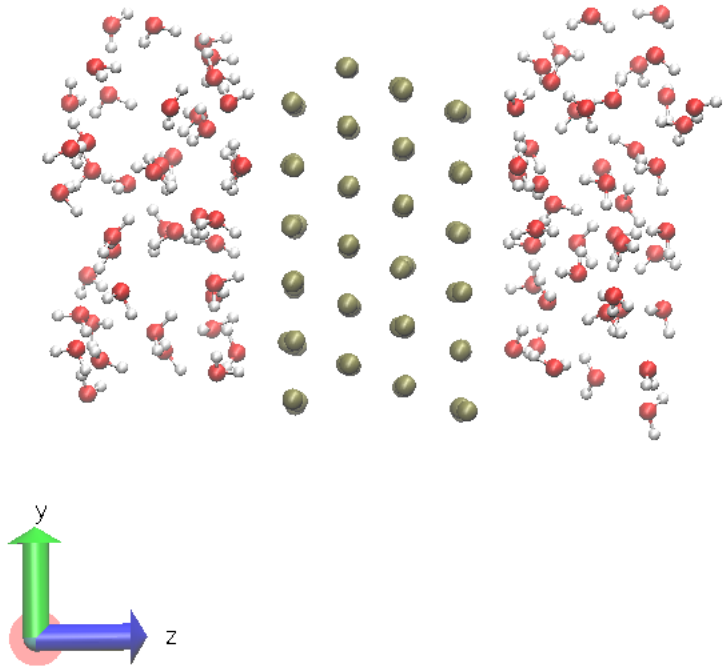

Figure 6-9: Distribution of water molecules on both side of Pt(111) surface, in new smaller system. The middle layers of the slab are fixed. The red sphere represent the 'Oxygen', white 'Hydrogen' and olive green 'Platinum'

noticed inside the second layer of water molecules. The second layer has a slightly negative charge in case of the larger system while it's slightly positive over here. To do a better comparison we analysed the values per unit area of the smaller as well as the larger system as shown in the Table 6.3. It can be seen from the table 6.3 that the total charge density on the electrodes in both cases is the same. As we move gradually to the first water layer the charge densities are similar, but differences appear in the second layer. The small

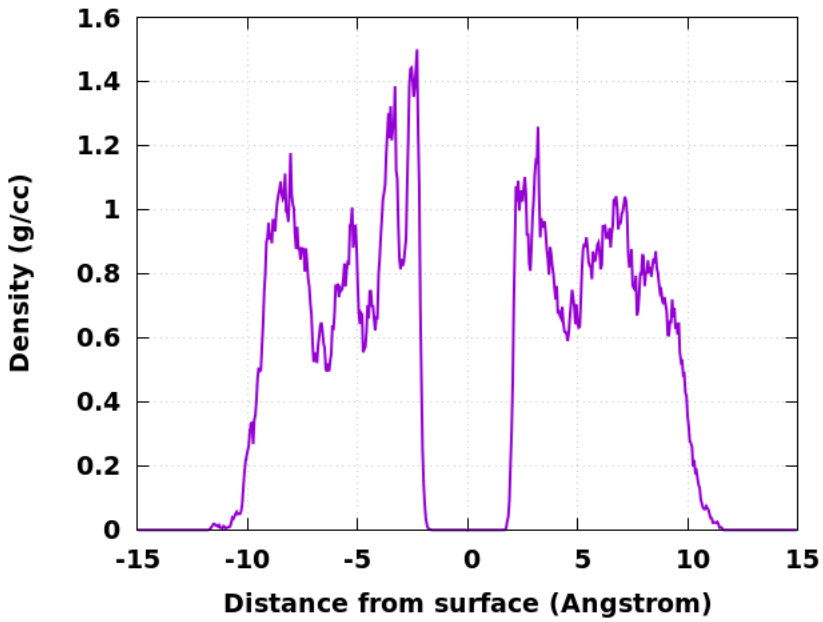

Figure 6-10: Distribution of water density in smaller system, measured as distance from the surface (surface=0Å)

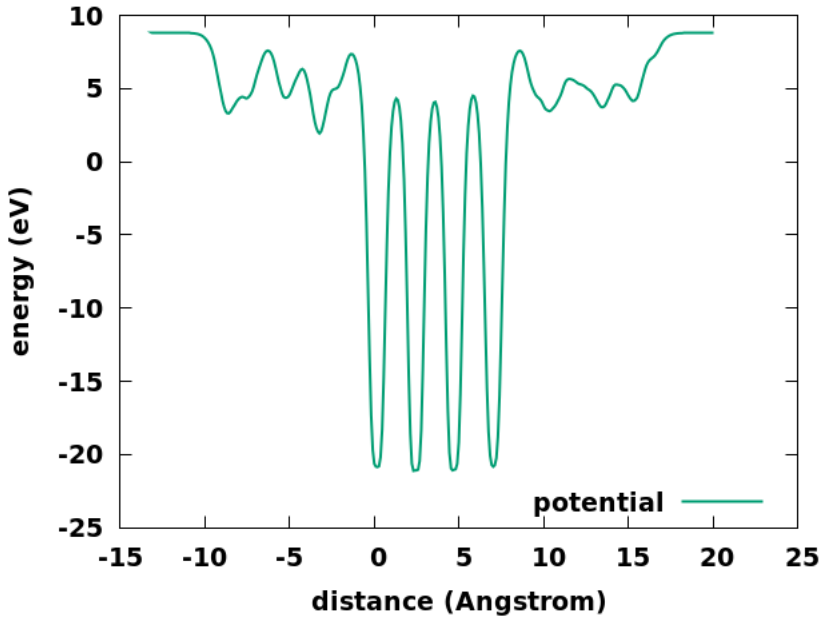

Figure 6-11: Average potential profile of Pt(111)-water (small system). The potential shows uniformity on both side of platinum surface.

system presented a less water density compared to the large system. In the large system, the average charge on the water in the first layer was $0.1|e|$. In the smaller system the

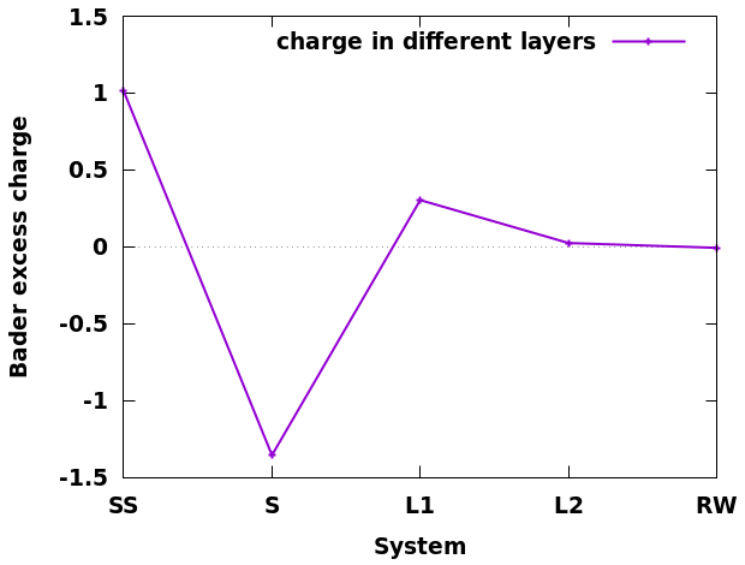

Figure 6-12: Charge variation in the small system, starting from the subsurface platinum layer (SS), surface platinum (S), first layer of water (L1), second layer of water (L2), rest of water (RW).

average charge on water in first layer is $0.12|e|$, which is an acceptable criteria. As we move further away in the system towards the second layer the differences start to increase. The nature of the charge is same in first and second layer of the small system, whereas we found oscillating nature of the charge in the large system. The average charge on water in the second layer in the small system has been reduced by one third of that of larger counterpart. From all this, we can conclude that the smaller system is good for studying surface properties involved with interaction of the first layer of water and metal electrode as it has been able to replicate the water density as well as charge density of the larger system. The small system needs an extension in the Z direction by adding more amount of water layer so that it can be represented correctly as in the present case there were not sufficient water molecule to study the second layer correctly. It was also found that charge on the subsurface and surface of smaller system electrode is very close to that observed in the larger system. The orientation of water molecule in the first layer of the smaller system is same as that of the larger system. From all these observations we can finally say that small system is sufficient to study the first layer of water in contact with an electrode.

Chapter 7

Conclusion and Future work

7.1 Conclusion

We started our simulation by doing convergency test to find the suitable parameters and we found that 8X8X8 K points are sufficient to model the platinum bulk and platinum surface. 7 layers of platinum best describe the surface as the bulk condition was reached in the middle of the slab but it was computationally very expensive so we used 4 layer platinum and fixing the middle layers to the bulk value and it was able to represent the surface correctly.

Work function 7 layers platinum Pt(111) and Pt(001)found to be 5.70eV and 5.69eV respectively. Work function 4 layers platinum Pt(111) and Pt(001)found to be 5.69eV and 5.63eV respectively. Which is in accordance with the other studies.

We started our study of electrode under bias by introduction of imbalanced population of ions in Pt/water, we created 12Na:10Cl, 10Na:10Cl and 10Na:12Cl systems. They are expected to generate a charge of -1, 0 and +1 |e| on each electrode surface, respectively. Correspondingly, a net +2, 0 and -2 |e| charge would be localised on the excess ions in solution (our system is globally charge neutral). However, deviations from this idealised picture are observed consisting in a charge transfer between the electrolyte solution and the Pt electrode. In particular, the charge on the electrode side of the DL amounts to -1.1, -0.6 and -0.03 |e|, the overall charge on DL amounts to 0.65, -0.28 and 1.5 |e|, for the

12Na:10Cl, 10Na:10Cl and 10Na:12Cl systems, respectively.

The density of first water layer is inversely proportional to the negative charge on the surface of the electrode, as the density of the first layer of water was lowest in the case of 12Na:10Cl and highest in the case of 10Na:12Cl. While the density of the second layer remains unaffected.

The orientation of the molecules in the first layer of water is independent of the status of charge, while the orientation of water molecule in the second layer is highly dependent on the charge on electrode. With increase in negative charge on the electrode there is increase in orientation H of water molecule in second layer towards the surface.

The charge density in first layer of water is highly responsive to the status of the charge on the electrode, so any change in the status of charge has immediate effect on the charge and density of first layer of water.

The charge in electrolytic system is spread in the system contrary to initial believe of charge being confined in the double layer.

Charge in the solvation shell of Cl, as well as Na has constant value of 0.8|e|, irrespective of the status of charge of the electrode.

The density of water is high close to the electrode surface, and its value changes to 1 g/cc as one goes in the middle.

Comparing the 10Na:12Cl-Pt and 10Na:12Cl-Ag systems, it can be seen that the Pt has more number of water molecules in the first layer compared to the Ag as the Pt is more electronegative. At the same time we note that the average charge on water is very similar in all Pt systems, thus differently charged electrode induce same charge per unit water (0.1|e|) in the first layer near the electrode while in the case of silver it's ten time lesser (0.01|e|), clearly showing the role of electronegativity. The charge distribution in the water molecule is more polarised in case of the Ag electrode. In first layer the water is polarised in such a way that the O atoms are slightly less negatively charged and the H atoms are slightly more positively charged than the average free water molecule. Overall the water molecules are positively charged. The charge on the electrodes of Pt and Ag are 0.03|e| and 1.0|e|, the reason being electronegativity of the electrode is playing a big

role in distribution of charge on the surface as well as in its vicinity. The charges in the solvation shell are unaffected by the nature of electrode as well as the status of charge as it can be seen in all the systems.

Now a few points about the small system: Before starting the *ab initio* MD we studied the surface coverage of Pt system (by putting a different number of water molecules on its surface). The work function shows a decreasing trend with increasing coverage, this result is similar to the study done by Sheng Meng [100]. Small system (constructed with 88 water molecules and 96 Pt atoms) mimics remarkable property of the large system studied (has 256 water molecules and 168 Pt atoms). After doing *ab initio* MD of the small system, we studied water density profile, which clearly shows the presence of the first layer of water, while the second layer is not very prominent due to the small size of the system.

To do a better comparison we analysed the values per unit area of the smaller as well as the larger system. We found that the total charge density on the electrodes in both cases is the same. As we move gradually to the first water layer the charge densities are similar, but differences appear in the second layer. The small system presented a less water density compared to the large system. In the large system, the average charge on the water in the first layer was $0.1|e|$. In the smaller system, the average charge on the water in the first layer is $0.12|e|$, which is an acceptable value. As we move further away in the system towards the second layer the differences start to increase. The nature of the charge is the same in the first and second layer of the small system, whereas we found the oscillating nature of the charge in the large system. The average charge on water in the second layer in the small system has been reduced by one-third of that of larger counterpart. It was also found that charge on the subsurface and surface of smaller system electrode is very close to that observed in the larger system. The orientation of water molecule in the first layer of the smaller system is same as that of the larger system.

From all this, we can conclude that the smaller system is good for studying surface properties involved with interaction of the first layer of water and metal electrode as it has been able to replicate the water density as well as charge density of the larger system.

The small system needs an extension in the Z direction by adding more amount of water layer so that it can be represented correctly as in the present case there are not sufficient water molecules to study the second layer correctly. This smaller system is not good for mimicking the system beyond the first water layer as it has a large difference in its charge as well as the water density distribution starting from the second layer.

7.2 Future work

In my PhD work, I extended the standard simulation methods towards a more realistic representation of the double layer of Pt-water solution interface and the effect of the application of bias on its structure. I substantially contributed to developing this model by revealing the structure and charge distribution in our complex model for Pt-water interface. However, the developed model is computationally very demanding and cannot be used straightforwardly to address water splitting. We used the knowledge about Pt water interface (acquired during the first part of my work) to develop simplified model systems to study water electrolysis in the form of a smaller system. We will like to move towards a more realistic description of the double layer of Pt-water interface, so in this context, the majority of the work should be dealing with the simulation of water splitting (in close proximity of the experiments). Our future work will be majorly based on the study of following:

1. Ions:

   As electrons help in conducting electricity in the solids, ions help to conduct electricity in the electrolytic solvent. The significant difference between ions and electrons is that the electrons have the same properties irrespective of the nature of the materials, whereas the ions have different shapes, size, charge, electronegativity, in this way studying of ions are very important. In solids the concentration of free electrons define the conductivity but in the electrolytic solution, there is not a general simple rule and conductivity depends on a lot of factors. The study of the ions can be broadly categorized as:

(a) Different types of ions will be introduced in solution e.g.(Sodium, Potassium, Hydronium, Chlorine, Bromine, Iodine, Hydroxyl). Effect of these ions will be studied on the electrolytic process.

(b) Mostly in experiments alkaline environment is used for the electrolysis of water, therefore dedicated model of solution hydroxyl ion will be addressed

(c) Effect of varying the concentration of unbalanced ions on the electrolyte and their effect on the state of charge (potential) of the electrode.

2. Electrode Surface:

This is a very important part of the electrolytic system. Usually, the electrodes are metals. They are the medium through which the potential is applied to the electrolyte. Their properties affect the response of the electrolyte. The general properties of the electrode can be broadly classified into:- conductivity, corrosion resistance, hardness, formability. The electrode is the place where both reactions of charge-transfer and mass transfer take place. To this end, it is very important to understand the properties and working principle of a surface. Experiments have been carried out to understand the nature of surfaces by using techniques like:- scanning probe microscopy, surface X-ray scattering and cyclic voltametry. But yet much has to be done to unreveal the process underlying for electrode functionality in its environment. The proper modelling of the electrode and interface is the most important among all, we will focus on:

(a) Relation between activity and surface orientation.

(b) Effect of work function of electrode on electrolytic interface.

(c) Equilibrium structure of the double layer with variation of applied potential.

(d) Reaction pathways and energy profiles for water splitting modelling explicitly the double layer where this reaction occurs.

(e) Effects of electrode coverage, surface defects on catalytic activity. Putting together the knowledge obtained from the analysis of different aspects of elec-

trolytic problem, it will be possible to develop comprehensive models for charge and mass transfer on model. A system of this kind is shown in the figure7-1 [11][12].

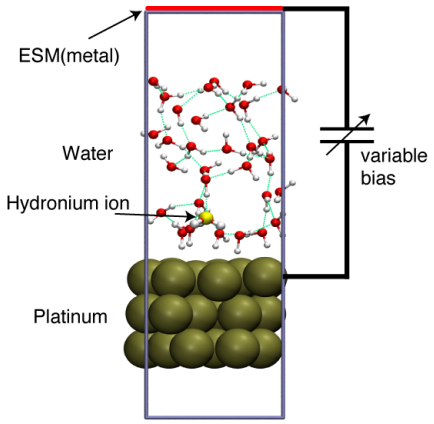

Figure 7-1: Electrolytic cell in working condition [11, 12]

Appendix A

Water Molecule

The first model system studied is an isolated water molecule. This was characterized in terms of geometrical structure and Bloch states. The isolated water molecule was modeled by using a supercell approach, where a water molecule was placed in a cubic box in vacuum periodically repeated to represent isolated molecules. The vacuum volume included in the cell must be large enough so that the different replicas of molecule do not interact with each other (with increasing the box size there is decreased interaction due to the periodic boundary conditions). We need to select a relevant quantity (the total energy) and look at its convergence as a function of the box size.

The first convergence test on the water molecule was performed by studying the total energy versus the energy cut-off. The energy cutoff is a parameter indicating how complete the plane wave basis set is. The larger it is, the more accurate is the representation of the electronic wave function, and more computationally demanding is the calculation. There is need to determine the minimum energy cut-off which serves the purpose in order to save computational time. This is similar to the calculation of sin(x) using Taylor expansion, as we keep adding the terms the precision keeps on increasing but there is no need to use infinite number of terms, we can stop at the number which gives the desired precision for calculation. Selecting an energy cut off introduces an error into the calculation. To have the error within given limits, a convergency test is done to find the appropriate value of the cut-off. We calculated the convergence of the energy vs energy cut-off and cell size

(Fig: A-1) and versus the box-size (Fig: A-2). The error ΔE is defined as the difference in the total energy from the corresponding higher energy cut-off and higher lattice parameter (for example in Fig: A-2 it is the difference in the energy value of two consecutive lattice sizes i.g. 7.94Å and 5.29Å, 10.58Å and 7.94Å...). When ΔE has the value less than 0.0136 eV, the box size corresponding to that will be used for further calculation.

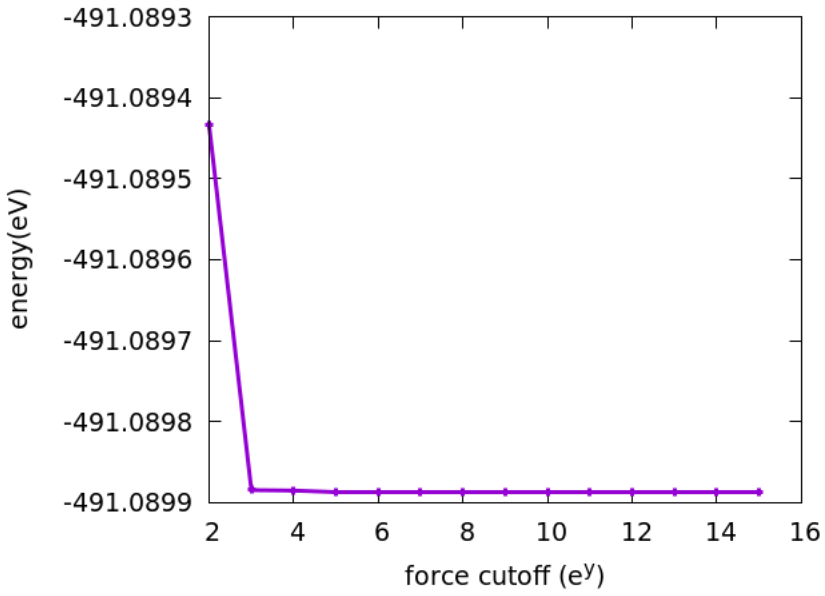

Figure A-1: Shown is the convergence of total energy as a function of force cutoff of a water molecule at a fixed box size.

In order to get an idea about the variation of the ΔE the curve Fig:A-3 was plotted. There is fluctuation in the value of ΔE in the range of -0.03 to +0.03 eV. There is fluctuation due to the error introduced through energy cut-off. The error in the evaluation of the total energy becomes less than the threshold of 0.013 eV at 13.2Å. So, we conclude that including 13.2Å of vacuum is large enough to represent isolated molecules. To check the electronic structure of the molecule, the electron density of the water molecule was also studied, which was generated by the DFT calculations of water molecules.

The study of the electron density helps in the understanding of the double layer and the solvation shell in the electrolyte. In fact we will be able to correlate this up with the orientation of water molecules and the charge/potential nearby it. The orientation of

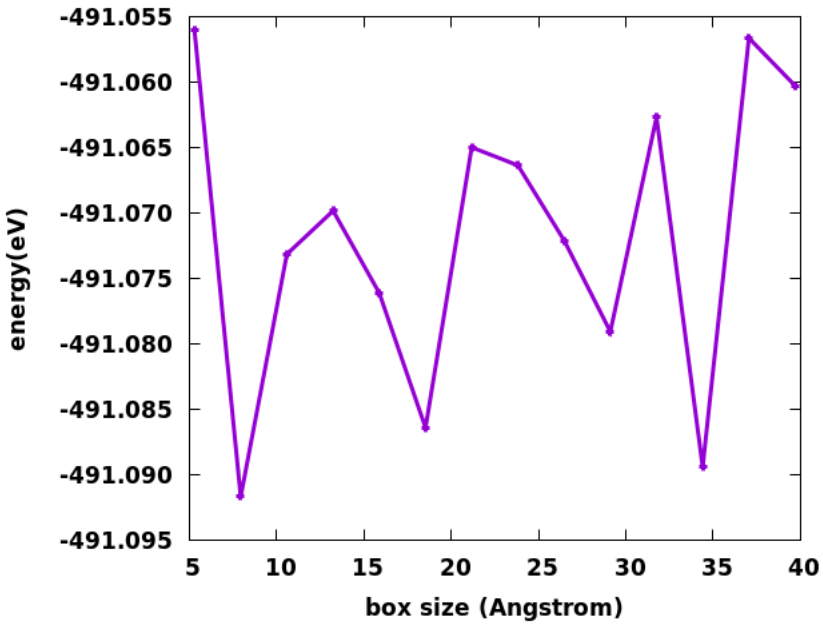

Figure A-2: Shown is the plot of variation of total energy of a water molecule as a function of box size.

water molecule with an electrode under bias can also be easily understood by knowing the charge density profile of the water in that given situation, it can also help in understanding the bond formation and bond breakage. As there are 8 electrons in a water molecule they will occupy the 4 orbitals. The single particle charge density isosurface are shown in figures A-4 and A-5. It is plotted using elecron density data obtained from DFT. The red and gray spheres are used to represent Oxygen and Hydrogen respectively.

In Fig: A-4(a), the charge density is spherical around the O, orbitals 2 to 4 have a P character in particular. In Fig: A-4(b), the charge density is confined in the O-H bond region. In Fig: A-4(c), the charge density is confined in the region between the hydrogens and opposite to it. In Fig: A-4(d), which is the HOMO (highest occupied molecular orbital) of the water molecule the density has a dumbbell shaped, and the bloch density is concentrated in the direction perpendicular to the plane of the bond. This may be useful in understanding the approach of an electrophile.

Fig: A-5 shows the charge density of the unoccupied orbitals of the water molecule. The important one is depicted in Fig: A-5(a). This is the LUMO (lowest unoccupied

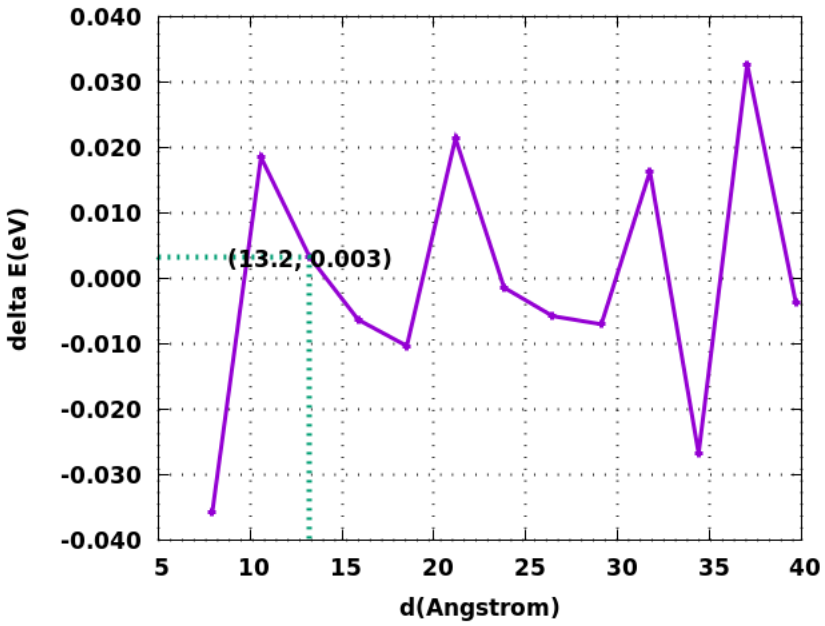

Figure A-3: Shown is the graph of ΔE as a function of box size for the water molecule, it can be seen that the ΔE fluctuates around 0

molecular orbital) of a water molecule.

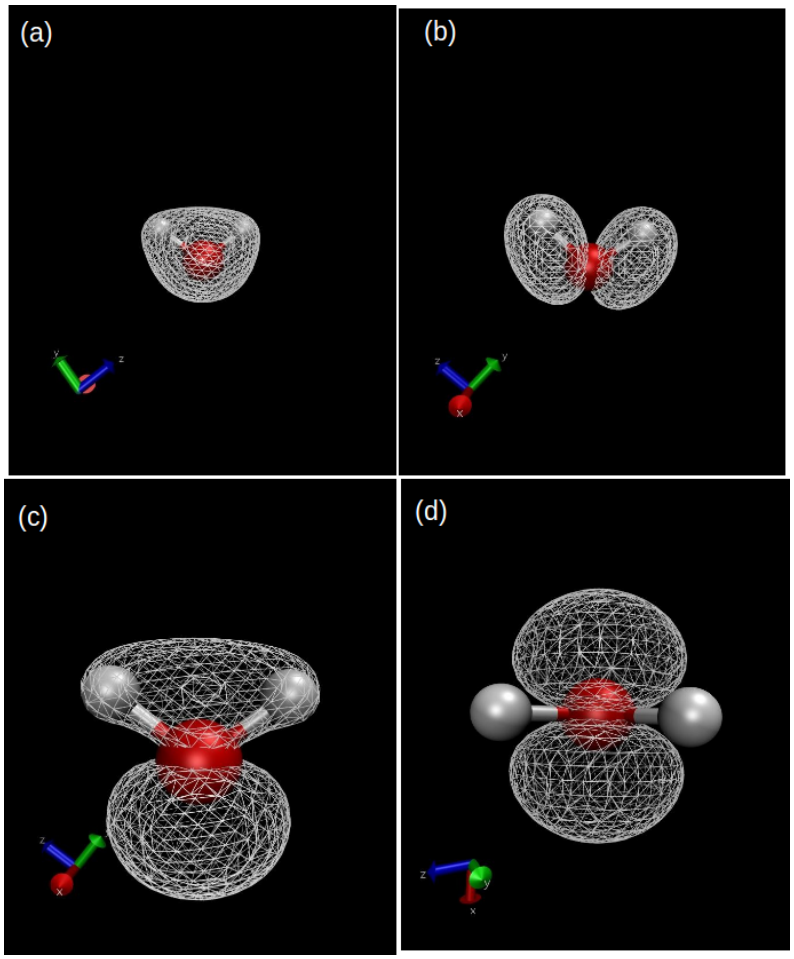

Figure A-4: Shown are the charge density isosurface of the occupied molecular orbitals of water, starting from lowest energy (a) to highest (d).

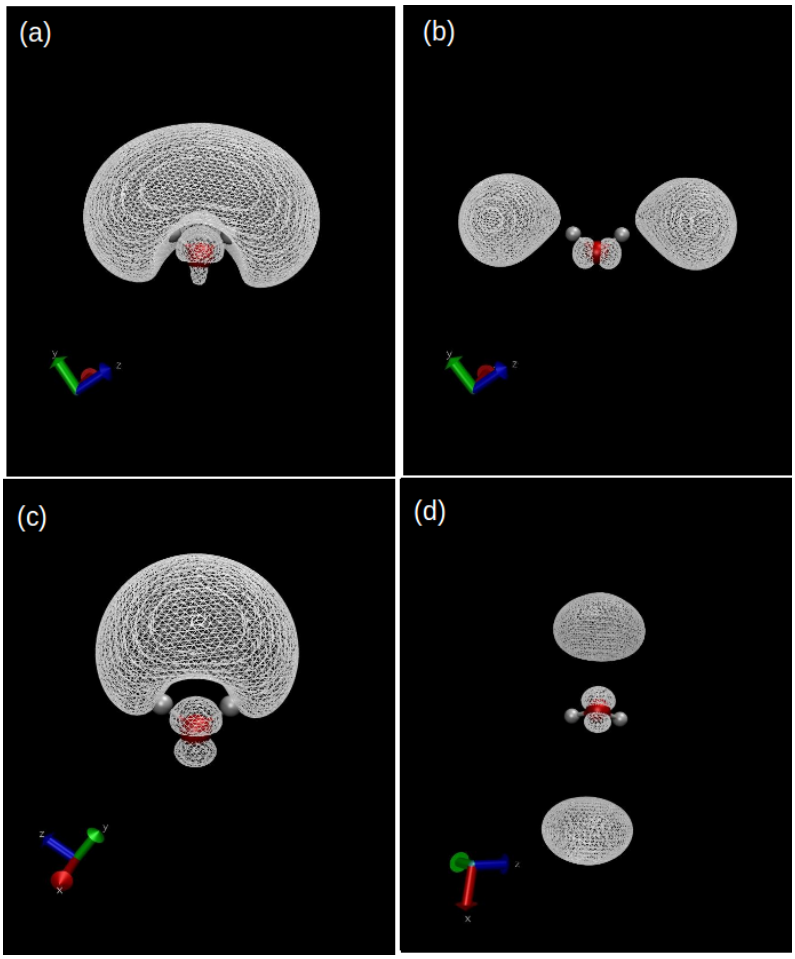

Figure A-5: Shown are the charge density isosurface of the unoccupied molecular orbitals of water starting from lowest energy (a) to highest (d).

Appendix B

Sum-Frequency-Generation Spectroscopy (SFG)

Is a tool used to characterize complex sample surfaces and interfaces. SFG vibrational spectroscopy has a advantage over the many techniques used to study interfaces is its unique ability to give details up to molecular levels. SFG uses second order nonlinear vibrational spectroscopic technique. The second order nonlinear effect allows for SFG to selectively probe interfaces in the regions where centrosymmetry is broken. SFG being a laser based vibrational spectroscopic technique allows to study complex interfaces in-situ. SFG has been successfully applied to study various systems including polymers, biomolecules, nanoparticles, ionic liquids and inorganic molecules. Here we discuss a surface-sensitive-Vibrational Density of States (ss-VDOS) which has been used to study the orientation of the O−H bonds and their environment. This methodology has been already successfully used to reproduce the Sum-Frequency-Generation (SFG) spectra at the water/CaF_2 interface [93].

ss-VDOS

In this method, we simulate the second order susceptibility tensor ($\boldsymbol{\chi}^{(2),R}$), the main

contribution to the SFG signal [101, 102, 103, 104]. In the classical limit [102], the PQR element of this tensor is obtained by evaluating the correlation function between the polarizability A_{PQ} and the dipole moment M_R:

$$\chi^{(2),R}_{PQR}(\omega) = \frac{i}{\omega T}\int_0^{+\infty} dt \exp(i\omega t)\langle \dot{A}_{PQ}(t)\dot{M}_R(0)\rangle \tag{B.1}$$

$$\approx \frac{i}{\omega T}\int_0^{+\infty} dt \exp(i\omega t)\langle \dot{\alpha}_{PQ}(t)\dot{\mu}_R(0)\rangle \,, \tag{B.2}$$

where P, Q, R are respectively the polarisation of the SFG, visible and IR beams, $\boldsymbol{\alpha}$ and $\boldsymbol{\mu}$ are the molecular polarizability tensor and the molecular dipole moment of a water molecule, respectively; ω is the frequency of the IR beam and $\langle \ldots \rangle$ stands for statistical average.

In our model, $\dot{\boldsymbol{\alpha}}$ and $\dot{\boldsymbol{\mu}}$ are obtained by a first order approximation based on the velocity, the orientation of the O$-$H bond and a parametrization of $\frac{\partial \boldsymbol{\alpha}}{\partial \mathrm{O}-\mathrm{H}}$ and $\frac{\partial \boldsymbol{\mu}}{\partial \mathrm{O}-\mathrm{H}}$. In proximity of an O$-$H bond, $\dot{X} = \{\dot{\alpha}, \dot{\mu}\}$ can be expressed as

$$\dot{X}(\omega) \approx x'(\omega)\frac{\partial X}{\partial \mathrm{O}-\mathrm{H}}\frac{d\mathrm{O}-\mathrm{H}}{dt} \,, \tag{B.3}$$

with $x'(\omega)$ being a linear function used to take into account the non-Condon effects [105, 101].

Appendix C

Solvation shell

Water being a polar solvent interacts differently with polar/ionic and nonpolar substances. In water there is a slightly positive charge on hydrogen atoms (usually represented by $\delta+$), and there is a slightly negative charge on the oxygen atom (usually represented by δ-). The charge difference makes the water polar and responsible for different interactions with cations and anions, while interacting with cations it forms a three dimensional spherical structure around with its oxygen pointing towards the cation while hydrogen atoms away from it, a two dimensional representation of it is shown in the figure C-1(b). While interacting with the anions it again forms a three dimensional spherical structure which has one hydrogen atom pointing towards the anion, a two dimensional representation is shown in the figure C-1(a). Therefore to study the solvation shell of anions and cations one need to plot the radial distribution function plot for hydrogen and oxygen with the respective ions being centre. The first minima of the G(r) curve is taken as cut off distance as it gives the distance which is suitable for calculating the total number of molecules in that solvation shell. Figures C-2 and C-3 show the radial distribution function of Cl-H and Na-O respectively.

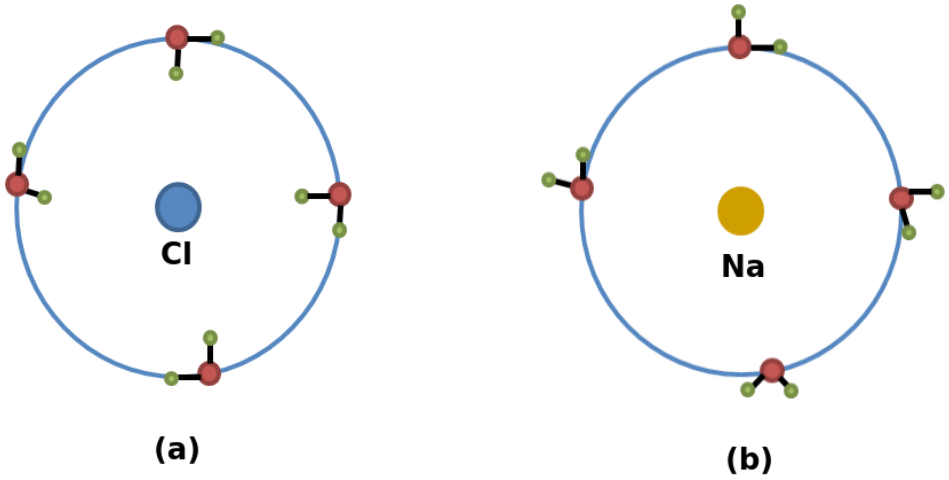

Figure C-1: The figure shows the solvations of anion (Cl) and cation (Na). It can be easily seen that in the anion solvation shell '(a)' hydrogen of water molecules are pointing towards Cl, while in the cation solvation shell '(b)' hydrogen of water molecules are pointing away from Na. Due to the polar nature of water molecule it is behaving in such a way.

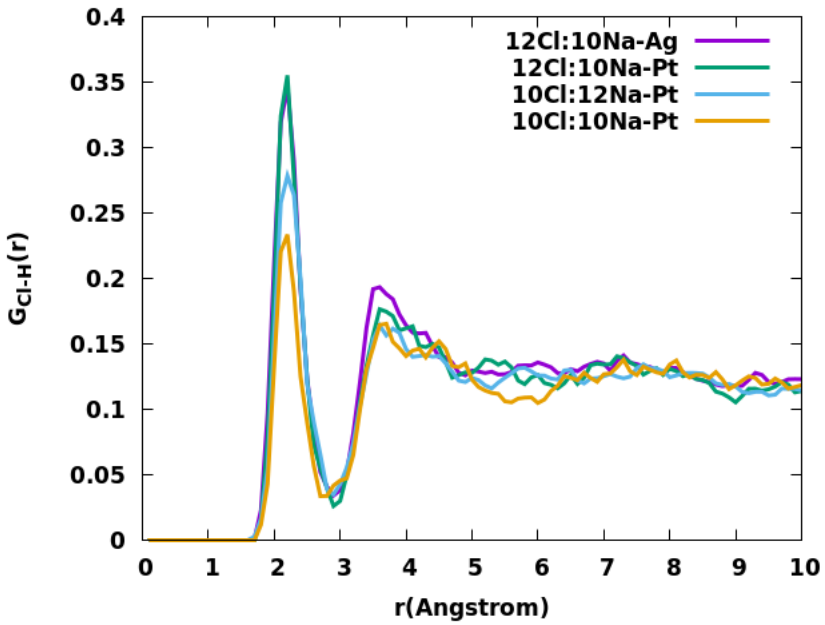

Figure C-2: The figure shows the radial distribution function of different systems for Cl-H. The first minima of G(r) curve is taken as cut off distance, defining the solvation shell.

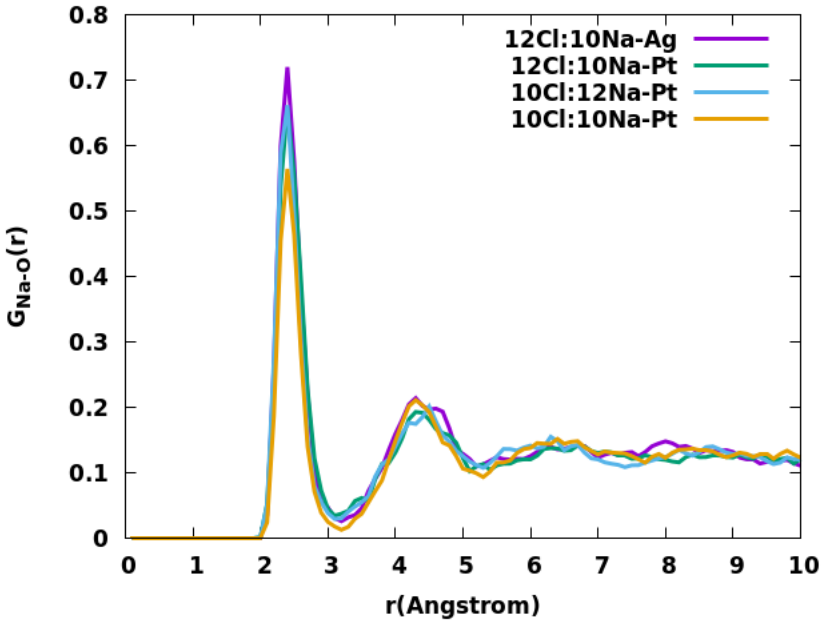

Figure C-3: The figure shows the radial distribution function of different systems for Na-O. The first minima of G(r) curve is taken as cut off distance, defining the solvation shell.

Appendix D

Timestep and K points

The timestep plays an important role in the MD simulations, so the selection of timestep should be done carefully otherwise it will lead to so many errors. Ideally, we should choose the longest time step as a smaller time step is inefficient (as it has longer calculation time compared to the smaller counterpart). Unfortunately, at larger time step MD integration becomes unstable with a sudden increase in energy with time, disturbing the normal structure of the atoms. Therefore it's necessary to find the appropriate one which is neither very large nor small, it's found by doing some trial runs with different time steps.

We know that by virtue of Bloch's theorem integrals in real space over the (infinitely extended) periodic system are replaced by integrals over the (finite) first Brillouin zone in reciprocal space. Such integrals are performed at a finite number of points in the Brillouin zone, called the K-point mesh by summing the function values of the integrand (for instance: the charge density). The convergence of the results are achieved by choosing a sufficiently dense mesh of integration points, therefore one of the major objective in convergency test to find a sufficiently dense mesh which can give a result within desired error limit, as denser mesh are computationally expensive. One important point to note is there is no variational principle governing the convergence with respect to the k-point mesh (e.g. total energy does not necessarily show a monotonous behaviour when the k-point mesh density is increased).

Appendix E

Publications

Manuscript stemming from this work:

1. The nanoscale structure of the Pt-water double layer under bias revealed: *Remi Khatib, Ashwinee Kumar, Stefano Sanvito, Clotilde S. Cucinotta and Marialore Sulpizi* (under revision 'npj Computational Materials').

2. Using first-principles molecular dynamics study to construct a very efficient electrolytic system : *Ashwinee Kumar, Stefano Sanvito, Clotilde S. Cucinotta* (in preparation).

Bibliography

[1] Y. Tamura, M. Takabayashi, and M. Takeuchi. The spread of fire from adjoining vehicles to a hydrogen fuel cell vehicle. *Chemical Reviews*, 39:6169–6175, 2014.

[2] M. A. Saleem, V. Desmaris, and P. Enoksson. Performance enhancement of carbon nanomaterials for supercapacitors. *Journal of Nanomaterials*, 10:1–17, 2016.

[3] S. Srinivasan. *Fuel Cells From Fundamentals to Applications*. Springer, 2006.

[4] A. Verdaguer, G. M. Sacha, H. Bluhm, and M. Salmeron. Molecular structure of water at interfaces: Wetting at the nanometer scale. *Chemical Reviews*, 106:1479–1210, 2006.

[5] C. D. Taylor, S. A. Wasileski, J. Filhol, and M. Neurock. First principles reaction modeling of the electrochemical interface: Consideration and calculation of a tunable surface potential from atomic and electronic structure. *Physical Review B*, 73(165402):1–16, 2006.

[6] J. Rossmeisl, E. Skulason, M. E. Bjorketun, V. Tripkovic, and J. K. Norskov. Modeling the electrified solid-liquid interface. *Chemical Physics Letters*, 167(2):103–128, 2008.

[7] W. W. Yi, S. S. Li, W. Yi, H. Fengbo, A. D. Kristopher, W. Yidong, X. Xie, N. S. Oleg, L. Jinshan, H. X. Dong, A. D. Karin, K. L. Peter, J. K. Laszlo, and L. Zi-Kui. Atomic and electronic basis for the serrations of refractory high-entropy alloys. *npj Computational Materials*, 3(1):23, 2017.

[8] D. N. Kouetcha, H. Ramézani, and N. Cohaut. Ultrafast scalable parallel algorithm for the radial distribution function histogramming using mpi maps. *The Journal of Supercomputing*, 73(4):1629–1653, 2017.

[9] S. A. Moiz, I. A. Khan, A. Younis, and K. Karimov. *Space Charge-Limited Current Model for Polymers Provisional chapter Space Charge-Limited Current Model for Polymers*, pages 91–117. Intech, 10 2016.

[10] A. Vilan and D. Cahen. Chemical modification of semiconductor surfaces for molecular electronics. *Chemical Reviews*, 10:1–17, 2016.

[11] M. Otani, I. Hamada, O. Sugino, Y. Morikawa, Y. Okamoto, and T. Ikeshoji. Structure of the water/platinum interface–a first principles simulation under bias potential. *Physical Chemistry Chemical Physic*, 10:3609–3612, 2008.

[12] M. Otani, I. Hamada, Y. Okamoto, and T. Ikeshoji. Reversible redox reaction and water configuration on a positively charged platinum surface: first principles molecular dynamics simulation. *Physical Chemistry Chemical Physic*, 13:20223–20227, 2011.

[13] M. A. Brown, Z. Abbas, A. Kleibert, R. G. Green, A. Goel, S. May, and T. M. Squires. Determination of surface potential and electrical double-layer structure at the aqueous electrolyte-nanoparticle interface. *Physical Review X*, 6:1–12, 2016.

[14] K. B. Oldham. A gouy-chapman-stern model of the double layer at a (metal)/(ionic liquid) interface. *Journal of Electroanalytical Chemistry*, 613(2):131–138, 2008.

[15] D. Marx. Proton transfer 200 years after von Grotthuss: insights from ab initio simulations. *Chemphyschem*, 7:1848–1870, 2006.

[16] O. F. Mohammed, J. Dreyer D. Pines, E. Pines, and E. T. J. Nibbering. Sequential proton transfer through water bridges in acid-base reactions. *Science*, 310:83–86, 2005.

[17] P. L. Geissler, C. Dellago, D. Chandler, J. Hutter, and M. Parrinello. Autoionization in liquid water. *Science*, 291:2121–2124, 2001.

[18] C. Cavazzoni, G. L. Chiarotti, S. Scandolo, E. Tosatti, M. Bernasconi, and M. Parrinello. Superionic and metallic states of water and ammonia at giant planet conditions. *Science*, 283:44–46, 1999.

[19] Q. Peng, A. K Dearden, J. Crean, L. Han, S. Liu, X. Wen, and S. De. New materials graphyne, graphdiyne, graphone, and graphane: review of properties, synthesis, and application in nanotechnology. *Nanotechnology, Science and Applications*, 7:1–29, 2014.

[20] A. Fujishima, X. Zhang, and D. A. Tryk. TiO_2 photocatalysis and related surface phenomena. *Surface Science Reports*, 63:515–582, 2008.

[21] J. H. Chang. *Investigation of the Interfaces between Cu(111)-based Electrodes and Water Using Density Functional Theory.* PhD dissertation, Graduate Department of Electrical and Computer Engineering University of Toronto, 2015.

[22] S. Plimpton. Fast parallel algorithms for short0-range molecular dynamics. *Journal of Computational Physics*, 117:1–19, 1994.

[23] H. J. C. Berendsen, D. V. D. Spoel, R. V. Drunen, and R. Gromacs. Fast parallel algorithms for short-range molecular dynamics. *Computer Physics Communications*, 91:43–56, 1995.

[24] N. Metropolis, A. W. Rosenbluth, M. N. Rosenbluth, and A. H. Teller. Equation of state calculations by fast computing machines. *The Journal of Chemical Physics*, 21:1087, 1953.

[25] J. Bonet and R. D. Wood. *Nonlinear Continuum Mechanics for Finite Element Analysis*. Cambridge University Press, 1997.

[26] K. Raghavan, K. Foster, K. Motakabbir, and M. Berkowitz. Structure and dynamics of water at the Pt(111) interface: Molecular dynamics study. *The Journal of Chemical Physics*, 94:2110–2117, 1991.

[27] H. Heinz, R. A. Vaia, B. L. Farmer, and R. R. Naik. Accurate simulation of surfaces and interfaces of face-centered cubic metals using 12-6 and 9-6 lennard-jones potentials. *The Journal of Physical Chemistry C*, 112:17281–17290, 2008.

[28] F. Iori, R. Felice, E. Molinari, and S. Corni. GolP: An atomistic force-field to describe the interaction of proteins with Au(111) surfaces in water. *Journal of Computational Chemistry*, 30:1465–1476, 2009.

[29] S. Schnur and A. Grob. Properties of metal-water interfaces studied from first principles. *New Journal of Physics*, 11:125003, 2009.

[30] T. Roman and A. Groß. Structure of water layers on hydrogen-covered Pt electrodes. *Catalysis Today*, 202:183–190, 2013.

[31] I. Tamblyn. Electronic Structure of Liquid Water and a Platinum Surface. *ArXiv e-prints*, pages 1–5, 2014.

[32] G. Cicero, J. C. Grossman, E. Schwegler, F. Gygi, and G. Galli. Water confined in nanotubes and between graphene sheets: A first principle study. *Journal of the American Chemical Society*, 130:1871–1878, 2008.

[33] Z. Huang and H. Lin. Stability of the high-spin ground state in the peierls-extended hubbard model. *The Journal of Chemical Physics*, 114:3284–3292, 2001.

[34] S. Meng, L. F. Xu, E. G. Wang, and S. Gao. Vibrational recognition of hydrogen-bonded water networks on a metal surface. *Physical Review Letters*, 89:176104–176108, 2002.

[35] J. Le, M. Iannuzzi, A. Cuesta, and J. Cheng. Determining potentials of zero charge of metal electrodes versus the standard hydrogen electrode from density-functional-theory-based molecular dynamics. *Physical Review Letters*, 119:16801–16807, 2017.

[36] S. Surendralal, M. Todorova, M. W. Finnis, and J. Neugebauer. First-principles approach to model electrochemical reactions: Understanding the fundamental mechanisms behind mg corrosion. *Physical Review Letters*, 120:246801–246806, 2018.

[37] M. Otani and O. Sugino. First-principles calculations of charged surfaces and interfaces: A plane-wave nonrepeated slab approach. *Physical Review B*, 73:115407–115412, 2006.

[38] M. Otani and O. Sugino. First-principles molecular dynamics simulation of biased electrode/solution interface. *Surface Science*, 601:5237–5240, 2007.

[39] J. Cheng, M. Sulpizi, and M. Sprik. Redox potentials and pka for benzoquinone from density functional theory based molecular dynamics. *The Journal of Chemical Physics*, 131(15):154504, 2009.

[40] F. Costanzo, M. Sulpizi, R. Guido D. Valle, and M. Sprik. The oxidation of tyrosine and tryptophan studied by a molecular dynamics normal hydrogen electrode. *The Journal of Chemical Physics*, 134(24):244508, 2011.

[41] J. Cheng, X. Liu, J. VandeVondele, M. Sulpizi, and M. Sprik. Redox potentials and acidity constants from density functional theory based molecular dynamics. *Accounts of Chemical Research*, 47(12):3522–3529, 2014.

[42] R. Subbaraman, D. Tripkovic, D. Strmcnik, K. Chang, M. Uchimura, P. A. Paulikas, V. Stamenkovic, and N. M. Markovic. Enhancing hydrogen evolution activity in water splitting by tailoring Li^+-$Ni(OH)_2$-Pt interfaces. *Science*, 334(6060):1256–1260, 2011.

[43] M. Born and K. Huang. *Dynamical theory of crystal lattices*. Oxford University Press, 1954.

[44] R. M. Martin. *Electronic Structure*. Oxford University Press, 2004.

[45] P. Hohenberg and W. Kohn. Inhomogeneous electron gas. *Phys. Rev.*, 136(3B):864–870, 1964.

[46] W. Kohn and L. J. Sham. Self-consistent equations including exchange and correlation effects. *Phys. Rev.*, 140(4A):1133–1138, 1965.

[47] D. M. Ceperley. Ground state of the electron gas by a stochastic method. *Phys. Rev.*, 45(7):566–569, 1980.

[48] J. P. Perdew and Y. Wang. Accurate and simple analytic representation of the electron-gas correlation energy. *Phys. Rev. B*, 45(23):13244–13249, 1992.

[49] M. Cococcioni. *A LDA+U study of selected iron compounds*. PhD dissertation, Scuola Internazionale Superiore di Studi Avanzati di Trieste, 2002.

[50] F. R. Mohamed. *Advanced methods in ab-initio molecular dynamics*. PhD dissertation, ETH Zurich, 2006.

[51] S. G. Louie, K. Ho, and M. L. Cohen. Self-consistent mixed-basis approach to the electronic structure of solids. *Physical Review B*, 19(4):1774–1782, 1979.

[52] J. VandeVondele, M. Krack, F. Mohamed, M. Parrinello, T. Chassaing, and J. Hutter. Quickstep: Fast and accurate density functional calculations using a mixed gaussian and plane waves approach. *Computer Physics Communications*, 167(2):103–128, 2005.

[53] A. D. Becke. Density-functional exchange-energy approximation with correct asymptotic behavior. *Phys. Rev. A*, 38:3098–3100, Sep 1988.

[54] T. W. Keal and D. J. Tozera. Semiempirical hybrid functional with improved performance in an extensive chemical assessment. *J. Chem. Phys.*, 123(121103):1, 2005.

[55] J. P. Perdew, M. Ernzerhof, and K. Burke. Rationale for mixing exact exchange with density functional approximations. *J. Chem. Phys.*, 105(22):9982–9984, 1996.

[56] E. Schwegler, J. C. Grossman, F. Gygi, and G. Galli. Towards an assessment of the accuracy of density functional theory for first principles simulations of water. ii. *Journal of Chemical Physics*, 121(11):5400–5409, 2004.

[57] J. Filhol and M. Neurock. Elucidation of the electrochemical activation of water over Pd by first principles. *Angewandte Chemie International Edition*, 45(3):402–406, 2006.

[58] M. T. Yin and M. L. Cohen. Theory of static structural properties, crystal stability, and phase transformations: Application to si and ge. *Physical Review B*, 26:5668–5687, 1982.

[59] H. J. Herrera-Suarez, A. Rubio-Ponce, and D. Olguin. Electronic band structure of platinum low-index surfaces: an ab initio and tight-binding study. ii. *Revista Mexicana de Fisica*, 58:46–54, 2012.

[60] N. E. Singh and N. Marzari. Surface energies, work functions, and surface relaxations of low-index metallic surfaces from first principles. *Physical Review B*, 80(235407):1–7, 2009.

[61] J. L. F. Da Silva, C. Stampfl, and M. Scheffler. Converged properties of clean metal surfaces by all-electron first-principles calculations. *Surface Science*, 600:703–715, 2006.

[62] S. Trasatti. Work function, electronegativity, and electrochemical behaviour of metals. *J. Elecfroanal. Chem.*, 33:351–78, 1971.

[63] M. Salmeron, S. Ferrer, M. Jazzar, and G. A. Somorjai. Photoelectron-spectroscopy study of the electronic structure of au and ag overlayers on pt(100), pt(111), and pt(997) surfaces. *Physical Review B*, 28(12):6758–6765, 1983.

[64] S. Goedecker, M. Teter, and J. Hutter. Separable dual-space gaussian pseudopotentials. *Physical Review B*, 54:1703–1710, Jul 1996.

[65] C. Hartwigsen, S. Goedecker, and J. Hutter. Relativistic separable dual-space gaussian pseudopotentials from H to Rn. *Physical Review B*, 58:3641–3662, Aug 1998.

[66] A. Y. Lozovoi, A. Alavi, J. Kohanoff, and R. M. Lynden-Bell. *Ab initio* simulation of charged slabs at constant chemical potential. *The Journal of Chemical Physics*, 115(4):1661–1669, 2001.

[67] J. K. Nørskov, J. Rossmeisl, A. Logadottir, L. Lindqvist, J. R. Kitchin, T. Bligaard, and H. Jónsson. Origin of the overpotential for oxygen reduction at a fuel-cell cathode. *The Journal of Physical Chemistry B*, 108(46):17886–17892, 2004.

[68] J. Staszak-Jirkovsky, R. Subbaraman, D. Strmcnik, and et.al. Water as a promoter and catalyst for dioxygen electrochemistry in aqueous and organic media. *ACS Catalysis*, 5(11):6600–6607, 2015.

[69] J. P. Perdew, K. Burke, and M. Ernzerhof. Generalized gradient approximation made simple. *Physical Review Letters*, 77:3865–3868, 1996.

[70] J. VandeVondele, F. Mohamed, M. Krack, J. Hutter, M. Sprik, and M. Parrinello. The influence of temperature and density functional models in *ab initio* molecular dynamics simulation of liquid water. *Journal of Chemical Physics*, 122(1):014515, 2005.

[71] D. Asthagiri, L. R. Pratt, and J. D. Kress. Free energy of liquid water on the basis of quasichemical theory and *ab initio* molecular dynamics. *Physical Review E*, 68:041505, 2003.

[72] I. W. Kuo, C. J. Mundy, M. J. McGrath, J. I. Siepmann, J. VandeVondele, M. Sprik, J. Hutter, B. Chen, M. L. Klein, F. Mohamed, M. Krack, , and M. Parrinello. Liquid water from first principles: Investigation of different sampling approaches. *Journal of Physical Chemistry B*, 108(34):12990–12998, 2004.

[73] W. Tang, E. Sanville, and G. Henkelman. A grid-based bader analysis algorithm without lattice bias. *Journal of Physics: Condensed Matter*, 21(8):084204, 2009.

[74] E. Sanville, S. D. Kenny, R. Smith, and G. Henkelman. Improved grid-based algorithm for bader charge allocation. *Journal of Computational Chemistry*, 28(5):899–908, 2007.

[75] G. Henkelman, A. Arnaldsson, and H. Jónsson. A fast and robust algorithm for bader decomposition of charge density. *Computational Materials Science*, 36(3):354–360, 2006.

[76] G. K. H. Madsen, C. Gatti, B. B. Iversen, L. Damjanovic, G. D. Stucky, and V. I. Srdanov. F center in sodium electrosodalite as a physical manifestation of a non-nuclear attractor in the electron density. *Physical Review B*, 59:12359–12369, May 1999.

[77] R. F. W. Bader. *Atoms in molecules : a quantum theory*. The International series of monographs on chemistry. Clarendon Press, Oxford, 1990.

[78] A. N. Frumkin, O. A. Petrii, and B. B. Damaskin. *Potentials of Zero Charge*, pages 221–289. Springer US, Boston, MA, 1980.

[79] J. Rossmeisl, Z.-W. Qu, H. Zhu, G.-J. Kroes, and J.K. Nørskov. Electrolysis of water on oxide surfaces. *Journal of Electroanalytical Chemistry*, 607(1-2):83–89, 2007. Theoretical and Computational Electrochemistry.

[80] P. Mirtaheri, S. Grimnes, and G. Martinsen. Electrode polarization impedance in weak NaCl aqueous solutions. *IEEE Transactions on Biomedical Engineering*, 52(12):2093–2099, Dec 2005.

[81] T. Pajkossy and D.M. Kolb. Double layer capacitance of Pt(111) single crystal electrodes. *Electrochimica Acta*, 46(20-21):3063–3071, 2001.

[82] A. Cuesta. Measurement of the surface charge density of co-saturated pt(111) electrodes as a function of potential: the potential of zero charge of pt(111). *Surface Science*, 572:11–22, 2004.

[83] A. Hodgson and S. Haq. Water adsorption and the wetting of metal surfaces. *Surface Science Reports*, 64(9):381–451, 2009.

[84] J. Carrasco, A. Michaelides, M. Forster, S. Haq, R. Raval, and A. Hodgson. A one-dimensional ice structure built from pentagons. *Nature Materials*, 8(5):427–431, May 2009.

[85] J. Carrasco, A. Hodgson, and A. Michaelides. A molecular perspective of water at metal interfaces. *Nature Materials*, 11(8):667–674, Aug 2012.

[86] A. Gross. Theory of solid/electrolyte interfaces. Ψ_k *Scientific Highlight Of The Month*, (125):1–32, 2014.

[87] N. S. Feibelman, P. J. Bartelt, K. N. C., and Thürmer. Pentagons and heptagons in the first water layer on Pt(111). *Physical Review Letters*, 105:026102, Jul 2010.

[88] N. S. Sakong, K. M. Mathew, G. R. Hennig, and A. Groß. Density functional theory study of the electrochemical interface between a Pt electrode and an aqueous electrolyte using an implicit solvent method. *The Journal of Chemical Physics*, 142(23):234107, 2015.

[89] K. Tonigold and A. Groß. Dispersive interactions in water bilayers at metallic surfaces: A comparison of the PBE and RPBE functional including semiempirical dispersion corrections. *Journal of Computational Chemistry*, 33(6):695–701, 2012.

[90] A. Glebov, A. P. Graham, A. Menzel, and J. P. Toennies. Orientational ordering of two-dimensional ice on Pt(111). *The Journal of Chemical Physics*, 106(22):9382–9385, 1997.

[91] E. H. G. Backus, N. Garcia-Araez, M. Bonn, and H. J. Bakker. On the role of fresnel factors in sum-frequency generation spectroscopy of metal-water and metal-oxide-water interfaces. *The Journal of Physical Chemistry C*, 116(44):23351–23361, 2012.

[92] R. Khatib and M. Sulpizi. Sum frequency generation spectra from velocity-velocity correlation functions. *The Journal of Physical Chemistry Letters*, 8(6):1310–1314, 2017.

[93] R. Khatib, E. H. G. Backus, M. Bonn, M. Perez-Haro, M. Gaigeot, and M. Sulpizi. Water orientation and hydrogen-bond structure at the fluorite/water interface. *Scientific Reports*, 6:24287, 2016.

[94] W. Liu, A. Tkatchenko, and M. Scheffler. Modeling adsorption and reactions of organic molecules at metal surfaces. *Accounts of Chemical Research*, 47(11):3369–3377, 2014.

[95] P. Mori-Sánchez, A. J. Cohen, and W. Yang. Localization and delocalization errors in density functional theory and implications for band-gap prediction. *Physical Review Letters*, 100:146401, Apr 2008.

[96] T. Schumann, L. Galletti, D. A. Kealhofer, H. Kim, M. Goyal, and S. Stemmer. Observation of the quantum hall effect in confined films of the three-dimensional dirac semimetal Cd_3As_2. *Physical Review Letters*, 120:016801, Jan 2018.

[97] T. A. Pham, D. Lee, E. Schwegler, and G. Galli. Interfacial effects on the band edges of functionalized si surfaces in liquid water. *Journal of the American Chemical Society*, 136(49):17071–17077, 2014.

[98] P. Pyykko. Relativistic effects in structural chemistry. *Chemical Reviews*, 88(3):563–594, 1988.

[99] F. Gossenberger, T. Roman, K. Forster-Tonigold, and A. Groß. Change of the work function of platinum electrodes induced by halide adsorption. *Beilstein Journal of Nanotechnology*, 5:152–161, 2014.

[100] S. Meng, E. G. Wang, and S. Gao. Water adsorption on metal surfaces: A general picture from density functional theory studies. *Physical Review B*, 69:195404, 2004.

[101] T. Ohto, K. Usui, T. Hasegawa, M. Bonn, and Y. Nagata. Toward *ab initio* molecular dynamics modeling for sum-frequency generation spectra; an efficient algorithm based on surface-specific velocity-velocity correlation function. *Journal of Chemical Physics*, 143(12):124702, 2015.

[102] A. Morita and T. Ishiyama. Recent progress in theoretical analysis of vibrational sum frequency generation spectroscopy. *Physical Chemistry Chemical Physics*, 10:5801–5816, 2008.

[103] A. Morita and J. T. Hynes. A theoretical analysis of the sum frequency generation spectrum of the water surface. ii. time-dependent approach. *Journal of Physical Chemistry B*, 106(3):673–685, 2002.

[104] M. Sulpizi, M. Gaigeot, and M. Sprik. The silica-water interface: How the silanols determine the surface acidity and modulate the water properties. *Journal of Chemical Theory and Computation*, 8(3):1037–1047, 2012.

[105] S. A. Corcelli and J. L. Skinner. Infrared and raman line shapes of dilute hod in liquid H_2O and D_2O from 10 to 90 degree. *Journal of Physical Chemistry A*, 109(28):6154–6165, 2005.